# Parametric Design and Multi-Objective Optimization of a 6,500 TEU Container Ship

Alexandros Priftis

Diploma Thesis


School of Naval Architecture and Marine Engineering
National Technical University of Athens

Thesis Supervisor: Prof. Apostolos D. Papanikolaou
Committee Member: Associate Prof. George Zaraphonitis
Committee Member: Assistant Prof. Nikolaos P. Ventikos

June 2015

# Abstract

The introduction of new and strict regulations by international organizations, as well as the constant endeavor of shipping companies for economic growth has led the shipbuilding industry to the introduction of new and cost-efficient designs in various types of merchant ships. In particular, container carriers, which are responsible for the shipping of millions of containerized goods every year, have recently started gaining in popularity among the ship owners around the globe. Hence, the competition between the international shipbuilders is getting stronger day by day, with each shipyard striving to offer the best container ship design that complies with both the existing and the imminent rules, yet without compromising the overall efficiency.

In order to improve a design, naval architects are encouraged to make proper use of CAD/CAE systems, which offer not only high convenience –by producing valuable results in short time– but also the much desired integration of design, engineering and manufacturing in a seamless operation. In the recent years, the optimization process has been quite popular in the field of engineering. As a result, software companies have excelled their products in such level that the consideration of design optimization in the design process has become of great value.

In this respect, our project deals with a case study of a mid-sized, 6,500 TEU container vessel. Firstly, the modeling of the ship, along with the creation of several subsystems that provide the necessary indicators takes place. Afterwards, an iterative optimization process begins, which results in a number of optimal designs, as far as certain objectives are concerned. Finally, an optimal design is selected, as a representative of the whole procedure. For this purpose, a powerful CAD/CAE software is used, CAESES/Friendship-Framework, which allows the user to create the parametric model, execute hydrostatic calculations and run multiple optimization cycles using various methods included in the software.



**Keywords:** Parametric Ship Design; Multi-Objective Optimization; Container Ship; CAD/CAE Systems; CAESES; Friendship-Framework

# Abstract in Greek

Η εισαγωγή νέων και αυστηρών κανονισμών από τους διεθνείς οργανισμούς στη ναυτιλία, καθώς και η συνεχής προσπάθεια των ναυτιλιακών εταιρειών να αναπτυχθούν οικονομικά έχουν οδηγήσει την ναυπηγική βιομηχανία στην εισαγωγή νέων και οικονομικά αποδοτικών σχεδίων στους διάφορους τύπους εμπορικών πλοίων. Συγκεκριμένα, τα πλοία μεταφοράς εμπορευματοκιβωτίων, που είναι αρμόδια για τη μεταφορά εκατομμυρίων συσκευασμένων αγαθών κάθε χρόνο, άρχισαν πρόσφατα να γίνονται δημοφιλή στους πλοιοκτήτες όλου το κόσμου. Ως εκ τούτου, ο ανταγωνισμός μεταξύ των ναυπηγείων γίνεται ισχυρότερος μέρα με τη μέρα, με το καθένα από αυτά να προσπαθεί να προσφέρει το καλύτερο δυνατό σχέδιο πλοίου μεταφοράς εμπορευματοκιβωτίων, το οποίο να συμμορφώνεται τόσο με τους υπάρχοντες, όσο και με τους επικείμενους κανονισμούς, χωρίς όμως να συμβιβάζει την αποδοτικότητα.

Προκειμένου να βελτιώσουν ένα σχέδιο, οι ναυπηγοί θα πρέπει να εκμεταλλεύονται κατάλληλα την χρήση CAD/CAE συστημάτων, τα οποία προσφέρουν όχι μόνο μεγάλη ευκολία –με την παραγωγή αποτελεσμάτων σε ελάχιστο χρόνο– αλλά και την πολυπόθητη ενσωμάτωση των φάσεων του σχεδίου, της μηχανικής και της κατασκευής σε μια ομαλή λειτουργία. Τα τελευταία χρόνια, η διαδικασία βελτιστοποίησης έχει γίνει ιδιαίτερα δημοφιλής στον τομέα της εφαρμοσμένης μηχανικής. Κατά συνέπεια, οι εταιρείες λογισμικού έχουν βελτιώσει τα προϊόντα τους σε τέτοιο επίπεδο, ώστε η χρήση της διαδικασίας βελτιστοποίησης στο στάδιο της σχεδίασης να έχει αποκτήσει ιδιαίτερο νόημα.

Η παρούσα εργασία εξετάζει τη μελέτη ενός μεσαίου μεγέθους πλοίου μεταφοράς εμπορευματοκιβωτίων, χωρητικότητας 6,500 TEU. Αρχικά πραγματοποιείται η διαμόρφωση του σκάφους, μαζί με τη δημιουργία διάφορων υποσυστημάτων, τα οποία παρέχουν τους απαραίτητους για την διαδικασία της βελτιστοποίησης δείκτες αποδοτικότητας. Κατόπιν, ξεκινά μια επαναληπτική διαδικασία βελτιστοποίησης, η οποία παράγει ορισμένα βελτιωμένα σχέδια, με βάση συγκεκριμένους στόχους. Τέλος, ένα βέλτιστο σχέδιο επιλέγεται ως αντιπροσωπευτικό της συνολικής διαδικασίας. Για το σκοπό αυτό, χρησιμοποιείται ένα προηγμένο CAD/CAE λογισμικό, το CAESES/Friendship-Framework, το οποίο επιτρέπει στο χρήστη να δημιουργήσει το παραμετρικό μοντέλο, να εκτελέσει υδροστατικούς υπολογισμούς και να τρέξει πολλαπλούς κύκλους βελτιστοποίησης, χρησιμοποιώντας διάφορες μεθόδους που περιλαμβάνονται στο λογισμικό.

**Λέξεις-κλειδιά:** Παραμετρική Σχεδίαση Πλοίου, Πολυκριτηριακή Βελτιστοποίηση, Πλοίο Μεταφοράς Εμπορευματοκιβωτίων, Συστήματα CAD/CAE, CAESES, Friendship-Framework

# Acknowledgements

At this point, I would like to thank my thesis supervisor, Professor Apostolos Papanikolaou, who gave me the opportunity to work on such an interesting and significant topic. He provided me with valuable guidelines in order to successfully complete my thesis, as well as my undergraduate studies in general. He has been and will always be a great inspiration to me.

Furthermore, I would like to thank Dr. Pierre Sames of DNV-GL for promoting the joint GL-NTUA CONTiOPT project regarding the formal safety assessment and optimization of container ships, which set the framework for this diploma thesis. Thanks are also due to Dr. Stefan Harries of Friendship Systems for providing the CAESES/Friendship-Framework software system, which was used in this thesis.

My sincere thanks also go to George Koutroukis, who was the first student of the Ship Design Laboratory of NTUA to work on this project and provided useful software tools and important data, on which this thesis is based.

I would also like to thank my friend and colleague Ilias Soultanias for helping me in the early stages of my project. His support and guidance have been of great value.

I am also thankful to Mrs. Aimilia Alisafaki for providing me with all the necessary information to begin my thesis and for her constant willingness to help.

Finally, I would like to express my gratitude to my family, who incessantly support me throughout my life.

Alexandros Priftis

June 2015

# Contents

# Introduction

The scope of this diploma thesis is to explore the potentials of parametric ship design and multi-objective optimization of a mid-sized container vessel. Both tasks are implemented using an advanced CAD/CAE software, Friendship-Framework. The ultimate purpose of the project is to produce an improved design in respect to several objectives, including a reduced required freight rate, an increased zero ballast TEU capacity, as well as a reduced energy efficiency design index.

Firstly, in section 1, the background of the container shipping industry is described. A brief history of the industry is presented, which allows us to understand how the method of containerization was introduced to the shipping world. Afterwards, a reference to container ship classes and their evolution follows. Finally, essential information regarding the global trade routes is provided, which helps the reader understand the current situation in the global trade market.

In section 2, the topic of ship design and CAD/CAE systems is analyzed. The introduction of the latter influenced the methods and techniques used in ship design. Their relationship is presented in this section. In addition, specific information regarding the container ship design is provided.

In section 3, the reader can find detailed information regarding the optimization and its establishment in the ship design process. Terms like multi-objective optimization, pareto optimality and design of experiment are sufficiently explained, as our project is based on these principles.

After the literature survey, the case study is presented in section 4. At first, there is an overview of the problem, while the purpose of the work is explained. Afterwards, the necessary information regarding the creation of the parametric model is provided, including both the geometric model and the subsystems, which supply us with the performance indicators needed for the optimization phase. An explanation of how the design optimization is being carried out follows.

Finally, in sections 5 and 6, the final results are presented, including detailed graphs and tables that illustrate the outcome of the whole procedure. The diploma thesis concludes with a brief summary and outline of the work undertaken, providing some perspectives for future research.

# 1 Container Shipping Industry

## 1.1 Introduction

It is widely known that international shipping is the backbone of global trade. Although the shipping industry is facing various challenges, particularly from the regulatory aspect, the global fleet is constantly growing and the competition is getting stronger. A little over half a century ago, when the first container ships were constructed, things were different. Neither were the designs optimized for maximum TEU capacity, nor were there many rules imposed, which would have a great impact on the operation of container ships. Nowadays however, the situation is completely different and a lot of effort is put on the improvement of ship design in order to follow the rapid changes in the shipping industry.

## 1.2 History of Container Shipping Industry

Container ships, as we know them today, have actually derived from another type of merchant vessels, the tankers. The first converted tankers, which were to be used as container carriers, appeared after the end of World War II. In 1951, the first purpose-built container ships commenced their operations in Denmark, Seattle, WA and Alaska. The first commercially successful container vessel was the *Ideal X*, owned by Malcom McLean and could carry 58 metal containers between Newark, NJ and Houston, TX [1].

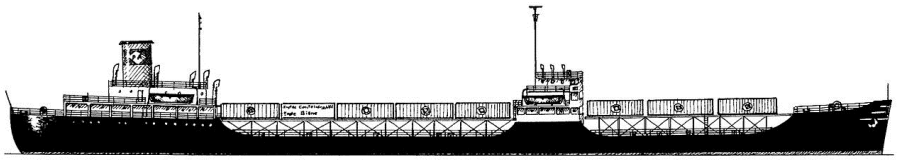

Figure 1: *Ideal X*

Malcom McLean is considered to be the pioneer of container shipping. It all started back in 1937, when he was the owner of a small trucking firm in North Carolina. A cargo ship back then would typically need much more time to be loaded with cargo, than modern container ships need today. Since the idea of containerization had not been invented yet, the methods used for the loading and the unloading of the cargo were both time-consuming and toilsome. This encumbrance and uncertainty in time schedule made this man come up with a new loading method that proved to be quite productive. The technique was based on the idea of loading the entire truck that carried the cargo onto the ship, instead of transferring the cargo from the truck to the vessel's holds. That

was the beginning of containerization, which later became the standard method for shipping goods around the globe [9].

Figure 2: Malcom McLean

Thanks to the special design of modern container ships, structures commonly found in the traditional general cargo vessels, such as individual hatches, holds and dividers, can be eliminated, thus increasing the overall capacity of the ship. A typical container ship's hull is divided into cells by vertical guide rails. The purpose of those cells is to hold the payload in containers. The most common types of containers are the TEUs and the FEUs, abbreviations that stand for Twenty-foot Equivalent Unit and Forty-foot Equivalent Unit respectively. However, there are also other types of units that are used for special cargo types, such as refrigerated ISO containers, suitable for transportation of refrigerated goods, or tanks, used for shipment of liquid materials [1].

| **Year** | **Vessel's Name** | **TEU Capacity** |
|---|---|---|
| 1968 | OCL Encounter Bay | 1,530 |
| 1972 | Hapag Lloyd Hamburg Express | 2,950 |
| 1988 | APL C-10 President Truman | 4,500 |
| 1998 | Susan Maersk | 8,680 |
| 2006 | Emma Maersk | 11,000 |
| 2015 | MSC Oscar | 19,224 |

Table 1: Largest container ships per decade

Today, the improvement of technology and engineering made the introduction of 19,224 TEU container carriers possible [4]. It seems that the increase in TEU

capacity will not be ceased anytime soon. However, that does not lead us to the fact that smaller container ships will disappear. A new trend, known as *cascading*, is the result of the high number of new building programs initiated by many liner companies. These orders consist primarily of very large container ships, such as Maersk's Triple-E class ships. The continued influx of such large vessels into the market has led to a large number of vessels being cascaded onto trade lines that historically have been served by smaller vessels [15].

In our case, this means that routes where 2,000-3,000 TEU container ships are preferred by charterers at this moment, could possibly attract vessels in the 6,000 TEU category in the following years. Since the former category of container ships is mainly used for the purpose of Short Sea Shipping, such changes in the market could make the latter category widely popular among both the charterers and the ship owners. As a result, an optimized design can play a pivotal role in the shipbuilding industry.

## 1.3 Container Ship Size Categories

Container vessels are categorized in seven major classes, as seen in table 2. The newest of them, called Ultra Large Container Vessels (ULCV), consists of the largest container ships to date, able to carry more than 14,500 TEUs. The size of Panamax vessels is limited by the Panama canal's lock chambers. The Post-Panamax category was once used to describe the vessels that had a beam of over 32.31 meters; however, the widening of Panama canal is causing some changes in the terminology. More specifically, the new locks, when the expansion project is completed, will be able to accommodate container ships with an overall length of over 366 meters, up to 49 meters wide and with a tropical fresh water draft of 15.2 meters. Container ships with a capacity of fewer than 3,000 TEUs are called Feeders, which are commonly used in short trade routes. This class is most likely to carry cargo cranes on board [1].

| **Name** | **TEUs** | **L (m)** | **B (m)** | **T (m)** |
|---|---|---|---|---|
| Small Feeder | up to 999 | – | – | – |
| Feeder | 1,000-1,999 | – | – | – |
| Feedermax | 2,000-2,999 | – | – | – |
| Panamax | 3,000-5,099 | 294.13 | 32.31 | 12.04 |
| Post-Panamax | 5,100-9,999 | 366.00 | 49.00 | 15.20 |
| New Panamax | 10,000-14,499 | 366.00 | 49.00 | 15.20 |
| ULCV | 14,500+ | 366.00+ | 49.00+ | 15.20+ |

Table 2: Container ship classes

## 1.4 Future Development of Container Ships

Looking at figure 3, we can clearly see that since the year 2000, the capacity of container vessels has been growing rather fast. As mentioned earlier, the largest container ship to date can carry 19,224 TEUs. However, it should be noted that there are several factors that could affect this trend. For instance, space limitations in commercial ports could render the entrance of ultra large container carriers impossible in the future. These limitations include air draft and under crane clearance, to name a few. Furthermore, the structural design of the hull has several limiting factors, considering the present typical layouts. Finally, it is imperative that future research is focused on ship stability, as increased beam can result in increased accelerations in ship motions, as well as high GM values [8].

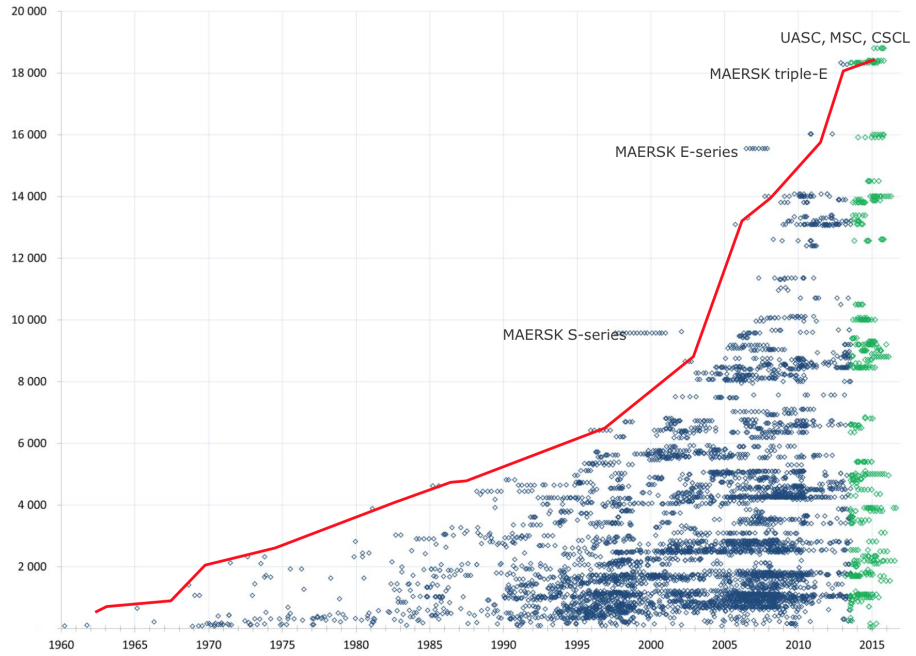


Figure 3: The evolution of container ships, 1960-2015

## 1.5 Slow Steaming

For a long time until a few years ago, the fuel prices were at such levels that enabled most container ship operators to use their vessels in speeds that could reach the number of 25 Knots. Container vessels carry valuable payload that needs to be shipped in short time to its destination. Hence, speeds in which other ship categories operate, such as bulk carriers or tankers that travel at around 15 Knots, could cause delays in this respect [23].

However, the recent notable increase in fuel prices introduced a new trend in the shipping industry, known as *slow steaming*. According to this practice, container ships cruise at considerably lower speeds, at around 18-20 Knots, as seen in figure 4. As a result, a significant decrease in fuel consumption and operational costs can be achieved, albeit accompanied by a prolongation of the voyage duration by a modest amount of time. Moreover, the decrease in the service speed of ships results in a much lower Energy Efficiency Design Index (EEDI). Therefore, many container carriers can comply with the international regulations regarding the environmental impact of merchant ships, evading the installation of expensive systems that aim to a reduction of the EEDI in existing vessels [25].

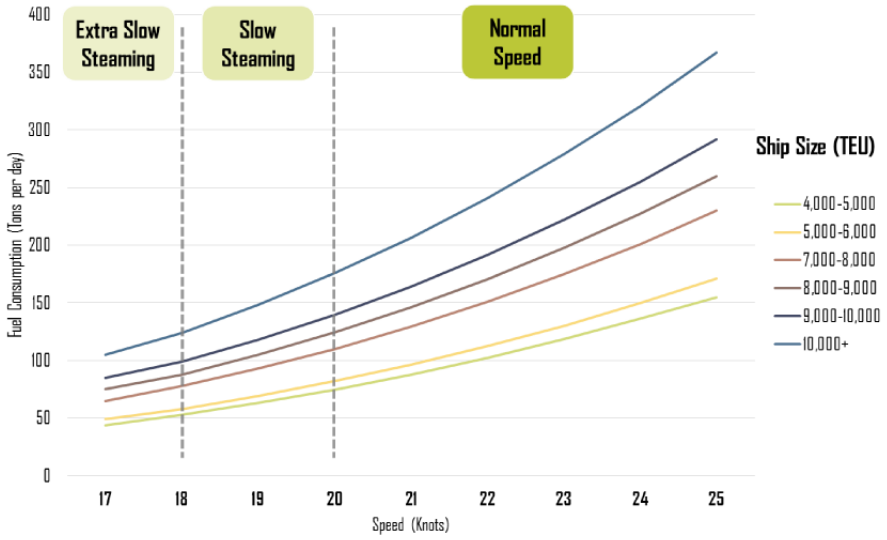


Figure 4: Fuel consumption per operational speed

## 1.6 Shipping Routes

A trade route is a logistical network identified as a series of pathways and stoppages used for the commercial transport of cargo. Allowing goods to reach distant markets, a single trade route contains long distance arteries, which may further be connected to smaller networks of commercial and non-commercial transportation routes (Donkin, 2003).

### 1.6.1 Global Trade Routes

Global containerized trade has been facing a constant growth since 1996. In 2013, there was a 4.6% growth, which can be translated to a total movement of

160 million TEUs in one year (Clarkson Research Services, 2014b). The three routes on the major East-West trade lane –the trans-Pacific, Asia-Europe and the transatlantic– bring together the manufacturing center of the world, Asia, along with North America and Europe, which are considered to be the major consumption markets [24]. The world's top trading routes by TEU shipments, according to [5], can be seen in table 3.

| **Route** | **West bound** | **East bound** | **North bound** | **South bound** |
|---|---|---|---|---|
| Asia-N. America | 7,739,000 | 15,386,000 | – | – |
| Asia-N. Europe | 9,187,000 | 4,519,000 | – | – |
| Asia-Mediterranean | 4,678,000 | 2,061,000 | – | – |
| Asia-Middle East | 3,700,000 | 1,314,000 | – | – |
| N. Europe-N. America | 2,636,000 | 2,074,000 | – | – |
| Australia-Far East | – | – | 1,072,016 | 1,851,263 |
| Asia-S. America | – | – | 621,000 | 1,510,000 |
| Europe-S. America | – | – | 795,000 | 885,000 |
| N. America-S. America | – | – | 656,000 | 650,000 |

Table 3: Top trade routes (TEUs shipped), 2013

### 1.6.2 The Asia-North America Route

In this project, one of the most profitable routes was selected for the investigation of the Required Freight Rate (RFR) in our model. The Asia-North America route is served by most shipping companies and can be found in various versions. One of them is the India-North America route that is usually served by container ships in the 6,000-7,000 TEU category. More information about the route chosen for our model can be found in section 4. Below, some examples of this route can be found:

- APL – IAX (India America Express)
- CMA CGM – Amerigo Express
- Hapag Lloyd – INDAMEX (India America Express)
- NYK – IEX (India East Coast Express)

All of the above routes include major hub ports of the Indian ocean, in countries like India, Pakistan and United Arab Emirates, as well as many ports in the east coast of the United States of America. Moreover, it should be noted that a few major ports of the Mediterranean sea are included in the routes, such as Port Said, Genoa and Valencia.

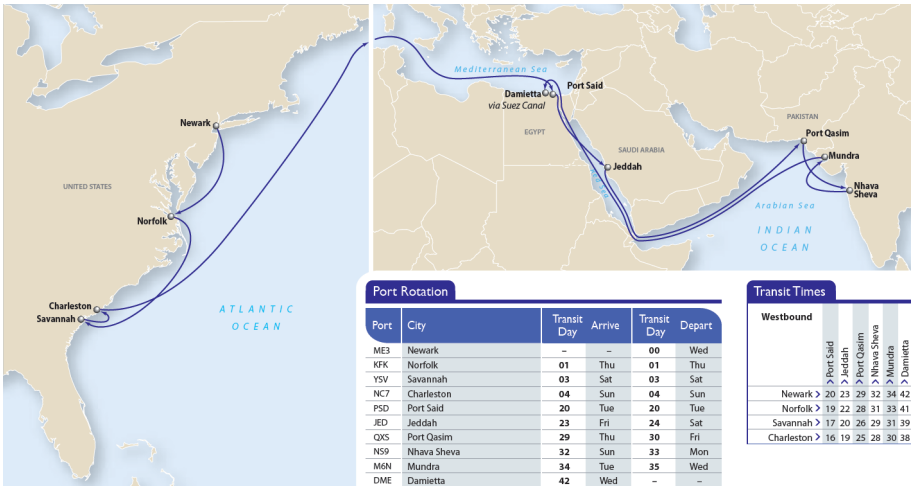


Figure 5: IAX (India America Express)

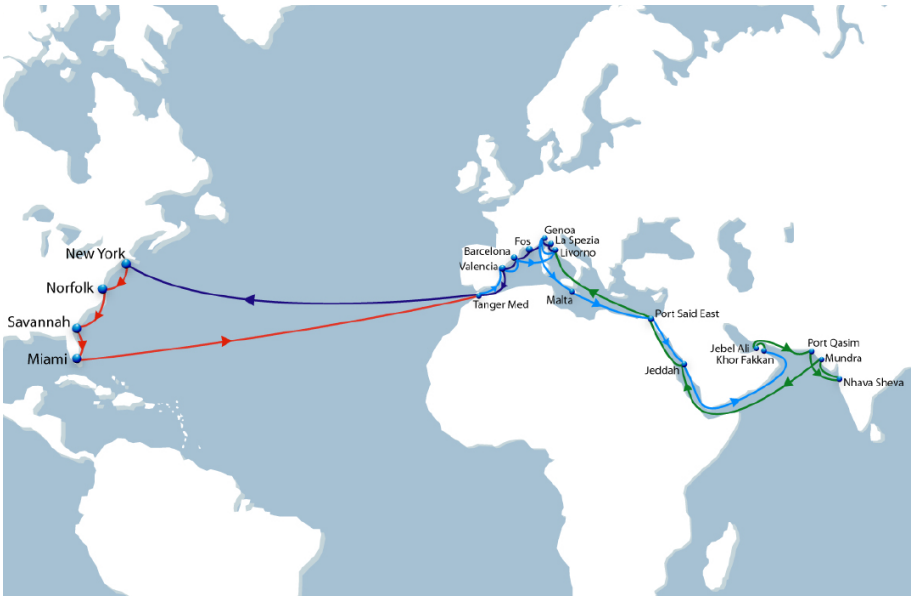


Figure 6: Amerigo Express

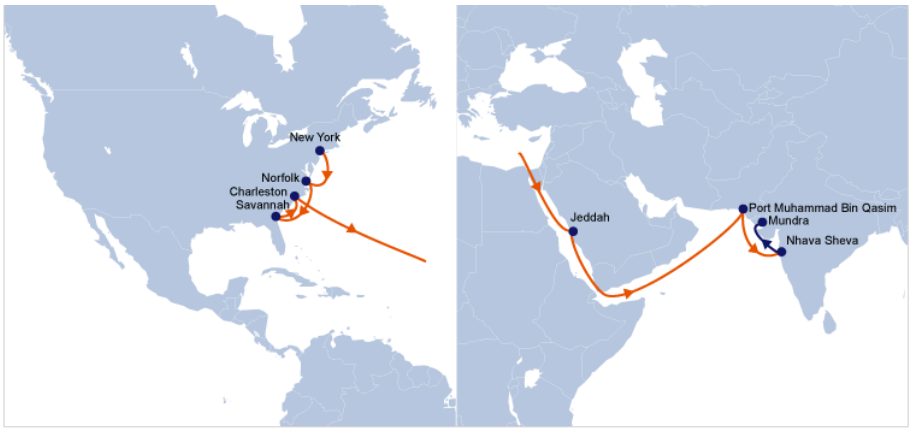


Frequency: weekly

North America ⟶ Indian Ocean

| From/To | Jeddah | Port Muhammad Bin Qasim | Nhava Sheva | Mundra |
|---|---|---|---|---|
| **Arrival Day** | FRI | THU | SUN | TUE |
| **New York** | 23 | 29 | 32 | 34 |
| **Norfolk** | 22 | 28 | 31 | 33 |
| **Savannah** | 20 | 26 | 29 | 31 |
| **Charleston** | 19 | 25 | 28 | 30 |

Figure 7: INDAMEX (India America Express)

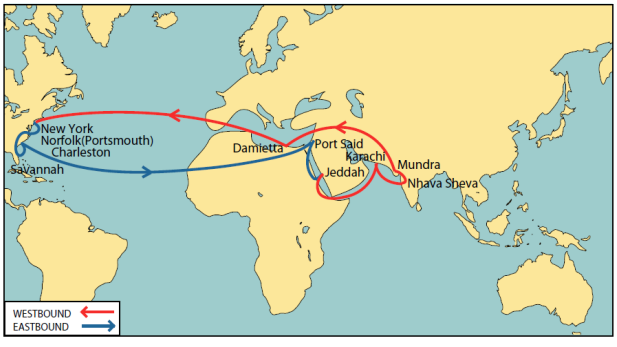


Port Rotation

| Origin | ETA/ETD |
|---|---|
| Port Muhammad Bin Qasim (Karachi) | THU/FRI |
| Nhava Sheva | SUN/MON |
| Mundra | TUE/WED |
| Damietta | WED/THU |
| New York | TUE/WED |
| Norfolk (Portsmouth) | THU/THU |
| Savannah | SAT/SAT |
| Charleston | SUN/SUN |
| Port Said | TUE/TUE |
| Jeddah | FRI/SAT |
| Port Muhammad Bin Qasim (Karachi) | THU/FRI |

Turnaround days 56
Weekly/Fixed Day Service

Figure 8: IEX (India East Coast Express)

# 2 CAD/CAE Systems and Ship Design

## 2.1 Introduction

Ship design was once considered a sequential and iterative process, where designers focused on one issue at a time. Many work cycles in the design process were necessary, in order to reach the final product. In each cycle, modifications and calculations took place, improving the model under development, created from square one. This method was accompanied by many difficulties, as no individual designer can either keep track of every subsystem of a complex design, or consider every possible option along with their advantages and disadvantages.

Times have changed and so have the ship design methods. The introduction of CAD/CAE (Computer Aided Design and Engineering respectively) systems in the shipbuilding industry has established new methods and techniques in the field of ship design, changing the way naval architects approach the ship design problem. Nowadays, a modern integrated approach to ship design brings together every task of the process simultaneously, which results in both shortening the overall time needed for the completion of the design and reducing the overall cost of the work [20].

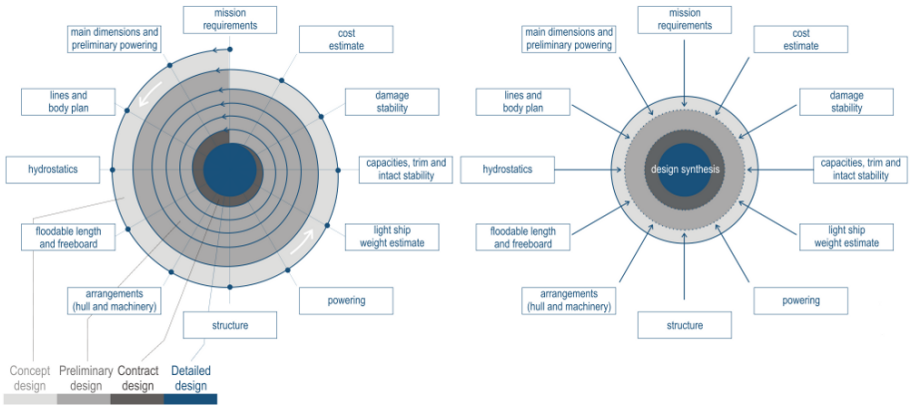


Figure 9: Traditional design spiral (left) vs. integrated approach (right)

## 2.2 Development of CAD/CAE Systems

The first use of CAD systems was intended for the building phase of ships. More specifically, a new method was developed, which enabled the numerical control of a flame cutting torch during the production of steel plates. In regard to ship design, the first CAD/CAE programs were used as a substitute of manual drafting, by producing elastic curves that would form the ship's lines. As technology

improved, these computer programs got more advanced, being able to produce more complex curves like Bezier, B-spline and NURBS curves. In the meantime, the increasing power of CAD software allowed them to handle more calculation problems, such as hydrostatic calculations, stability problems and simulation of different loading cases. Today, software developers are trying to incorporate the optimization process in naval architecture programs in order to provide a more complete and thorough solution to CAD/CAE software alternatives [17].

## 2.3 Ship Design Methods

### 2.3.1 Traditional Design

As mentioned earlier, the ship design problem was at first considered a sequential process. The traditional approach of ship design can be divided in four phases [14]:

**Conceptual model:** this phase is primarily concerned with the owner's requirements and the ultimate purpose is to set the type and calculate the main dimensions and form coefficients of the ship, in order to satisfy the owner's needs.

**Preliminary model:** following the conceptual model phase, naval architects proceed to a more detailed study. A preliminary design is created, including weight calculations, deadweight analysis, stability calculations and a first draft of the ship's lines.

**Final design model:** during the next phase, a final design is presented to the client. Final plans are created, detailed hydrostatic and hydrodynamic calculations based on the final hull form are executed and the internal arrangement of the ship is finalized.

**Detailed and faired hull model:** the last phase of the design process includes the final touches to the design. The naval architects perform a final checkup, in order to ensure that the ship complies with every rule and regulation. Structural analysis is carried out in detail so as to control the ship's strength in several conditions.

When every aspect of the design is ready, the contract can be signed between the shipbuilder and the client, in order for the construction phase to commence. It should be noted that in the approach described above, a lot of iterations occur, because the results of calculations may not be satisfactory immediately, as the compliance with the international and domestic regulations often contradict with the hull form and the ship's internal arrangement.

### 2.3.2 Integrated Design

From the description of the traditional design procedure, we can conclude that the use of CAD systems is applicable in various aspects of ship design. The integration of such software has changed the design practice followed by naval architects, as in this case the multiple iterations are superfluous. In particular, CAD/CAE systems are able to incorporate constraints in the design process, like environmental rules or stability criteria. As a result, every calculation is based on these constraints and the outcome always complies with every requirement. Hence, the design is always valid and no checkups or new set of calculations are required in order to finalize the design.

In addition, the power of computer hardware and software allows the designer to execute analytical calculations in a very short time, compared to the case where no CAD software is utilized. Finally, the much desired integration of design, engineering and manufacturing results in an automated production process, which eliminates unnecessary delays in the construction of the ship. Thus, the time needed for the completion of a project is reduced. All in all, it can be understood that the benefits of CAD/CAE systems justify their use in ship design to the fullest.

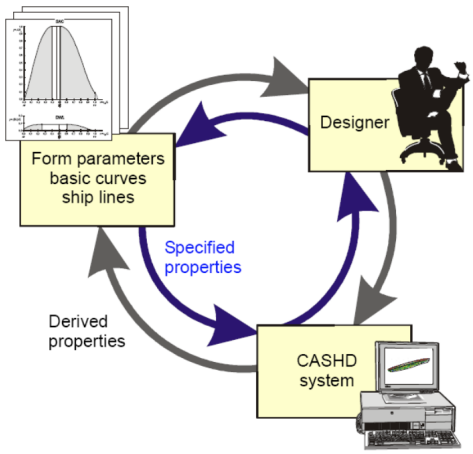


Figure 10: Conventional vs. parametric modeling

## 2.4 Parametric Modeling

The principle behind CAD systems and integrated design is the parametric modeling. In modern CAD/CAE tools, the extent to which parameters are used in ship design, demonstrates three main geometric modeling methods [22]:

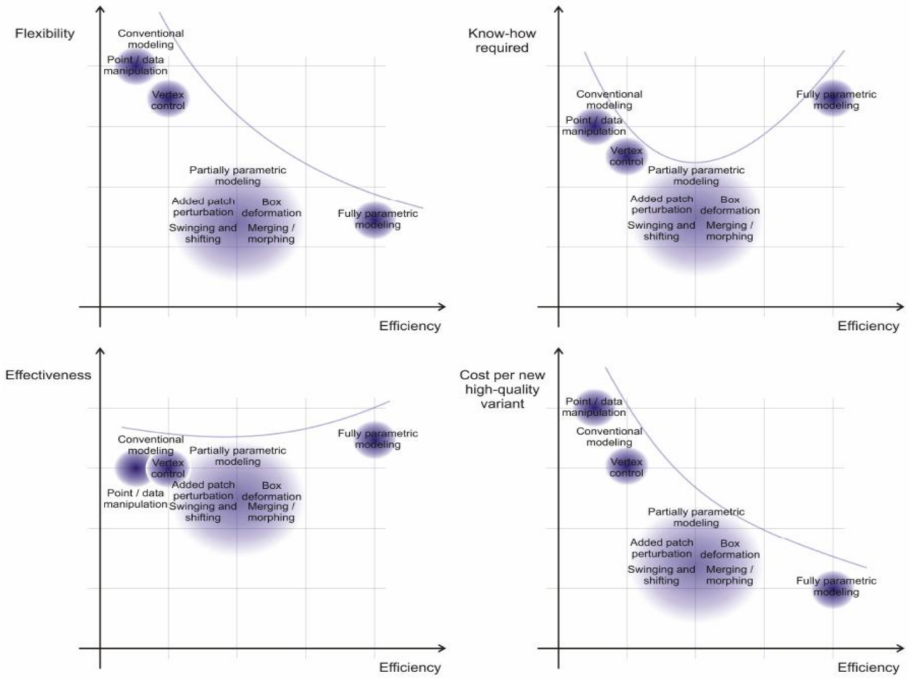


Figure 11: Geometric design methods

**Conventional design:** the designer has full control of the design and the curves defining it. Changes in the geometric model can only be achieved by moving curve points manually. In this case, the designer must pay attention to the result, as it is his/her job to deal with geometric constraints, as well as the fairing of the curves. The overall procedure is time-consuming and leads to a single final design.

**Semi-parametric design:** in this case, the role of CAD tools is not restricted to the graphical user interface. Software, such as Friendship-Framework, Aveva Marine and Rhinoceros, are able to modify a given hull form by adjusting parameters included in the creation of various curves. Design variants can be produced either by advanced transformations, such as the Lackenby transformation, or by distortion. This method can best be described as partially parametric, since changes are applied to the existing design in a certain degree only. The advantages of this method, compared to conventional design, sum up to the ability of creating multiple design variants in short time.

**Fully parametric design:** the model is generated automatically by relationships between several parameters defined by the designer. Every curve is created by the program, taking into account these parameters, while the designer can also set design constraints, so as to confine the design space according to his/her preferences. In addition, hull fairness is achieved automatically and the results are satisfactory. The software gives back the necessary performance indicators, which allow the naval architect to evaluate the result and make the necessary adjustments instantly.

Apart from the geometry of the ship, a wide range of computations is integrated into the process. Hence, there is no need for repetitive calculations. The final product includes a wide range of variants, from which the designer can select the optimal, based on the task's requirements.

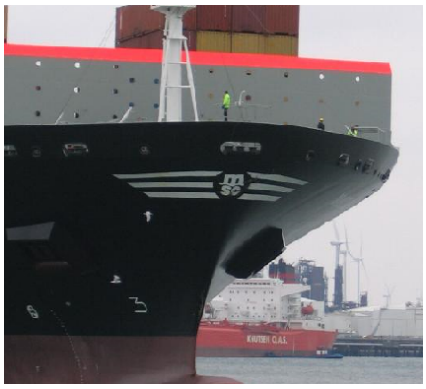

(a) Bow

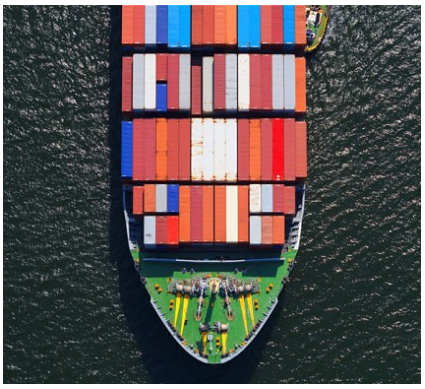

(b) Main deck

Figure 12: Container ship design characteristics

## 2.5 Container Ship Design

Container ship design follows the principles described above. However, some differences in respect to the design procedure can be observed, compared to the design of other ship types, like tankers or bulk carriers. The most significant one pertains to the principal dimensions of the hull. Since container ships carry their payload in standardized units (mainly TEUs and FEUs), their hull dimensions are estimated based on the unit's dimensions. Hence, the length, breadth and depth are multiples of the unit's matching dimensions. Of course, more aspects are taken into account in this estimation procedure, such as several required minimum distances in specific parts of the hull. Some examples include the double bottom, double side, forward collision bulkhead as well as the bay spacing [19].

Another characteristic of container ship design is the low block coefficient $c_B$ value. While crude oil tankers' typical $c_B$ values are in most cases above 0.8, container vessels' hulls have a $c_B$ of less than 0.7. The reason behind this is the service speed of the latter ship type. The typical speed of container carriers used to be 25 Knots, until recently, when the values dropped by around 5 Knots. Still, the difference between these ships and other merchant vessel categories is considerable. Bulk carriers and tankers have a service speed of around 14 Knots. Due to the higher Froude numbers that container ships operate in, it

is imperative that the friction resistance is kept low. This can be achieved by producing slender hulls with low $c_B$ values [19].

Finally, a special feature of container carriers is the large flare angle of the ship's bow (figure 12a). Although the hull of a container ship needs to be slender, designers try to maximize the main deck area, in order to boost the TEU capacity above the main deck of the ship (figure 12b). The larger the area on the main deck, the higher the number of TEUs that can be stored on deck [19].

# 3 Design Optimization

## 3.1 Introduction

Optimization is a process inextricably linked with human activity. The desire to consciously optimize the outcome of decisions is a uniquely human character trait (Nowacki, 2003).

Ship design traditionally has been based on a sequential and iterative approach. There have been several attempts from researchers to solve the ship design problem using various optimization methods. Through the optimization process, a selection of the best solution among many feasible ones can be achieved. A problem may be approached in various ways, depending on the desired outcome of the process. Optimization methods are used in different areas, such as structural engineering or mechanical design. The result is the creation of much improved designs in a short time span [21].

Decision making, a vital part of the optimization procedure, is mainly the choice of one or more design alternatives from a list of several options. The ultimate aim is to select the best design, so as to maximize the positive outcome and minimize the negative one. Since both the positive and the negative results are closely related, it is the human factor that leads to the final result of the whole procedure [16].

## 3.2 Optimization in Naval Architecture

In the 1960s, the utilization of computers for parts of the design process began. In the meantime, the first CAD programs made their appearance. These programs were mainly used for the optimization of design variables for specific economic criteria or for the mathematical parametric exploration of the design space on the basis of simplified ship models [18]. In ship aerodynamics, optimization methods have been utilized by Day, in order to investigate the aerodynamic lift distribution of a heeled yacht in a wind gradient.

As far as ship design is concerned, there have been numerous approaches to optimization. For example, Murphy et al. and Nowacki et al. have modeled the ship design problem as a single-objective optimization problem. Sen has modeled it as a generalized goal programming problem instead. Pal and Keane et al. used more traditional techniques, while Bras et al. approached the design problem as a Decision Support Problem Technique (DSPT) one. On the other hand, there are researchers, like Ray and Sha, that used a multi-criteria optimization model, which incorporates not only accepted naval architectural estimation methods, but also a decision system handler and a nonlinear optimization tool [21].

## 3.3 Ship Design and Holistic Optimization

According to the great philosopher Aristotle, *holism* means that the whole is more than the sum of the parts. In ship design, this means that the ship is considered to be a system that incorporates various subsystems and their components. For instance, one subsystem can be related to the cargo storage and handling, whereas a different one can be connected to the ship's propulsion. These systems are serving well-defined ship functions, which can be divided into several categories. When addressing the ship design problem, the naval architect should take into account the whole ship's life cycle. Hence, the design ought to be divided into stages that reflect different phases of the whole design development. From the above, it can be understood that the optimal design of a ship, with respect to its whole life cycle, can best derive from a holistic optimization of the ship system for its life cycle [18].

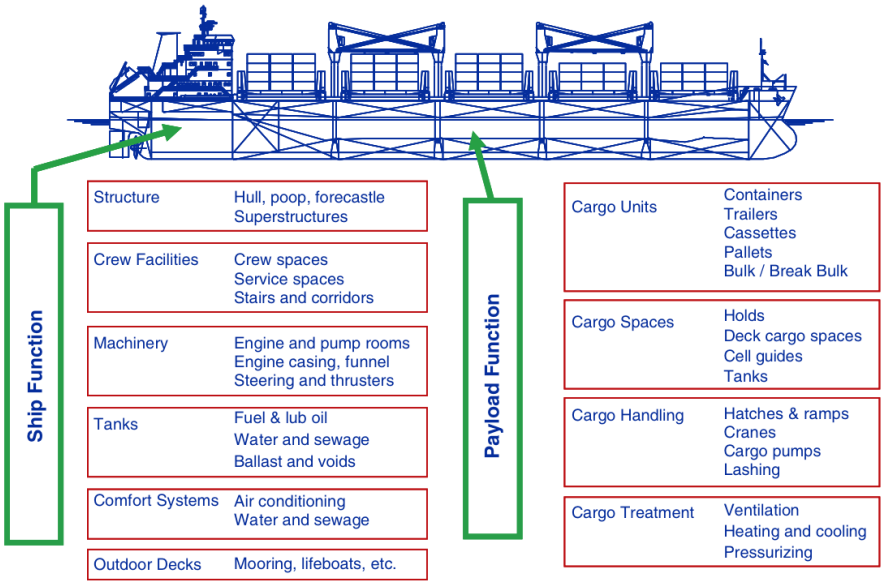


Figure 13: Ship functions according to Levander

The ship model is created based on the purpose of the vessel, the owner's special requirements, as well as several constraints that must be taken into account, such as international rules and regulations or safety criteria. Then, after the first phase of the design is finished, which results to a thorough and complete model of the ship, the optimization cycles inaugurate. The ultimate purpose of this phase is usually to optimize the ship in regard to cost or operational efficiency by trying to achieve the lowest required freight rate possible, or in regard to passenger safety or satisfactory protection of cargo. Of course, when environmental regulations are taken into account, the environmental footprint of the ship is monitored throughout the optimization process and its minimization

is included in the main objectives. The final result does not always include a straightforward solution and it is a common practice for the designers to select one among the many optimal designs, by mitigating the significance of every objective [18].

## 3.4 The Generic Ship Design Optimization Problem

The generic ship design optimization problem describes the exhaustive multi-objective and multi-constrained optimization with the least reduction of the entire real design problem. Its basic elements can be defined as follows [18]:

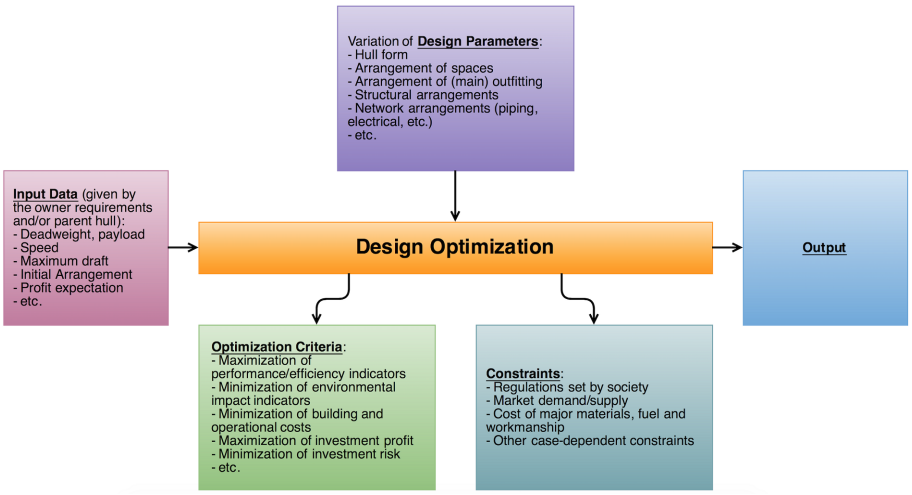


Figure 14: The generic ship design optimization problem

**Optimization criteria (merit functions, goals):** a list of mathematically defined performance/efficiency indicators. As far as the ship design problem is concerned, the criteria are usually complex nonlinear functions of the design parameters and are defined by algorithmic routines in CAD procedures.

**Constraints:** a list of mathematical defined criteria in regard to case-specific constraints. The latter include international or domestic laws and regulations, such as SOLAS or MARPOL regulations, operational costs, etc.

**Design parameters:** a list of parameters used to describe the design under optimization. This includes, among others, the internal arrangement of the vessel, the hull form, structural arrangements and piping and electrical networks.

**Input data:** data including owner's specific requirements, drawings or other qualitative information crucial to the optimization procedure. Typical examples of input data include the deadweight of the ship, maximum draft, profit expectation, etc.

**Output:** the entire set of design variables, for which the optimization criteria obtain the mathematically extreme values. In the case of a multi-objective optimization process, the sum of the optimal solutions to the problem lies on the so-called pareto front. The designer has to make the final decision, as compromises have to be made regarding the objectives of the optimization.

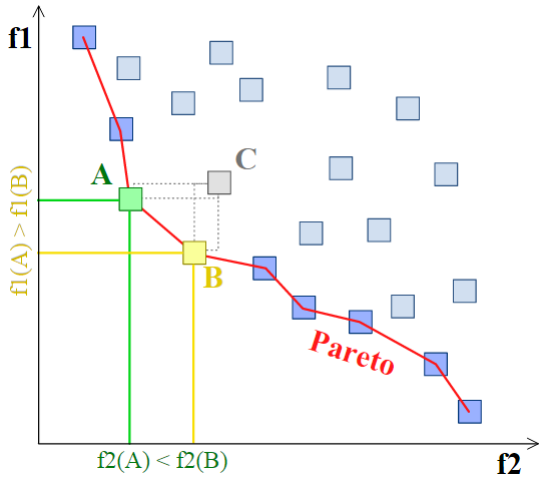


Figure 15: Pareto frontier

## 3.5 Pareto Optimality

When multi-objective optimization methods are utilized, it is very important to understand the way systems react to different conditions, as design variables change. In most cases, the models cannot combine the best performance in every objective. That is why decision making plays a critical role in optimization. The result of the decision process is to find the best compromised solution. This solution can be found in the pareto front and is one of the so-called pareto optimal solutions. Pareto optimal solutions is a set of feasible outcomes, in which no single objective can be improved without degrading the achievement of at least one other objective [16].

Looking at figure 15, we can understand how pareto optimality works. The boxed points represent feasible choices. Smaller values are preferred to larger ones. Point $C$ does not lie on the pareto frontier as it is dominated by both points $A$ and $B$. On the other hand, $A$ and $B$ are not strictly dominated by any other, so they do lie on the frontier [2].

## 3.6 Design of Experiment

Design of Experiment (DoE) is a systematic method, used to determine the relationship between factors affecting a process and the output of that process. In other words, it is used to find cause-and-effect relationships. This information is needed to manage process inputs in order to optimize the output. Through this procedure the feasibility boundaries are detected, allowing the designer to detect the trends of the design variables in regard to the optimization objectives.

There are many methods which can be used for the DoE. In our project, the Sobol sequence was utilized, producing an acceptable result. This particular design engine is included in the software used for the creation of the container ship model, namely Friendship-Framework. Sobol sequence (or also known as $LP_T$ sequence) is categorized as a space-filling design. This design is a quasi-random sequence. Using this method, test sequences are generated randomly in the design boundary. It is important to note that these sequences are iteratively generated in a uniform distribution, so as to secure the overall coverage of the design space, while overlapping of previous set of sequences is avoided throughout the process [7].

## 3.7 Multi-Objective Genetic Algorithm NSGA-II

Non-dominated Sorting Genetic Algorithm II (NSGA-II) is a popular non-domination based genetic algorithm used for multi-objective optimization problems. It was developed by Professor K. Deb et al., as an improvement over the NSGA, which received a lot of criticism for its computational complexity and lack of elitism [10].

In NSGA-II, the population is initialized at first, as usual. Then, based on non-domination, the population is sorted into each front. The first one is a completely non-dominant set, the second is dominated by individuals in the first front only and the front goes so on. Individuals in every front receive rank (fitness) values, with the ones in the first front receiving a fitness value of 1, the ones in the second front a fitness value of 2 and so on. Along with the fitness values, a parameter called crowding distance is calculated for each individual. This parameter measures the proximity of an individual to its neighbors. It should be noted that large average crowding distance will result in a better diversity in the population [10].

In the next phase, parents are selected from the population, taking the rank and the crowding distance into account. The new population generates offspring from crossover and mutation operators. Then the same sorting procedure as above is implemented, based on non-domination and only the best $N$ individuals are selected, where $N$ is the population size [10].

# 4 Case Study

## 4.1 Overview

In this diploma thesis, our work is focused on a typical Post-Panamax container ship, able to carry 6,500 TEUs. The main objective is to optimize the model in order to achieve the following:

- minimization of the Required Freight Rate (RFR)
- maximization of the $\frac{zero\ ballast\ TEU\ capacity}{maximum\ TEU\ capacity}$ ratio
- minimization of the Energy Efficiency Design Index (EEDI)
- maximization of the $\frac{TEUs\ above\ the\ main\ deck}{TEUs\ below\ the\ main\ deck}$ ratio
- minimization of the overall resistance of the ship

Some of these objectives are related to each other. However, for the scope of this work, all of the above objectives are monitored throughout the whole process, in order to perform a more detailed study.

The diagram in figure 16 illustrates the workflow of the project.

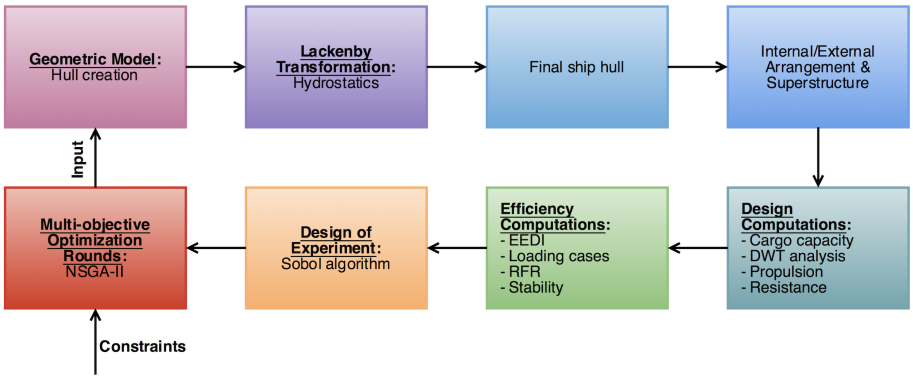


Figure 16: Thesis workflow

Since everything is built from square one, the first step is to gather all the necessary information regarding the specific container ship type. As far as the geometric model is concerned, the two main sources of information are a list of similar vessels obtained from a ship database, along with some data of an existing, similar sized container carrier. Several elements from these two sources, combined with essential information gathered from previous studies [16, 22] conducted in the Ship Design Laboratory of the National Technical

University of Athens and a pre-installed model of a container ship hull included in Friendship-Framework, contribute to the creation of the geometric model.

After the creation of the geometric model, all the necessary subsystems are defined. More specifically, systems that calculate the TEU capacity, the resistance and propulsion of the ship, as well as the stability and the loading cases investigated in this project are created. These systems provide the performance indicators that are used in the optimization phase.

The optimization procedure consists of two main phases. The first one deals with the exploration of the design space. For this purpose, the design of experiment is conducted, using the Sobol algorithm. Through this process, the investigation of the feasibility boundaries is achieved, allowing us to detect the trends of the design variables in regard to the optimization objectives. After the completion of this procedure, the formal optimization phase starts, using the NSGA-II algorithm. This phase is composed of two rounds, in order to ensure that the optimal solution is found.

After each formal optimization round, an evaluation of the results takes place using Microsoft Excel. More specifically, the results are extracted from Friendship-Framework and sorted, after their normalization, in order to ensure that the best solution is found following this process. Several scenarios are created, with each one focusing on a different objective, so as to observe how the generated variants react to different situations.

## 4.2 Phase 1: Hull Creation

The first step in our project is to create the parametric model of the container ship type under investigation. Below, the methods and the steps followed in order to achieve that are presented.

### 4.2.1 Data Collection

The only way to produce a sufficiently detailed model is to gather as much information as possible. It is of high importance to create a parametric model that approximates a real vessel, as this ensures that the results of the study will be accurate.

As mentioned previously, the main source of information is not only a list of similar ships obtained from a ship database, but also detailed data of a similar sized container carrier. The former information comes from an official database of merchant vessels and includes the main dimensions of the ships, their displacement and deadweight values, their service speed, as well as the power of their main engine. At this stage of our project, the main dimensions are required in order to create the hull of the parametric model. After the main dimensions are set, an adjustment of some of the form factors follows, in order to finalize the displacement of the ship.

The list of the similar ships is presented in table 4.

| **TEUs** | **$L_{OA}$ (m)** | **$L_{BP}$ (m)** | **Beam (m)** | **Draft (m)** | **Depth (m)** |
|---|---|---|---|---|---|
| 6,208 | 299.00 | 287.00 | 40.00 | 14.03 | 23.90 |
| 6,214 | 299.90 | 283.80 | 40.00 | 14.03 | 23.90 |
| 6,310 | 295.18 | 276.00 | 40.00 | 14.02 | 24.30 |
| 6,332 | 300.00 | 283.00 | 42.80 | 13.50 | 24.20 |
| 6,350 | 293.19 | 276.00 | 40.10 | 14.02 | 24.30 |
| 6,402 | 293.87 | 281.40 | 40.00 | 14.04 | 24.20 |
| 6,415 | 304.00 | 292.00 | 40.10 | 14.00 | 24.50 |
| 6,418 | 318.24 | 302.28 | 42.92 | 14.00 | 24.10 |
| 6,435 | 306.00 | 292.00 | 40.05 | 14.50 | 24.50 |
| 6,478 | 318.41 | 306.58 | 40.06 | 14.00 | 24.20 |
| 6,479 | 303.83 | 292.00 | 40.00 | 14.00 | 24.20 |
| 6,589 | 305.60 | 293.16 | 40.00 | 14.00 | 24.20 |
| 6,627 | 300.27 | 286.06 | 40.30 | 14.00 | 24.10 |
| 6,655 | 304.07 | 292.00 | 40.00 | 14.22 | 24.60 |
| 6,661 | 304.06 | 292.07 | 40.00 | 14.02 | 20.14 |
| 6,690 | 299.90 | 283.80 | 42.83 | 14.03 | 24.40 |
| 6,732 | 300.00 | 286.56 | 40.00 | 14.52 | 24.20 |
| 6,763 | 304.00 | 286.00 | 40.00 | 14.00 | 24.50 |
| 6,802 | 299.90 | 286.00 | 42.84 | 14.00 | 24.50 |

Table 4: Similar container ships

Apart from the list, detailed information (including several plans) of a 6,300 TEU container vessel is available. Important data is extracted from both the general arrangement plan and the midship section plan, in order to adjust several details in the stern and bow sections, as well as the radius of the midship section. More specifically, through these plans, parameters such as the radius and position of the propeller tube, the diameter of the propeller and the vertical position of the beginning of the transom are set. The result is the creation of a detailed container ship hull, which resembles as much as possible modern container vessels of this size.

### 4.2.2 Building the Parametric Model

After gathering all of the above information, the creation of the model within the Friendship-Framework environment begins. For this purpose, a pre-installed model of a container ship hull is used as a reference for our project. A ship's hull is a complex 3D object, composed by several points, curves and surfaces. Our model follows the same design process as the pre-installed one.

The program itself follows some specific principles regarding the design procedure. First and foremost, it should be noted that the models created in the

program are fully parametric ones, thus providing all the desired advantages described in paragraph 2.4. The whole concept of design is based on relations and dependencies between the elements used to create the final model. That means that a change made in one object is passed onto other elements that are related to the altered one.

Apart from the usual elements that define the 3D object –points, curves and surfaces– two additional features of the program are utilized to simplify the design process. These are the *parameters* and the *curve engines*. The main role of the parameters is to make the change of values in various objects (e.g. points) much simpler and faster. More specifically, instead of searching through numerous elements in order to make the desired change in the model, values of these elements are linked to parameters. Hence, adjusting the parameters' values, the properties of an object are automatically modified accordingly.

As far as the curve engines are concerned, their main role is to create complex surfaces. That can be achieved by relating the so-called feature definitions with curves and parameters. Feature definitions, or just features, is the software's approach for programming several commands, creating macros and subroutines that can be used in several ways, decreasing the time needed to complete tasks within the program. In this case, a cross section of a surface is defined using a feature. At this point, the feature refers to a 2D depiction of a section. Along a third axis, a number of parameterized curves can be defined, thus storing the distribution of the related parameters along this particular direction. The curve engine generates several cross sections, based on the information stored in the feature. The final result is the creation of the surface, using meta surface technology.

Although the overall procedure is highly automated, the designer ought to examine the outcome and make the necessary modifications in case of odd and unacceptable results.

### 4.2.3 Initial Geometric Model

The geometric model is divided in four main sections:

- main frame
- aft body
- fore body
- main deck

In order to sufficiently set up the model, several parameters are defined in this stage. The main parameters include the length between perpendiculars, beam, draft and depth of the ship. However, more parameters are created, in order to control various parts of the hull. In particular, the bilge height and width, the

stem and the stern overhang, the position of the propeller tube and the vertical start position of the transom are defined before creating the parametric model.

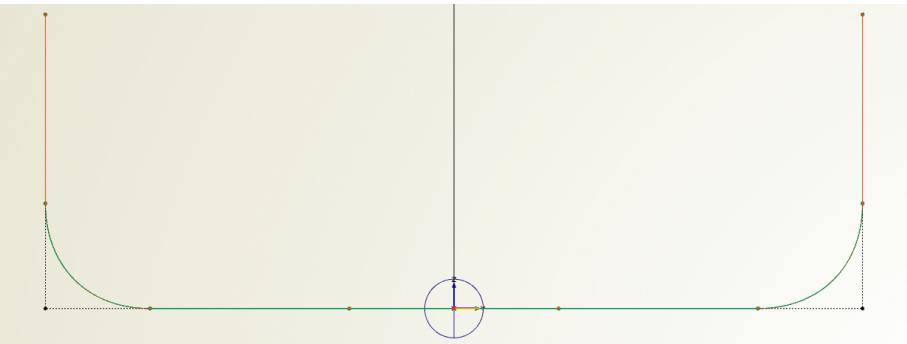

Figure 17: Main frame

**Main frame:** the main frame consists of the bottom part of the hull (represented by a straight horizontal line), the sides of the hull (represented by two straight vertical lines) and the bilge. Parameters such as the deadrise, the bilge height and width are used to easily control the overall outcome (figure 17).

**Aft body:** the aft body is composed by several functions. These include the stern bossing, the Center Plane Curve (CPC), the Flat of Bottom (FoB) and the Flat of Side (FoS). Using these functions, along with several curve engines and features, the corresponding surfaces are created. The result is the complete definition of the aft part of the container ship hull. The whole definition is based on the geometry of the main frame, which develops all the way to the transom (figure 18).

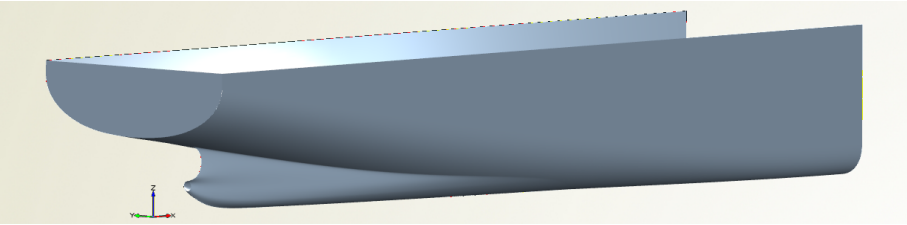

Figure 18: Aft body

**Fore body:** this part of the hull is more complex, therefore more functions are needed in order to design the forward part of the ship. As far

as the hull in general is concerned, functions like the Design Water Line (DWL), the FoB, the FoS, the Sectional Area Curve (SAC), the stem, as well as the flare at the bottom, deck and the DWL are used to create a detailed model of the hull. Apart from these functions, several curves are defined to create the bulb. More specifically, the elevation and the beam, among others, are curves that control the surface of the bulb. Of course, numerous parameters are used in this case, so as to control many details regarding the bulbous bow of the ship (figure 19).

**Main deck:** this part of the hull does not require any new elements to be defined, as through several features, two curves –the plane curve and the deck curve– are created and used as input to create the surface of the deck.

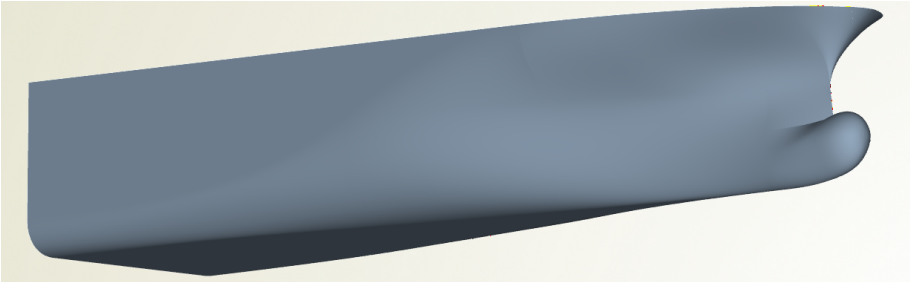

Figure 19: Fore body

## 4.3 Phase 2: Lackenby Transformation

After the completion of the initial geometric model, a hydrostatic calculation is performed, in order to determine the basic properties of the hull. This is achieved using an in-built hydrostatic connection. After running the connection, the SAC becomes available and is used as input in the Lackenby transformation. The ultimate purpose is to produce the final hull of the model by adjusting the prismatic coefficient $c_P$ and the Longitudinal Center of Buoyancy (LCB).

The Lackenby transformation is used in semi- and fully parametric designs to produce hull variants. The source is the base model and the modifications resulting in different products are based on the following:

- change in the prismatic coefficient
- change in the longitudinal center of buoyancy
- change in the forward position of the parallel mid body
- change in the aft position of the parallel mid body

Shift functions for both the aft and the fore bodies of the hull are used. These functions control the extent to which each section has to move, so as to achieve the desired changes in the SAC. In order to avoid several problems that might occur when quadratic polynomials are utilized, Friendship-Framework employs B-splines, thus enabling the model to control the regions of application, as well as the slopes at both ends of the shift functions [6].

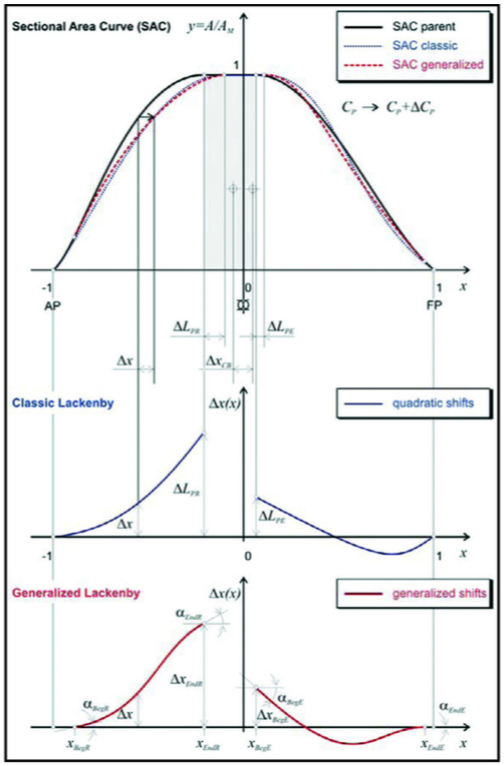


Figure 20: Classic Lackenby shift and new generalized Lackenby method

## 4.4 Phase 3: Cargo Arrangement and Superstructure

Although until this step, one hull has been created, from this point onwards, two slightly different ship models are designed. The only aspects that differentiate these two designs are the superstructure and, consequently, the internal and external arrangement of the cargo stowage area.

As far as the first variant (Model-1) is concerned, both the superstructure and the engine room are traditionally positioned at the aft part of the ship, as in most –if not all– ships belonging to the 6,000-7,000 TEU category. Therefore, the funnel is attached to the crew accommodation and the internal and external

cargo arrangement is split in two parts; a few bays are located aft of the superstructure, while the majority of them is located between the superstructure and the front collision bulkhead.

On the other hand, the second variant (Model-2) illustrates a more modern and radical approach, usually found in larger container carriers. In this case, a twin-isle arrangement is employed, with the engine room positioned at the aft part of the hull, whereas the biggest part of the superstructure, which includes the crew accommodation and the wheelhouse, is located at the fore part. The funnel and the stores area are located above the engine room, near the stern of the vessel. As a result, the cargo area is divided into three separate segments; one small area behind the engine room, a large one between the engine room and the accommodation, plus another small one in front of the accommodation.

The latter arrangement provides both advantages and disadvantages. A small decrease in cargo capacity can be observed, when the exact same hull is used. However, the *On deck/In hold* cargo ratio increases, improving the port efficiency aspect of the ship. When the optimization cycles begin, the results will indicate which of the two options is more profitable.

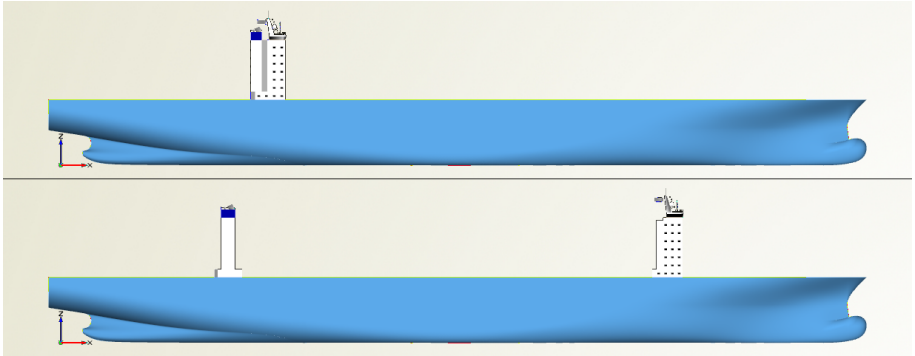

Figure 21: Traditional arrangement (above) vs. twin-isle arrangement (below)

### 4.4.1 Superstructure

Since the general arrangement plan of a similar, real container ship is available, the main dimensions of its superstructure are measured and then used as input in a built-in feature, which creates the deckhouse and the funnel of the ship. In particular, the length and the beam of the structure are defined in the feature, along with the number of different decks and the height of each one. During the design of the Model-1, featuring a superstructure where the accommodation and the funnel are joined, no modifications are needed, however, in Model-2, changes in the feature's code have to be made, so as to divide the funnel from the rest of the superstructure. The result in both cases is satisfactory, creating a typical container ship superstructure.

### 4.4.2 Cargo Storage

After the definition of the superstructure, the cargo arrangement both below and above the main deck follows. In both cases, an advanced feature is used, developed during previous studies at the Ship Design Laboratory of the National Technical University of Athens. The source code however is modified extensively, to improve the overall outcome. Hence, the process becomes much more automated, as during the optimization cycles, where multiple variants of the base model are created, even a slight change in some parameters results in different internal and external cargo arrangements.

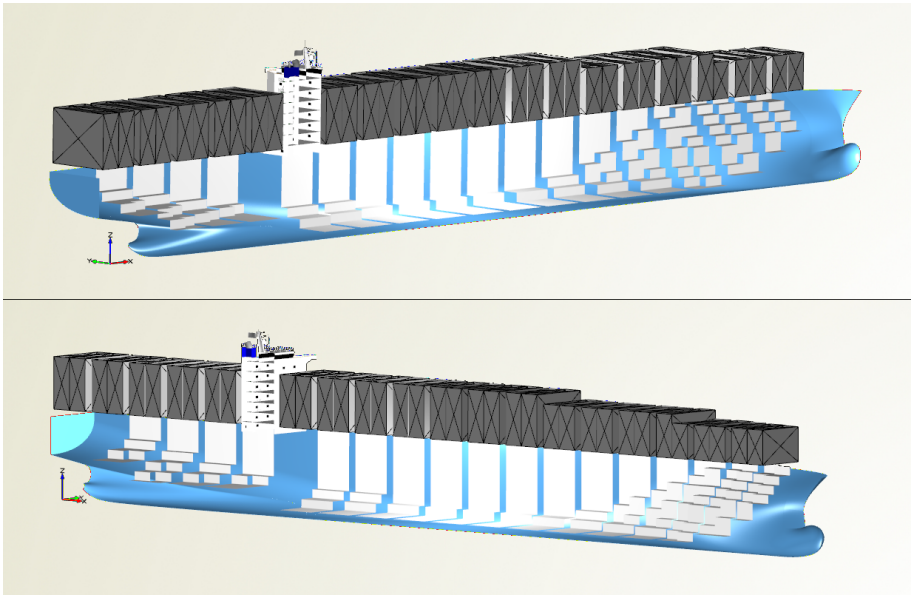

Figure 22: Model-1 cargo storage arrangement

The feature responsible for the development of the internal cargo storage arrangement creates the surface on which the TEUs are stored, while monitoring the distance of this inner surface from the outer cell of the hull. This distance in our model is represented by two design variables, the double side and the double bottom parameters, which vary throughout the multiple models created by the program during the optimization stage. Moreover, the cargo space behind the engine room is automatically designed to leave sufficient space for the propeller axis above the double bottom.

The feature responsible for the development of the cargo storage arrangement above the main deck is designed in such way, so as to take the visibility line rule into account. The visibility line is included in the IMO SOLAS regulations and it is of high importance to check the compliance in our case, since it is the container ship type that would most likely not comply with the rule, due to the high

stack of TEUs above the main deck. The feature automatically takes as input the visibility line defined in our model, thus preventing an excessive vertical stowage of containers above the main deck that would result in disobedience to the rule. In addition, the feature follows the deck line and monitors the available space along the beam of the ship, in order to define the proper amount of TEU rows above the main deck.

In both cases, several parameters are set, used to define the cargo space. More specifically, the bay spacing is defined, which determines the distance between each bay, so that various parts of the hull structure can be installed to support the payload. In addition, the dimensions of the standardized TEU unit are defined.

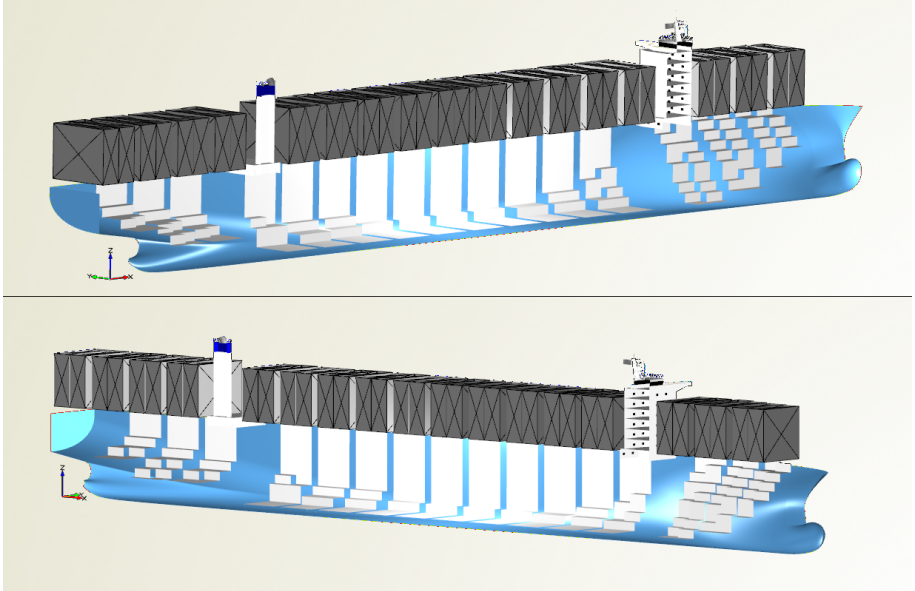

Figure 23: Model-2 cargo storage arrangement

The result of the computations performed within the features is limited to one bay length, including the spacing between the bays along the ship. The benefit of this tactic is that the maximum cargo storage capacity is ensured, taking advantage of as much of the available space as possible. Furthermore, it should be mentioned that the code of both features is appropriately programmed, so that the space dedicated to the engine room (in both variations of the base model) and the space below the accommodation (in the twin-isle variant) are left empty, as they should be reserved for the installation of the main engine and the allocation of various tanks.

## 4.5 Phase 4: Design Computations

This part of the project is one of the most time-consuming ones, since all of the subsystems that are responsible for the computations regarding the cargo capacity, the deadweight analysis, the propulsion and resistance of the ship are built at this stage. The computations described below are identical in both variants of the model.

### 4.5.1 Cargo Capacity

After the hull of the model is completed, including the superstructure and the internal and external cargo storage arrangement, it is possible to continue with the calculation of the actual TEU capacity of the ship. To accomplish this, two features are created, one for the capacity calculation below the main deck and another one for the capacity calculation above the main deck. Apart from the actual measurement of the TEUs below and above the main deck, these features are designed to calculate vertical and longitudinal moments, as well as vertical and longitudinal centers of gravity, which are used as input in other computations.

### 4.5.2 Hydrostatics

Before proceeding to the remaining computations, a hydrostatic calculation has to be run first. Earlier, the same action took place, however, that was before the final hull was generated. Since its characteristics have changed after the last hydrostatic calculation, a new run is necessary for the following steps of the project. The methodology and tools used to get the results are the same as mentioned earlier in paragraph 4.3.

### 4.5.3 Resistance

Another essential element needed for the design computations is the resistance of the ship. For this purpose, a popular method for the prediction and calculation of the resistance is used, namely the Holtrop and Mennen method [13]. Since this method requires numerous calculations for various aspects of the overall resistance, a custom feature is developed, requiring a limited amount of input, so as to be as straightforward as possible.

According to Holtrop and Mennen, the total resistance can be subdivided into:

$$R_{Total} = R_F \cdot (1 + k_1) + R_{App} + R_W + R_B + R_{Tr} + R_A$$

where:

- $R_F$: frictional resistance according to the ITTC-1957 friction formula
- $1 + k_1$: form factor describing the viscous resistance of the hull form in relation to $R_F$
- $R_{App}$: resistance of appendages
- $R_W$: wave-making and wave-breaking resistance
- $R_B$: additional pressure resistance of bulbous bow near the water surface
- $R_{Tr}$: additional pressure resistance of immersed transom stern
- $R_A$: model-ship correlation resistance

Each one of the different resistance categories can be calculated through a series of formulas that differ, depending on several parameters and ratios. Within the custom feature, subroutines responsible for the calculation of form factors, like $k_1$ or the Froude and Reynolds numbers are included, in order to create a seamless computation procedure. However, specific input has to be defined first.

A critical parameter in this computation is the vessel's speed. In order to set the value of this parameter, a look into the current trends takes place first. In the past few years, the operational speed of merchant vessels, especially container ships, has declined significantly, creating the slow steaming trend, described in paragraph 1.5. Taking into account this common practice, the service speed of our model is set to 20 Knots.

Another mandatory parameter for the resistance calculation is the wetted surface of the hull. This can be calculated using a simple feature that takes as input the hull's sections and the draft of the ship.

Further elements needed for the calculations, such as the waterline length, the beam and hydrostatic data, are already known from previous stages of this project.

### 4.5.4 Propulsion

This stage is closely related to the previous one. The Holtrop and Mennen method includes formulas for the calculation of the Effective Horsepower (EHP) and the Shaft Horsepower (SHP). First of all, the EHP is calculated, since the total resistance and the speed of the vessel are known, from the following formula:

$$EHP = R_{Total} \cdot V_S$$

Having already found the necessary propulsion and efficiency factors from the resistance computations, the calculation of SHP is now possible, using the following formula:

$$SHP = \frac{EHP}{\eta_R \cdot \eta_0 \cdot \eta_S \cdot \frac{1-t}{1-w}}$$

The final result is increased by a small percentage, in order to include a bad sea state as well as a fouled hull condition.

Moreover, the estimation of the auxiliary power follows, using the methodology described in [19]. More specifically, the auxiliary power is calculated based on the following formula:

$$P_{B_{Aux}} = 100 + 0.55 \cdot P_{B_{ME}}^{0.7}$$

The outcome is modified, in order to match the final required value, according to existing formulas.

Finally, the fuel consumption is calculated, based on existing methods. The Specific Fuel Oil Consumption (SFOC) of the main engine is set to 175 g/KWh, while the SFOC of the auxiliary engines is set to 185 g/KWh.

### 4.5.5 Lightship

Several methods are used to calculate our model's lightship weight and its center of gravity, as described in [19]. The selection of the methods, described below, is based on the available data.

Even though the chosen methods provide an approximation of the desired values, several attempts are made in order to achieve the most accurate result. In particular, several parameters needed for the computations derive from detailed calculations performed by Friendship-Framework, such as the volume of the hull. Moreover, the same calculation procedures are applied to the reference 6,300 TEU container ship. The purpose of this action is to calculate correction factors that will improve the final outcome of our model's lightship computation, since the actual lightship weight and center of gravity of the reference ship are known.

First of all, the calculations for the reference ship are performed in Microsoft Excel. Afterwards, a custom feature is developed in Friendship-Framework, including the same techniques used in the first step, so as to determine the model's lightship characteristics. It should be noted that the feature takes as input the data from the calculations performed in Microsoft Excel, so as to include the correction factors in the model's lightship computation.

The lightship weight can be subdivided into:

$$LS = W_{ST} + W_{OT} + W_M$$

where:

- $W_{ST}$: steel weight, including the weight of the hull, the superstructure and the hatches
- $W_{OT}$: outfitting weight, including the weight of the ship's equipment and the lashes
- $W_M$: machinery weight

**Hull weight calculation:** the technique used in this case is the Schneekluth method. The information needed includes the hull volume, the ship's main dimensions –length, beam, draft and depth– as well as several form factors. As mentioned above, some parameters, such as the volume of our model's hull, are calculated from the software itself, for a more detailed measurement.

**Superstructure weight calculation:** the Müller-Koster method is utilized, in order to calculate the superstructure weight. The area of each deck is measured, either using the general arrangement plan –in case of the reference ship– or by integrating the feature responsible for the creation of the deckhouse and the funnel, along with the necessary commands, in the lightship feature –in case of our model.

**Hatches weight calculation:** this weight group is calculated using the Schneekluth method.

**Outfitting weight calculation:** the formula described in [19] uses as input the length and the beam of the ship and delivers the weight of equipment of the accommodation and overall ship arrangements.

**Lashes weight calculation:** the weight of lashes is calculated using a simple formula, also described in [19].

**Machinery weight calculation:** the final weight group is calculated, based on the main engine's power.

As far as the longitudinal and vertical centers of gravity are concerned, they also calculated using formulas described in [19] and will be used later in the trim and stability calculations. Their values are corrected accordingly, based on the correction factors calculated above.

### 4.5.6 Deadweight Analysis

During this stage, the analysis of the deadweight takes place. As the trim and stability booklet of an already built, similar sized container vessel is available, an overview of the various weight categories helps us understand how weights like crew, stores, oil, fresh water and provisions are distributed throughout the ship. The weight calculations are based on empirical methods used mostly in the early stages of ship design. For this purpose, some elements have to be outlined, on which most of the related calculations are based.

First of all, the total number of crew members is defined. Taking the reference ship into account, it seems that 30 is a sufficient number for the crew complement of our model. As far as the range of the vessel is concerned, a hypothetical operational profile has to be set. As mentioned in paragraph 1.6.2, the route selected for our case is the India-North America one, which is mostly operated by container ships in the 6,000-7,000 TEU category. Searching through the internet, a real route between these regions was found and was selected for our model. The ports of call, along with some additional information can be found in tables 5 and 6, illustrating the operational profile of our container ship model.

| **Port** | **Time at port (h)** | **Distance (nm)** |
|---|---|---|
| Jawaharlal Nehru, IND | 36 | – |
| Salalah, OMN | 12 | 1,143 |
| Suez Canal, EGY | 15 | 2,052 |
| Algeciras, ESP | 12 | 2,326 |
| Newark, NJ, USA | 15 | 3,515 |
| Charleston, SC, USA | 10 | 780 |
| Savannah, GA, USA | 10 | 91 |
| Houston, TX, USA | – | 1,554 |

Table 5: Trade route (West-bound)

| **Port** | **Time at port (h)** | **Distance (nm)** |
|---|---|---|
| Houston, TX, USA | 23 | – |
| Savannah, GA, USA | 10 | 1,563 |
| Norfolk, VA, USA | 10 | 588 |
| Newark, NJ, USA | 13 | 347 |
| Algeciras, ESP | 18 | 3,557 |
| Suez Canal, EGY | 22 | 2,326 |
| Djibouti, DJI | 12 | 1,420 |
| Salalah, OMN | 9.5 | 770 |
| Jebel Ali Dubai, ARE | 12 | 999 |
| Port Qasim, PAK | 20 | 746 |
| Pipavav, IND | 15.5 | 445 |
| Jawaharlal Nehru, IND | – | 189 |

Table 6: Trade route (East-bound)

After evaluating not only the distance between each port, but also the transit time required in the real timetable found on the internet, it is reckoned that our model can attain a decent voyage time frame while cruising at 20 Knots. Furthermore, by examining the data found in tables 5 and 6, the average time of the ship staying at port for cargo loading/unloading purposes can be calculated. Taking into account the overall route distance in nautical miles, as well as the

operational speed of the vessel, the information essential for the next steps can be found at table 7.

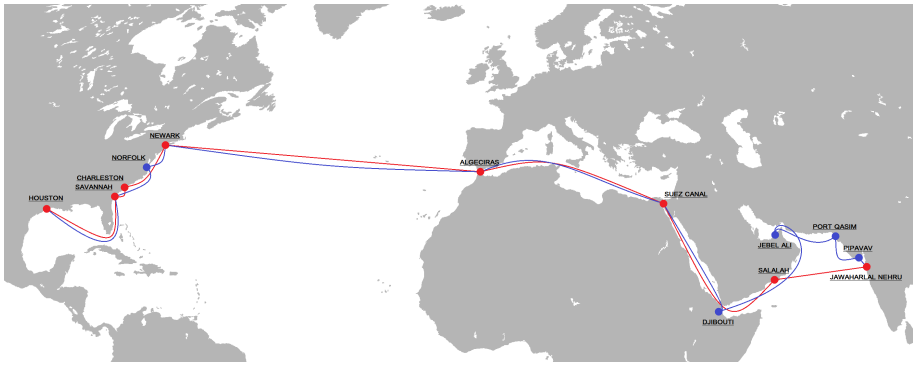


Figure 24: Route map

| | |
|---|---|
| **Operational speed (Knots)** | 20 |
| **Transit time (days)** | 63 |
| **One-way route distance (nm)** | 12,205 |
| **Average time at port (h)** | 15.3 |

Table 7: Operational profile

At this point, all the necessary input data are known. Therefore, it is possible to calculate the deadweight. The latter can be subdivided into:

$$DWT = W_{DO}+W_{FO}+W_{LO}+W_{Crew}+W_{FW}+W_{Payload}+W_{Provisions}+W_{Stores}$$

where:

- $W_{DO}$: diesel oil weight. It depends on the power and the SFOC of the auxiliary engines, as well as the range of the ship
- $W_{FO}$: fuel oil weight. It depends on the power and the SFOC of the main engine, as well as the range of the ship
- $W_{LO}$: lube oil weight. It is reckoned as a small percentage of the combined fuel and diesel oil weight
- $W_{Crew}$: weight of the crew members, as well as their belongings
- $W_{FW}$: fresh water weight, depending on the number of the crew, as well as the range of the ship

- $W_{Payload}$: payload weight, already calculated in the cargo capacity feature
- $W_{Provisions}$: provisions weight. It depends on the number of the crew and the range of the ship
- $W_{Stores}$: stores weight. Its value is based on the corresponding value found in the trim and stability booklet of the reference ship, since no empirical formula exists for the calculation of this weight group

Along with the weight computations, the longitudinal and vertical centers of gravity of each group are calculated, in order to be used as input in the trim and stability calculations.

### 4.5.7 Tanks Allocation

The final design computation that has to be performed is the allocation of the necessary tanks in the model's hull. The tanks created in the model are mainly the ones containing the fuel, diesel and lube oil, as well as the water ballast tanks.

The former category is created by specifying the position of the tanks by generating the necessary sections along the hull. Then, a feature calculates the volume of the tanks and checks if the result is greater than or equal to the required volume, which is defined by the overall weight of the oil consumables, calculated during the deadweight analysis.

As far as the water ballast tanks are concerned, the situation is slightly different. Four main tank groups are created:

- Aft Peak Tank (APT)
- bilge tanks
- double bottom tanks
- Fore Peak Tank (FPT)

The APT and FPT are produced effortlessly. First, the necessary sections of the hull in the stern and the stem overhang areas are generated. Then the height, to which the tanks extend, is defined. Finally, two hydrostatic computations are run, in order to obtain the desired values, namely the volume and the longitudinal and vertical centers of gravity of the tanks.

In the case of the bilge and the double bottom tanks, the same method is utilized –section generation and hydrostatic computation runs. However, several small tanks are created –one for each corresponding cargo hold– instead of a big one, so that a more precise loading condition can be created at a later stage.

## 4.6 Phase 5: Efficiency Computations

Now that the model is properly defined, the efficiency computations can commence. These calculations produce the required performance indicators that will be used in the optimization process. The computations described below use information and data derived from the design computations and are identical in both variants of the model.

### 4.6.1 Energy Efficiency Design Index

The Energy Efficiency Design Index (EEDI) calculates a vessel's energy efficiency, based on a complex formula. The ship's emissions, its capacity and speed are taken into account. The lower EEDI, the more efficient the ship. Ships are required to meet a minimum energy efficiency requirement [11].

The EEDI assesses the energy consumption of the vessel at normal seafaring conditions, taking into account the energy required for propulsion and the hotel load for the crew. However, energy consumed for cargo maintenance and for maneuvering or ballasting is not considered (figure 25).

The required EEDI represents a minimum energy efficiency requirement for new ships, depending on ship type and size. This began with a baseline value in 2013 and is raised successively in three steps until 2025. The baseline for the required EEDI is calculated from the EEDI of vessels built after the millennium. In our case, the requirements referring to the container ship type are used to calculate the required EEDI.

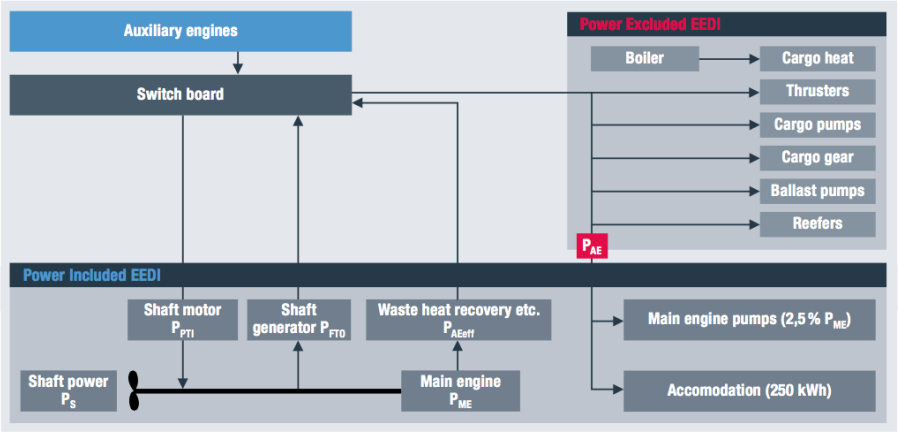


Figure 25: Energy consumption

According to [12], the formula for the calculation of the required EEDI is the following:

$$EEDI_{Req} = a \cdot b^{-c} \cdot \left(1 - \frac{x}{100}\right)$$

where:

- $a$: for container ships, $a$ equals to 174.22
- $b$: for container ships, $b$ stands for the deadweight of the ship
- $c$: for container ships, $c$ equals to 0.201
- $x$: reduction factor. At first it is equal to zero, but after each five years the number increases by ten

The attained EEDI calculation can be roughly described by the following formula:

$$EEDI_{Att} = \frac{(Ship\ emissions) - (Efficiency\ technologies)}{(Transport\ work)}$$

The ship emissions include the main engine, auxiliary engines, as well as the shaft generators and motors emissions. The efficiency technologies include several arrangements, modifications or installations to the hull or the propulsion system, which result in increased efficiency (figure 26). Hence, these technologies should be taken into account in the calculation of the attained EEDI as a reduction factor. Finally, the transport work takes into account the cargo loading of the ship, as well as its service speed.

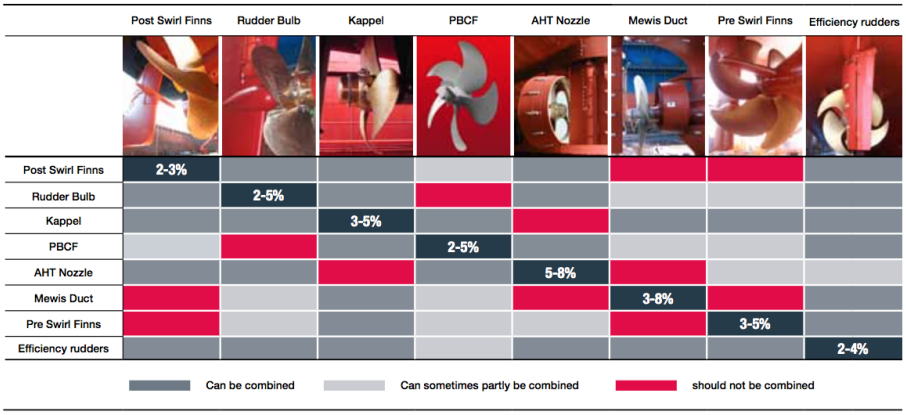


Figure 26: Efficiency technologies

The formula for the calculation of the main engine emissions according to [12] can be found below:

$$\left(\prod f_j\right) \cdot \left(\sum P_{ME} \cdot C_{F_{ME}} \cdot SFOC_{ME}\right)$$

where:

- $f_j$: correction factor to account for ship specific design elements. If no ship specific design elements are installed, the factor is set to one
- $P_{ME}$: 75% of MCR of the main engine
- $C_{F_{ME}}$: conversion factor fuel oil to $CO_2$
- $SFOC_{ME}$: specific fuel oil consumption of the main engine at 75% MCR

The formula for the calculation of the auxiliary engines emissions according to [12] can be found below:

$$P_{AE} \cdot C_{F_{AE}} \cdot SFOC_{AE}$$

where:

- $P_{AE}$: auxiliary power demanded for the operation of the main engine
- $C_{F_{AE}}$: conversion factor fuel oil to $CO_2$
- $SFOC_{AE}$: specific fuel oil consumption of the auxiliary engines

The formula for the calculation of the transport work according to [12] can be found below:

$$f_i \cdot f_l \cdot f_w \cdot f_c \cdot Capacity \cdot V_{Ref}$$

where:

- $f_i$: correction factor to account for ship specific design elements which reduce the capacity
- $f_l$: correction factor to account for general cargo ships
- $f_w$: correction factor to account the decrease of speed in representative sea conditions
- $f_c$: cubic capacity correction factor for chemical tankers
- $Capacity$: for container ships, capacity is defined as 70% of the deadweight at summer load draft
- $V_{Ref}$: reference speed of the ship at EEDI conditions

Both the required and the attained EEDI values are calculated in our model through a custom feature that uses the necessary input, either from rules and regulations, such as [12], or from calculations performed in other computations within our model. Apart from the actual values, a *Attained/Required* ratio is calculated to be used later as a performance indicator.

### 4.6.2 Required Freight Rate

One of the most important efficiency computations is the calculation of the Required Freight Rate (RFR). For this purpose, another custom feature is developed, which includes a detailed economic model for our container ship, taking into account several parameters.

More precisely, according to the model used in our case, the RFR calculation is based on the following formula:

$$RFR = \frac{(Total\ annual\ cost)}{(Round\ trips) \cdot (TEUs)}$$

The total annual cost can be divided into the following subcategories:

- capital cost
- fuel cost
- operation cost

The capital cost is mainly based on the building costs of the ship. It is calculated from the following formula:

$$\left[\left(m_{St_{Ref}} - m_{St}\right) \cdot C_{St} + (Building\ cost)\right] \cdot (1+d)^t \cdot \frac{d}{(1+d)^{t-1}}$$

where:

- $m_{St_{Ref}}$: reference steel mass
- $m_{St}$: actual steel mass
- $C_{St}$: cost of steel
- $d$: discount rate
- $t$: operation time of the ship. In our case, we assume the vessel will be operating for 25 years
- *Building cost*: overall cost for the construction of the ship. It is divided into four subcategories; hull construction, machinery, pipes and other components cost. The formula for the calculation of the building cost is the following:

$$1.7618 \cdot [150.7 \cdot L \cdot B \cdot D + 216 \cdot P_{B_{ME}} + 200 \cdot P_{B_{Aux}} + 144 \cdot (P_{B_{ME}} + P_{B_{Aux}})]$$

where:

- $L$: length of the ship
- $B$: beam of the ship
- $D$: depth of the ship
- $P_{B_{ME}}$: main engine power
- $P_{B_{Aux}}$: auxiliary engines power

The fuel cost is relative to the fuel consumed during two different states; underway and while located at ports. In each case, the load of the main and auxiliary engines varies. Moreover, there is a difference between the cost of heavy fuel and the diesel oil. According to [3], the oil prices are the following:

| **Location** | **IFO380 ($)** | **MGO ($)** |
|---|---|---|
| Singapore | 304.00 | 514.00 |
| Rotterdam | 284.50 | 522.50 |
| Houston | 276.00 | 593.00 |
| Fujairah | 330.00 | 850.00 |

Table 8: Oil prices (March 2015)

The formula used to calculate the fuel cost while underway is the following:

$$P_{B_{ME}} \cdot L_{ME} \cdot SFOC_{ME} \cdot \frac{Route}{V_S} \cdot C_{HFO} \cdot 10^{-6}$$

On the other hand, the calculation of the fuel cost when the ship stays at port is based on the following formula:

$$(P_{B_{ME}} \cdot L_{ME} \cdot SFOC_{ME} \cdot C_{HFO} + P_{B_{Aux}} \cdot L_{Aux} \cdot SFOC_{Aux} \cdot C_{MGO}) \cdot t_P \cdot 10^{-6}$$

where:

- $P_{B_{ME}}$: main engine power
- $L_{ME}$: main engine load
- $SFOC_{ME}$: specific fuel oil consumption of the main engine
- $C_{HFO}$: fuel oil cost
- $P_{B_{Aux}}$: auxiliary engines power
- $L_{Aux}$: auxiliary engines load
- $SFOC_{Aux}$: specific fuel oil consumption of the auxiliary engines

- $C_{MGO}$: diesel oil cost
- $t_P$: overall time during which the ship is located at port

After the fuel cost for one route is calculated, the annual cost is found by multiplying the former value with the number of round trips taken per year.

Finally, the operation cost consists of the following expenses:

- crew cost
- stores cost
- maintenance cost
- insurance cost
- administration cost
- port cost

The calculation of the above values is based on numerical coefficients and the main dimensions of the ship.

### 4.6.3 Trim and Stability

One of the most important computations in our model is the trim and stability calculations. This step is required for the implementation of the next one, namely the generation of the loading cases. Within the current computation, essential parameters are determined, such as the values of the GZ-$\varphi$ curve, the trim of the ship, as well as the KG and LCG values that will be used in the loading cases computation.

Normally, an external software would be employed at this stage, as complex computations need to be performed to get the desired results. However, in this case, a custom feature developed during previous studies [22] at the Ship Design Laboratory of the National Technical University of Athens is used instead.

The program creates the GZ-$\varphi$ curve, by running several hydrostatic computations at various heeling angle values. Moreover, the code incorporates the stability criteria as appointed by the IMO and a check is performed, to ensure that the model complies with these regulations. If the latter is not the case, the KG and LCG values are modified and the whole process restarts, until the criteria are met.

The stability criteria that should be met in our model, are the following:

- initial GM value needs to be 0.15 m or higher

- the area below the GZ-φ curve between $0^o$-$30^o$ needs to be 0.055 m-rad or higher
- the area below the GZ-φ curve between $0^o$-$40^o$ needs to be 0.09 m-rad or higher
- the area below the GZ-φ curve between $30^o$-$40^o$ needs to be 0.03 m-rad or higher
- maximum GZ value should occur at a heeling angle of $30^o$ or higher
- maximum GZ value should be 0.2 m or higher
- trim value at the full load departure condition should not exceed 0.5% of $L_{BP}$

### 4.6.4 Loading Cases

The last efficiency computation required is the generation of the loading conditions. Two different conditions are investigated in this project. Both of them require several parameters and elements determined in previous stages. These parameters consist of various weight groups, as well as their longitudinal and vertical centers gravity which represent the data used as input in this computation. These groups include the displacement, the lightship, the payload, divided into the below and above main deck TEUs, the consumables and the water ballast.

As far as the water ballast is concerned, several groups are defined, in order to fill only the minimum required space with sea water. The groups created are the following:

- aft peak tank
- fore peak tank
- double bottom tanks
- bilge tanks
- fore peak tank, along with no. 1 water ballast tank

One or more of the above groups are used whenever the stability or the trim conditions are not satisfied.

The conditions investigated in this project are the following:

- maximum TEU condition
- zero ballast condition

As far as the former condition is concerned, the main objective is to max out the cargo capacity. However, that affects the homogeneous weight per container. Water ballast is loaded for trimming purposes.

On the other hand, the latter condition is defined as a condition where no water ballast is loaded for stability reasons. Hence, the number of TEUs aboard the ship is restricted due to limitations described in the trim and stability computation stage. The objective in this case is the maximization of the number of loaded TEUs.

## 4.7 Phase 6: Design of Experiment

Before proceeding to the formal optimization rounds, a Design of Experiment (DoE) is conducted first. This process will allow us to examine the design space and the response of several parameters to the change of the model's main characteristics. The algorithm utilized in this phase is the Sobol algorithm. The selection of the specific algorithm is described in paragraph 3.6. Through the DoE, the investigation of the feasibility boundaries is ultimately achieved, allowing us to detect the trends of the design variables in regard to the optimization objectives.

In our case, the design engine is assigned to create 500 variants of our model. Since two versions –Model-1 and Model-2– are built, the DoE is conducted twice, once for each variant. In order to start the DoE, the design variables and the constraints need to be defined first. At this point, no objectives need to be determined, since only the feasibility boundaries are investigated. However, several parameters are evaluated through this process, including the main dimensions of the ship, its form factors, the wetted surface of the hull, the TEU capacity, as well as the RFR and the EEDI.

The design variables, including both the base model's and the extreme values, are presented in table 9.

| **Design variable** | **Min. value** | **Base model value** | **Max. value** |
|---|---|---|---|
| Bays | 18 | 19 | 20 |
| Rows | 14 | 16 | 18 |
| Tiers in hold | 8 | 9 | 10 |
| Tiers on deck | 6 | 6 | 8 |
| Double bottom (m) | 1.9 | 2.0 | 2.6 |
| Double side (m) | 2.0 | 2.1 | 3.0 |
| $\Delta c_P$ | -0.06000 | -0.01125 | 0.06000 |
| $\Delta$LCB | -0.02600 | -0.00375 | 0.02600 |

Table 9: Design variables

Taking a closer look at table 9, it can be understood that the main dimensions of the ship are actually closely related to the design variables in this project.

In other words, each of the main dimensions –length, breadth, depth– derives from the number of bays, rows and tiers respectively. In our model, the engine room length is a multiple of the number of bays. Since the length between perpendiculars consists of the engine room and the cargo area –which is also a multiple of the number of bays– it is clear that the length of the ship can be described by the amount of the bays.

Moreover, the number of rows, along with the value of the double side, describes the beam of the ship. As far as the depth is concerned, its value derives from the double bottom clearance and the number of tiers below the main deck. The only parameter that belongs to the main dimensions group and is not included in the design variables is the draft of the ship. This value is set as a fixed number from the beginning of the project, taking into account the draft values of both the similar ships (table 4) and the 6,300 TEU reference vessel.

The constraints are set, so as to have a clear view of which of the subsequent variants violate several criteria that must be met. For instance, various stability criteria are included in the constraints. In case one of them is violated, the variant cannot be considered as a satisfactory alternative to the base model, even if some of the objectives are improved. In table 10, all of the constraints that are set in our model, are presented.

| **Constraint** | **Value** |
|---|---|
| *Attained/Required* EEDI ratio | $\leq 1$ |
| GZ area between $0^o$-$30^o$ | $\geq 0.055$ m-rad |
| GZ area between $0^o$-$40^o$ | $\geq 0.09$ m-rad |
| GZ area between $30^o$-$40^o$ | $\geq 0.03$ m-rad |
| Initial GM | $\geq 0.15$ m |
| Angle at $GZ_{max}$ | $\geq 30^o$ |
| $GZ_{max}$ value | $\geq 0.2$ m |
| Homogeneous weight per TEU (Max. capacity) | $\geq 6$ t |
| Homogeneous weight per TEU (Z.B. capacity) | $\geq 7$ t |
| Trim at FLD | $\leq 0.5\%$ $L_{BP}$ |

Table 10: Constraints

When the run ends, a wide variety of results are displayed, which inform us about the design space. It is worth mentioning that the TEU capacity of the model is not constrained, thus the maximum and minimum number of TEU capacity of the variants is not limited to the 6,000-7,000 area. In section 5 several diagrams are presented, illustrating how our model responds to the modification of its design variables.

## 4.8 Phase 7: Multi-Objective Optimization Rounds

The last step to complete our work is to run the formal optimization rounds. To achieve that, the NSGA-II algorithm is utilized, which produces satisfactory

results. In order to ensure that the optimal design is found, two rounds are run for every version of our model. In particular, during each run, five generations are created, having a population size of fifty, each.

Since the DoE provided fairly decent results, the same baseline model is used for the first round. The best variant produced during the first round is then used as the baseline model for the second and final optimization round.

In addition, the design variable extents remain the same, as the design space seems to be well defined. As far as the constraints are concerned, apart from the ones defined in the previous stage (table 10), two additional constraints are set to delimit the maximum TEU capacity of the ship variants. Therefore, an upper and lower limit is defined, as described in table 11.

| | |
|---|---|
| **Min. TEU capacity** | 6,000 |
| **Max. TEU capacity** | 7,000 |

Table 11: Additional constraints

Unlike the previous phase, in this case, apart from the evaluation of various parameters of the model, several objectives are defined. These are the main objectives that are mentioned at the beginning of this section:

- minimization of the Required Freight Rate (RFR)
- maximization of the $\frac{zero\ ballast\ TEU\ capacity}{maximum\ TEU\ capacity}$ ratio
- minimization of the Energy Efficiency Design Index (EEDI)
- maximization of the $\frac{TEUs\ above\ the\ main\ deck}{TEUs\ below\ the\ main\ deck}$ ratio
- minimization of the overall resistance of the ship

The evaluation of the results of both optimization rounds is based on the above objectives, as well as on some utility functions. The objectives are in fact existing parameters of the model which are monitored through the optimization process and their minimization is pursued by the algorithm. Hence, the objectives which need to be maximized, such as the TEU capacity in the zero ballast condition, are changed to differences from a higher value. As a result, the minimization of that difference leads to the maximization of the objective.

As mentioned in section 3, the results of a multi-disciplinary optimization procedure might not provide a straightforward solution to a problem. Although the algorithm used for the optimization provides some improved designs, it is not always clear which one is the best. For this reason, several case scenarios are created, so as to determine the optimal of the top solutions to the problem.

In our project, three distinctive scenarios are defined, where the significance of each objective is acknowledged differently, as shown in table 12.

After obtaining the results of each run, the data is normalized according to the scenarios. Afterwards, the normalized data is ranked, in order to find the optimal variant of our model. In most cases, a specific variant dominates in every scenario. In this case, the selection of the optimal solution is unambiguous. However, if the process does not lead to a clear-cut result, the decision lies with the designer. As far as our project is concerned, the normalization of the data provided concrete results.

| **Objective** | **Scenario 1** | **Scenario 2** | **Scenario 3** |
|---|---|---|---|
| RFR | 20% | 50% | 20% |
| Capacity ratio | 20% | 20% | 50% |
| EEDI | 20% | 10% | 10% |
| Stowage ratio | 20% | 10% | 10% |
| Total ship resistance | 20% | 10% | 10% |

Table 12: Case scenarios

The above procedure is utilized both after the end of the first optimization run, in order to determine the new, improved baseline model for the second run, and after the end of the final run, so as to determine the optimal final design.

# 5 Results

## 5.1 Introduction

In section 4 the development of the model was thoroughly presented and a detailed explanation of each phase took place. In the current section, the results of our work are displayed, demonstrating how the design optimization worked, as well as how much our base model was improved and how the objectives reacted to the change of the design variables. Moreover, a comparison of the optimal variant with existing similar container ships is made, in order to illustrate the differences in their main characteristics.

## 5.2 Base Model

Before proceeding to the actual results, some essential information about the base model is presented, in order to have a clear perspective of the initial hull. The principal data of the base model can be found in table 13.

| | | | |
|---|---|---|---|
| **$L_{BP}$ (m)** | 290.76 | **Bays** | 19 |
| **Beam (m)** | 39.01 | **Rows** | 16 |
| **Depth (m)** | 24.28 | **Tiers in hold** | 9 |
| $c_B$ | 0.6994 | **Tiers on deck** | 6 |
| $c_M$ | 0.9821 | **Double bottom (m)** | 2.00 |
| $c_P$ | 0.7121 | **Double side (m)** | 2.10 |
| **Displacement (t)** | 113,852 | **$\Delta c_P$** | -0.01125 |
| **Wetted surface ($m^2$)** | 15,104 | **$\Delta$LCB** | -0.00375 |

Table 13: Base model principal data

| **Objective** | **Model-1** | **Model-2** |
|---|---|---|
| RFR ($/TEU) | 634.68 | 644.10 |
| Capacity ratio | 0.5193 | 0.5292 |
| EEDI | 9.21 | 9.20 |
| Stowage ratio | 0.9451 | 1.0145 |
| Total ship resistance (KN) | 1,635 | 1,635 |

Table 14: Base model objective values

The data in table 13 refers to both initial model variants. However, other elements, like the lightship or the TEU capacity, slightly vary between these two variants. It is worth mentioning though that this does not affect the optimization process, as these elements will fluctuate much more during the optimization rounds.

## 5.3 Design of Experiment

During the Design of Experiment (DoE) phase, the response of our model to the variation of the design variables becomes fathomable. Friendship-Framework provides us with useful data, including various diagrams that illustrate this response. By observing these diagrams, we can evaluate the design space, as well as how the initial model can be improved.

In figure 27, the correlation between the maximum number of TEUs that can be stored aboard the ship and the number of bays is presented. It can be understood that the higher the number of the bays, the higher the maximum TEU capacity of the ship. However, since the number of rows and tiers above and below the main deck can also vary, it is clear that in each case –18, 19 or 20 bays– the TEU capacity can range between 5,000 and 10,000 TEUs.

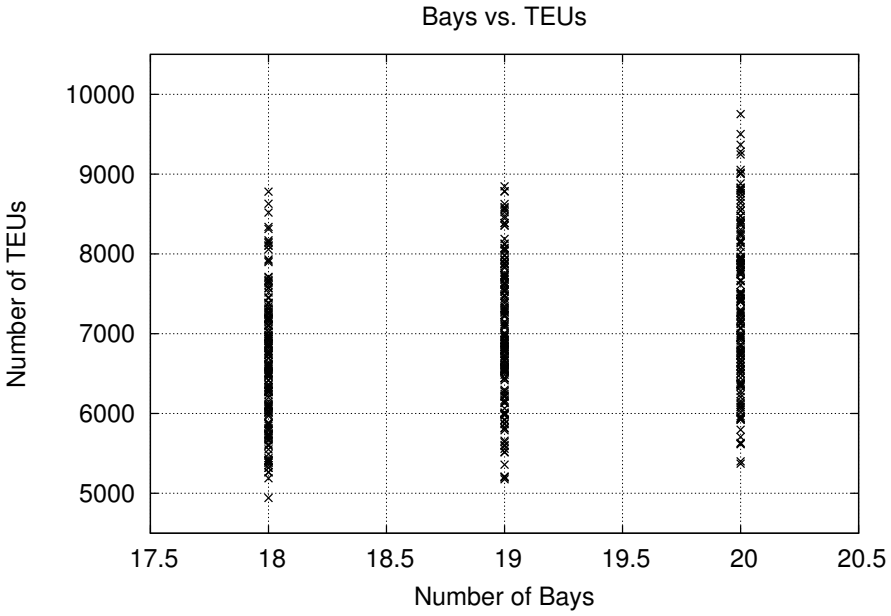


Figure 27: DoE – Bays vs. TEUs

In figure 28, the cargo capacity versus the number of rows is displayed. Here the results are more coherent, since there is an obvious increase in the TEU capacity, as the number of rows increments. More precisely, in the case of 14 rows, the maximum TEU capacity that can be reached is 7,500 TEUs. On the other hand, when the model features 18 rows, the cargo capacity can vary between 6,000 and 10,000 TEUs.

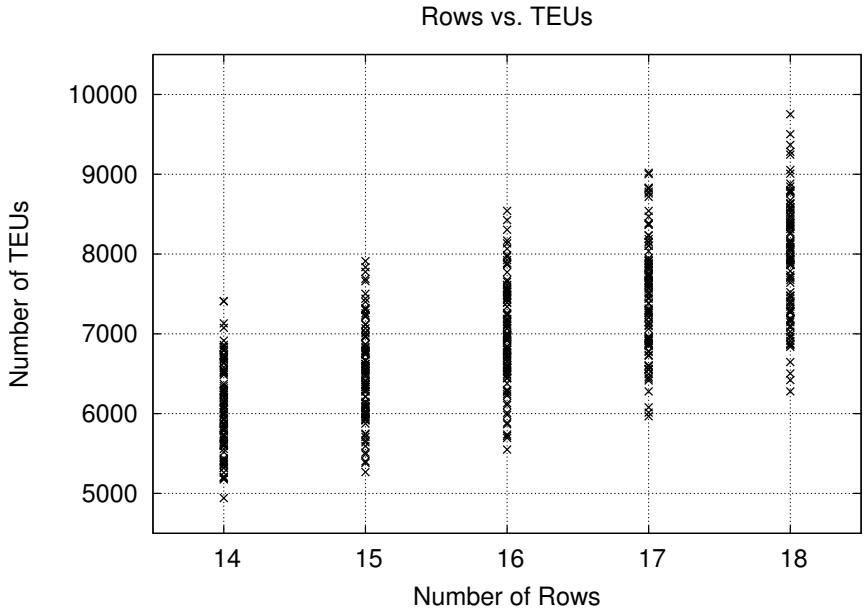


Figure 28: DoE – Rows vs. TEUs

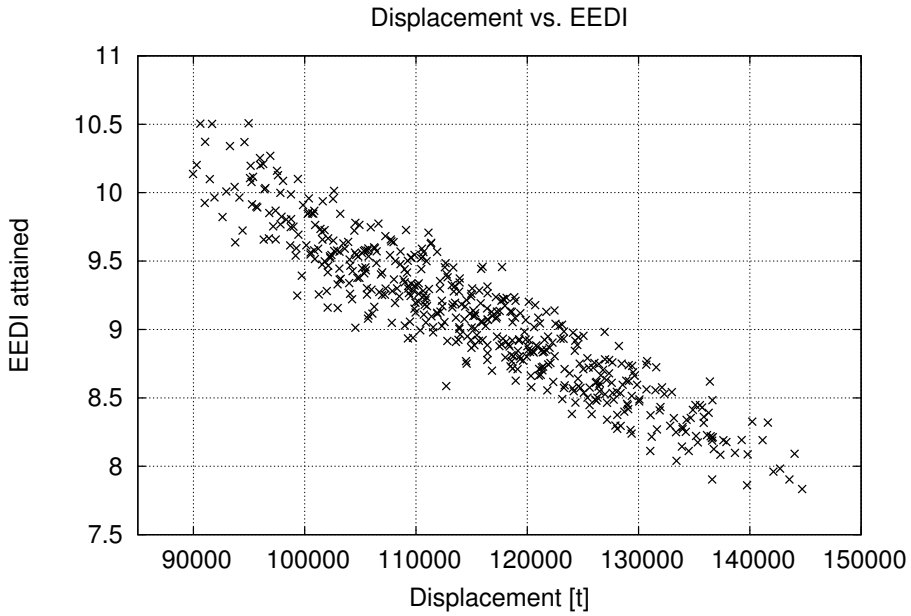


Figure 29: DoE – Displacement vs. EEDI

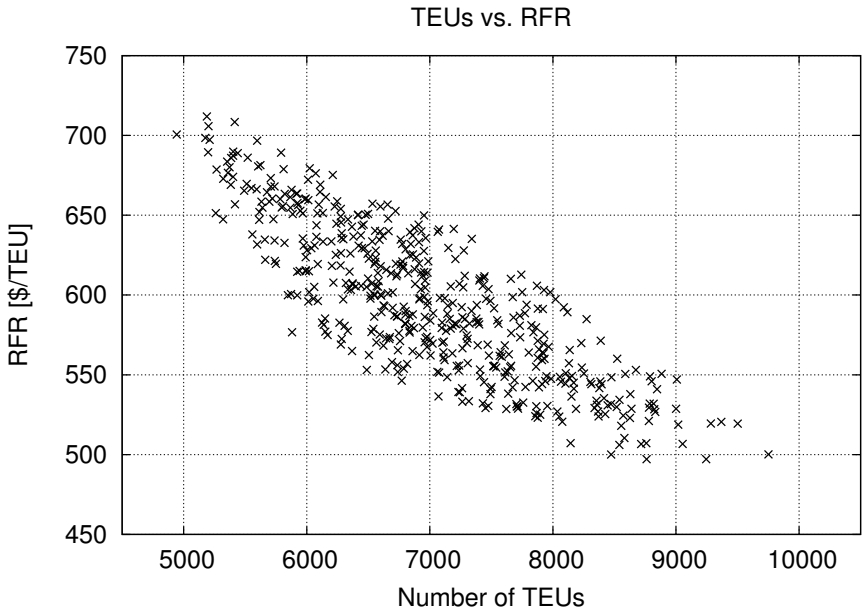


Figure 30: DoE – TEUs vs. RFR

In figure 29, the change of the EEDI in regard to the displacement can be observed. Since the formula used to calculate the attained EEDI contains the transport work (paragraph 4.6.1), which is relative to the deadweight of the vessel, it is clear that changes in the displacement of the model result in variation of the attained EEDI. An increase in the displacement of the model normally means an increase in the deadweight also. Since the deadweight is inversely proportional to the attained EEDI, as the displacement of the model increments, the index declines.

Finally, as far as the RFR is concerned, by looking at figure 30, we can observe the correlation between the RFR and the cargo capacity of our model. It is evident that the lower the number of TEUs transported, the higher the RFR of the ship. This can be explained by looking at the formula used to calculate the RFR in paragraph 4.6.2. The cargo capacity is inversely proportional to the RFR value, hence a decrease in the rate can be observed, as the TEU capacity expands.

The diagrams above refer to the Model-1 variant, however the response of the Model-2 variant is very similar to the former, hence there is no need for presenting at this stage the results of Model-2's DoE. In appendix A, more diagrams, including ones regarding Model-2's response, can be found.

## 5.4 Multi-Objective Optimization Rounds

After completing the DoE phase for both base model variants, the multi-objective optimization commences. As mentioned in section 4, in each case, two rounds are run, so as to ensure that the best design is found. As in DoE's case, Friendship-Framework supplies us with plenty of tables containing useful data, so that we can have a precise idea of each variant.

### 5.4.1 Model-1

As far as Model-1 variant is concerned, after the two NSGA-II rounds and the evaluation of both rounds' results, we concluded that the optimal design was produced during the first round. This design (Des0129), along with the base model, is marked differently in the diagrams displayed below, in order to stand out from the rest of the produced variants and to understand the level of improvement of the model. Since the second round did not generate a more superior design in respect to the five objectives, only diagrams of the first round are presented.

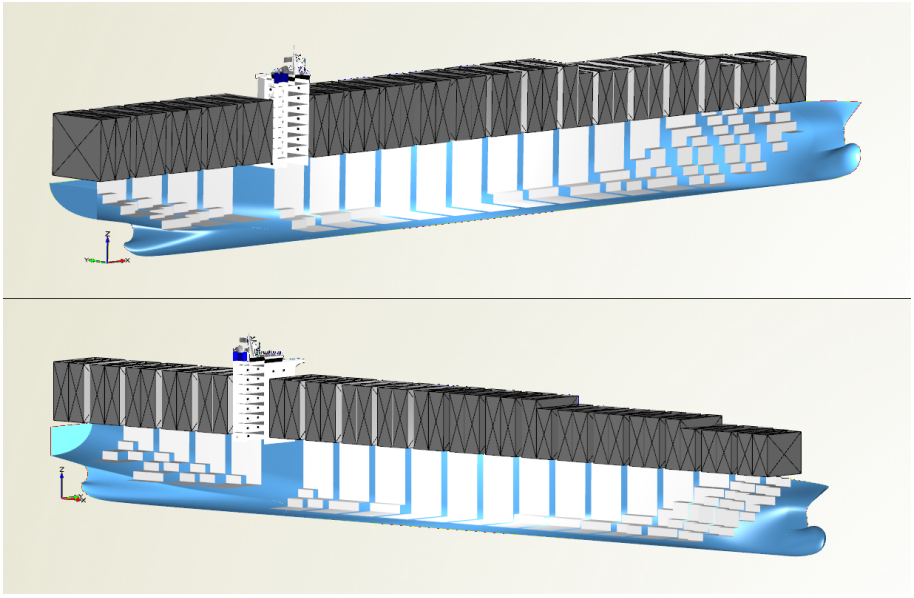

Figure 31: Des0129 model

Before proceeding to the diagrams, the final form of Des0129 can be seen in figure 31, while its principal data are presented in table 15.

| | | | |
|---|---|---|---|
| **Bays** | 20 | **Max. TEU capacity** | 6,918 |
| **Rows** | 16 | **Z.B. TEU capacity** | 3,583 |
| **Tiers in hold** | 8 | **RFR ($/TEU)** | 579.99 |
| **Tiers on deck** | 7 | **Capacity ratio** | 0.5179 |
| **Double bottom (m)** | 2.00 | **EEDI** | 8.58 |
| **Double side (m)** | 2.63 | **Stowage ratio** | 1.3191 |
| $\mathbf{\Delta} c_P$ | 0.02416 | **Total ship resistance (KN)** | 1,688 |
| **ΔLCB** | 0.00102 | **Wetted surface ($m^2$)** | 15,945 |

Table 15: Des0129 principal data

In figure 32, the values of the attained EEDI in respect to the number of bays are presented. Low values in variants having 20 bays are noticeable, whereas in case of 18 and 19 bays, the range of EEDI values is bigger, running from around 8.25 to 10. A decrease in the attained EEDI can be noticed between the base and the improved model.

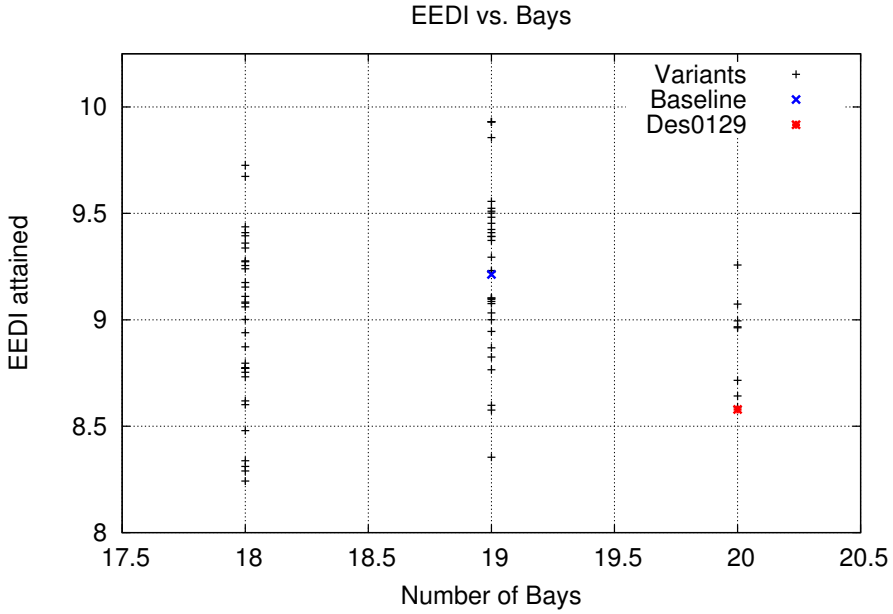


Figure 32: NSGA-II – EEDI vs. Bays

By looking at figure 33, we can observe the correlation between the stowage and the capacity ratio. Optimally, high values for both ratios are desired. However, a decrease in the stowage ratio is observed, as the capacity ratio rises. A few variants though deviate from this behavior and achieve high stowage and capacity ratios. Among these designs is Des0129. All in all, between the base and the improved model, we notice an impressive increase in the stowage ratio, while the capacity ratio remains nearly the same in both cases.

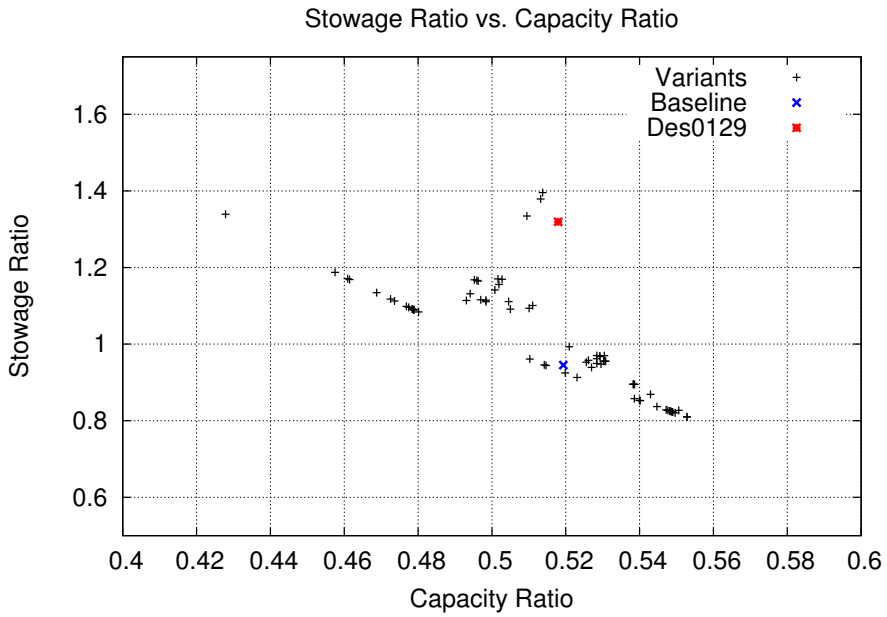


Figure 33: NSGA-II – Stowage ratio vs. Capacity ratio

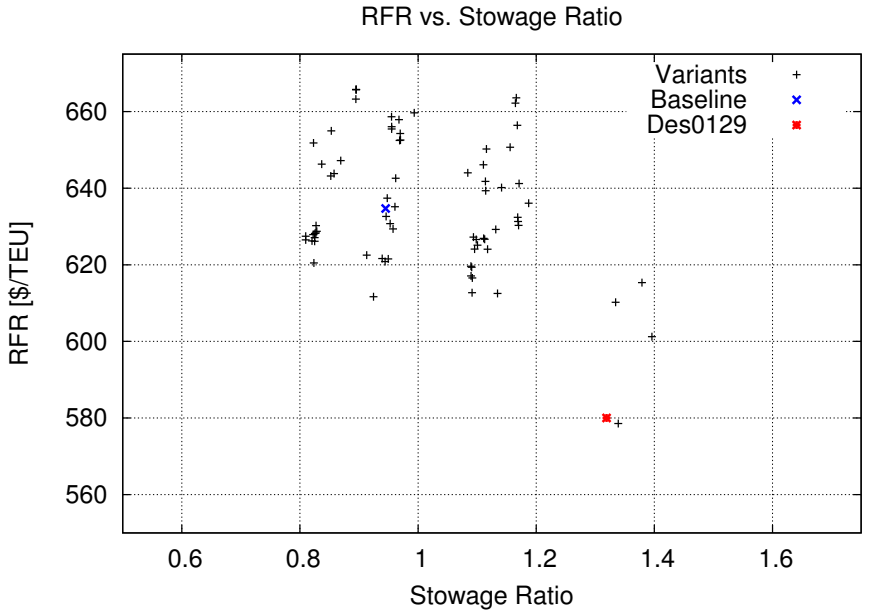


Figure 34: NSGA-II – RFR vs. Stowage ratio

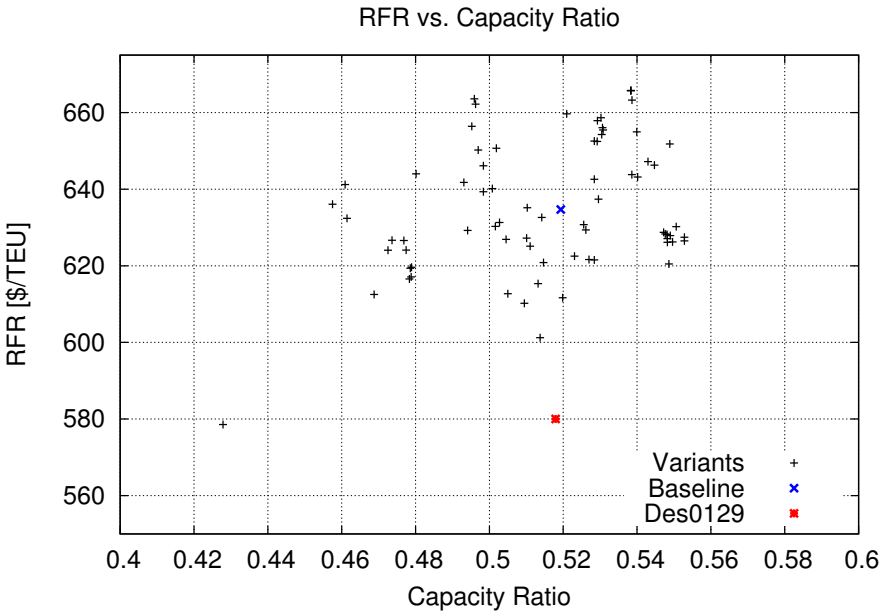


Figure 35: NSGA-II – RFR vs. Capacity ratio

The relationship between RFR and the stowage ratio is displayed in figure 34. Here, an optimal solution would be characterized by a low RFR value and a high stowage ratio. Most of the design variants range between 620 $/TEU and 675 $/TEU as far as the RFR is concerned, while their stowage ratios range between 0.8 and 1.2. However, a few generated designs present lower RFR values and slightly higher stowage ratios. Des0129 is located in this area of the diagram, achieving both a satisfactory freight rate and a high stowage ratio.

Finally, the RFR in regard to the capacity ratio is presented in figure 35. The optimal variant is located far from most of the generated designs in the diagram, along with another variant. Both of these designs feature a low freight rate, however, Des0129 features an adequate capacity ratio, which is almost the same as our base model's one.

In order to select the optimal design, namely Des0129, a decision making process takes place. The results from the optimization runs are normalized and evaluated, taking into account the three scenarios described in paragraph 4.8. Figures 36, 37 and 38 demonstrate the superiority of Des0129, compared to the best generated designs.

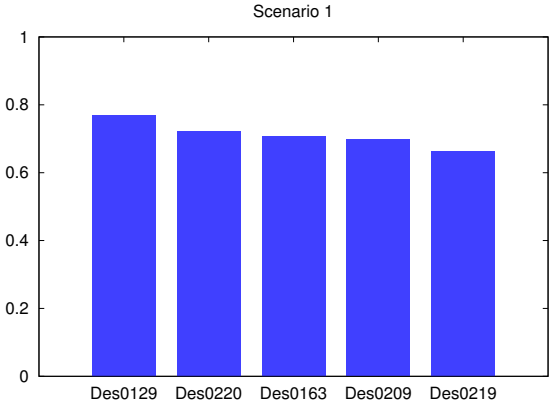


Figure 36: Scenario 1 ranking

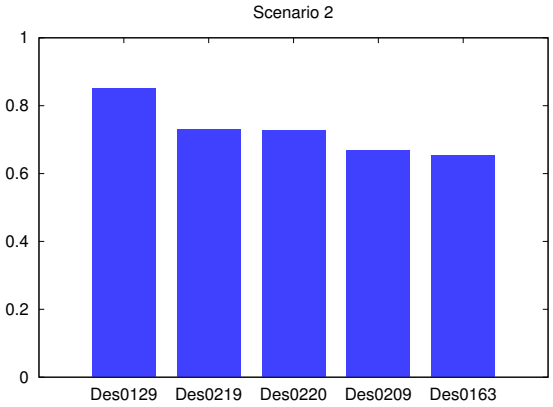


Figure 37: Scenario 2 ranking

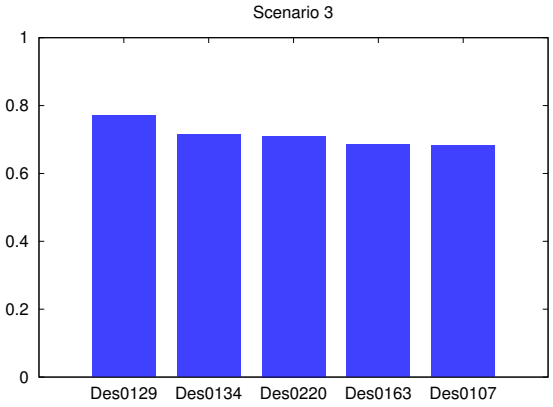


Figure 38: Scenario 3 ranking

### 5.4.2 Model-2

Following the same steps as in Model-1's case, after the optimization rounds, an optimal variant was found, named Des0080. The diagrams presented below, show the differences and improvements between the base model and the improved one. The configuration of Des0080 can be seen in figure 39, while its main characteristics are found in table 16.

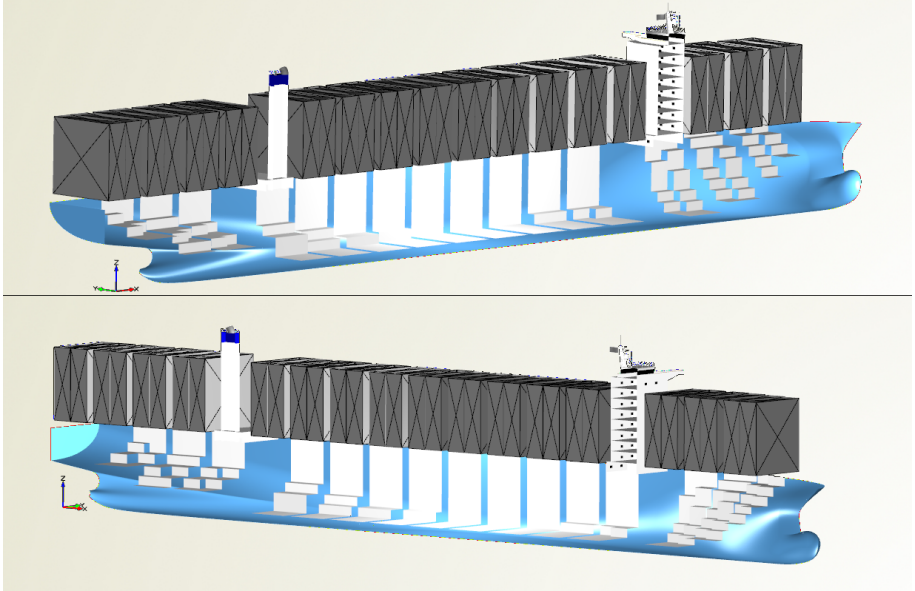

Figure 39: Des0080 model

| | | | |
|---|---|---|---|
| **Bays** | 18 | **Max. TEU capacity** | 6,980 |
| **Rows** | 17 | **Z.B. TEU capacity** | 3,730 |
| **Tiers in hold** | 8 | **RFR ($/TEU)** | 562.93 |
| **Tiers on deck** | 8 | **Capacity ratio** | 0.5344 |
| **Double bottom (m)** | 2.52 | **EEDI** | 8.98 |
| **Double side (m)** | 2.69 | **Stowage ratio** | 1.6250 |
| **Δ**$c_P$ | -0.02636 | **Total ship resistance (KN)** | 1,582 |
| **ΔLCB** | 0.01825 | **Wetted surface ($m^2$)** | 14,279 |

Table 16: Des0080 principal data

Overall, several differences can be spotted between Des0080 and Model-1's optimal variant. Des0080 features 18 bays, instead of 20 that Des0129 has. Moreover, the number of rows is increased by one in this case. As far as the tiers

are concerned, the ones below the main deck are equal, while one extra tier is present above the main deck in Des0080's case. Finally, both the double bottom and the double side values are higher in Des0080 than in Des0129. Nevertheless, the maximum TEU capacity of both variants achieved is nearly the same.

As before, some representative diagrams demonstrating the optimization results are displayed. Des0080, along with the base model, is marked differently, in order to stand out from the rest of the produced variants.

Unlike Model-1, Des0080 features one bay less than the initial model. Looking at figure 40, we see a 2% decrease in the attained EEDI value. Moreover, we can observe a steady decline in the EEDI values as the number of bays increases.

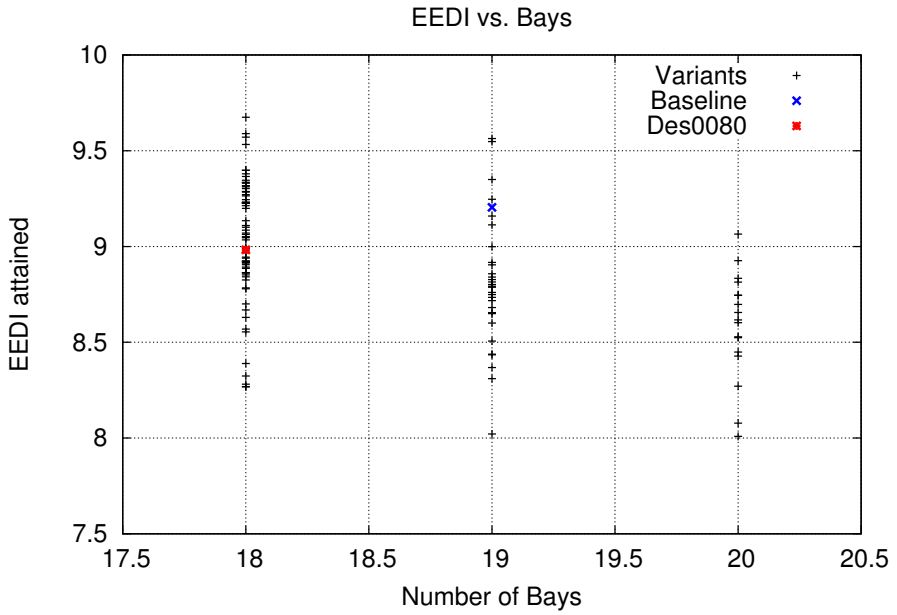


Figure 40: NSGA-II – EEDI vs. Bays

As far as figure 41 is concerned, the situation resembles Model-1's case. A general decline in capacity ratio can be observed, as the stowage ratio rises. However, our improved model, along with a couple of generated variants, seems to achieve high values in both ratios. Des0080 in particular, manages to increase its capacity ratio by little, while boosting its stowage ratio by more than 60%, compared to the baseline model.

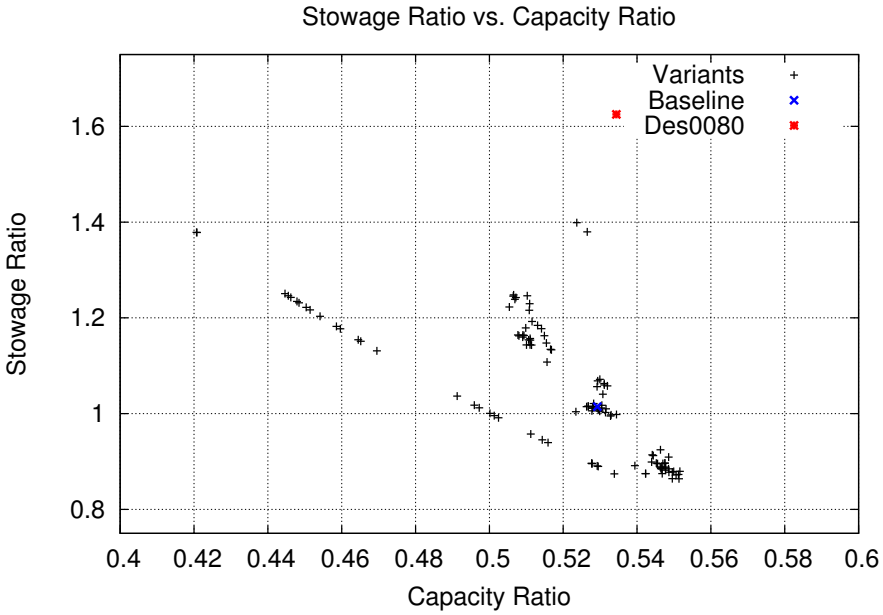


Figure 41: NSGA-II – Stowage ratio vs. Capacity ratio

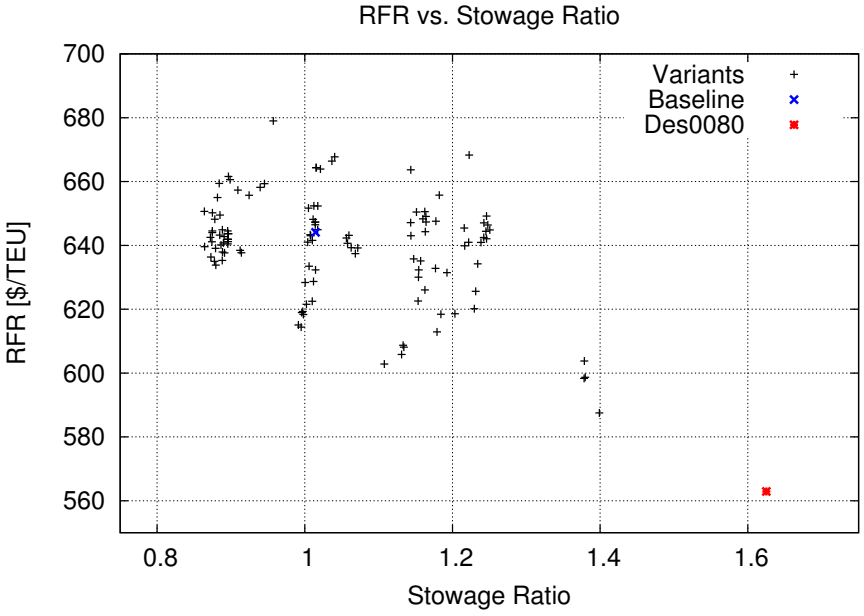


Figure 42: NSGA-II – RFR vs. Stowage ratio

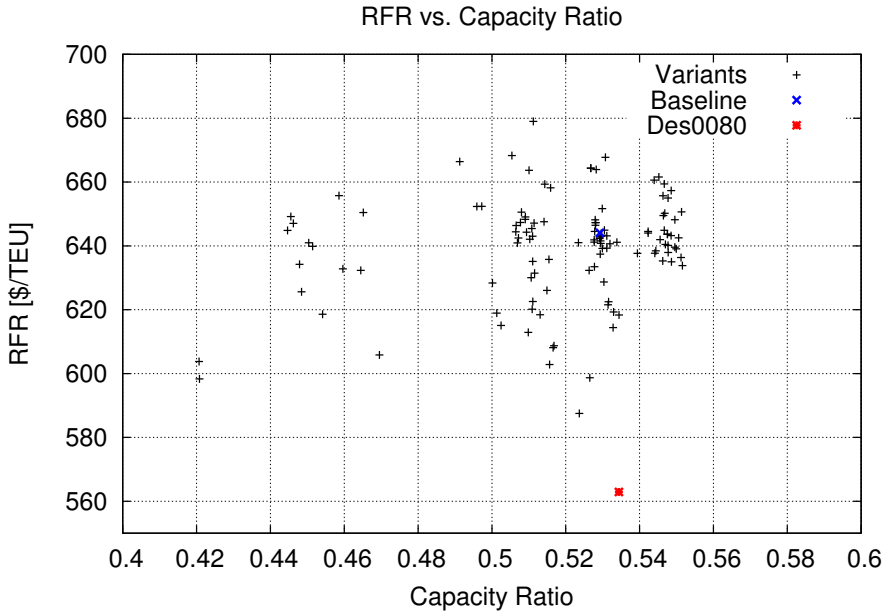


Figure 43: NSGA-II – RFR vs. Capacity ratio

The correlation between RFR and stowage ratio is found in figure 42. Looking at the position of the design variants in the diagram, it becomes fathomable that as the ratio values rise, the RFR values descend. Des0080 is positioned far from most of the variants, including the base model, achieving both the highest stowage ratio and the lowest freight rate.

Finally, in figure 43 we can observe the relation between the RFR and the capacity ratio. Most of the design variants are characterized by adequate capacity ratios, however the freight rate is kept relatively high. Yet, Des0080 manages to combine satisfactory results in both objectives. In particular, the RFR value sees a sharp decrease of around 12.5%, compared to the base model.

As previously, a decision making process takes place, which leads us to the optimal design. The results from the optimization runs are normalized. Then, the evaluation process takes place, taking into account the three scenarios described in paragraph 4.8. Figures 44, 45 and 46 substantiate the selection of Des0080, since it ranks first in every scenario. More specifically, Des0080 reaches values of higher than 0.8 in each case, being the only one of the top ranked variants to achieve that.

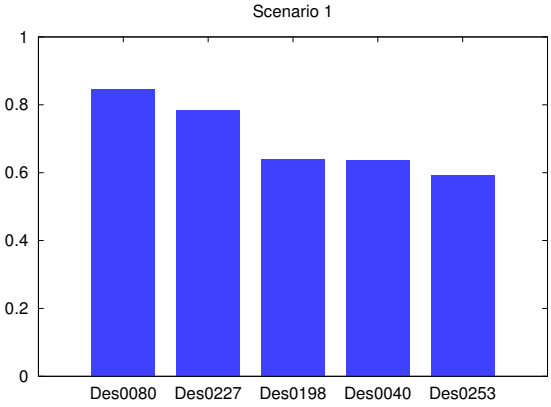


Figure 44: Scenario 1 ranking

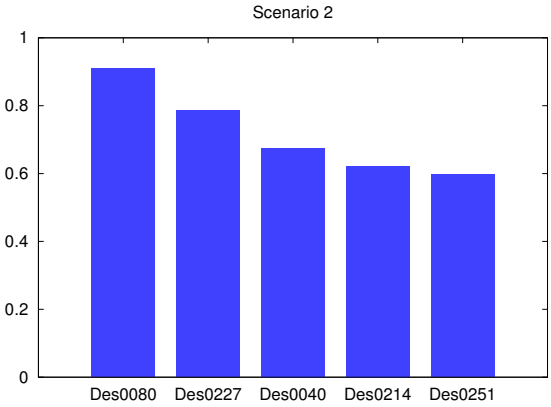


Figure 45: Scenario 2 ranking

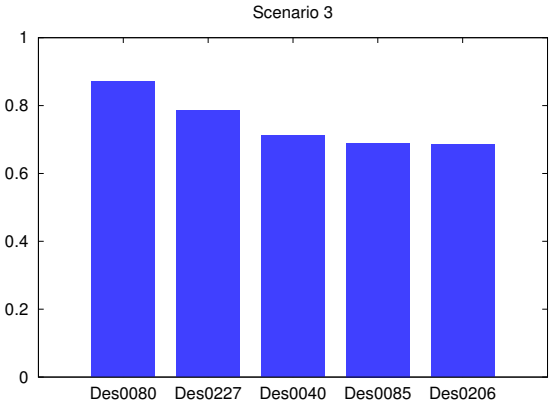


Figure 46: Scenario 3 ranking

## 5.5 Optimal Design Selection

In the previous paragraph, the optimal result of each initial model variant (Model-1 and Model-2) was presented. Since the scope of this diploma thesis is to determine the best container ship design derived from the optimization rounds, a comparison between Des0129 and Des0080 is inevitable.

Firstly, a comparison regarding the main characteristics of Des0129 and Des0080 is made in table 17.

| **Data** | **Des0129** | **Des0080** |
|---|---|---|
| $L_{BP}$ (m) | 305.53 | 276.00 |
| Beam (m) | 39.01 | 41.45 |
| Depth (m) | 21.69 | 22.21 |
| $c_B$ | 0.7269 | 0.6859 |
| $c_M$ | 0.9821 | 0.9832 |
| $c_P$ | 0.7401 | 0.6976 |
| Displacement (t) | 124,337 | 112,611 |
| Deadweight (t) | 97,241 | 88,683 |
| Lightship (t) | 27,096 | 23,928 |
| Weight per TEU (Max. capacity) (t) | 8.29 | 7.69 |
| Weight per TEU (Z.B. capacity) (t) | 25.37 | 22.42 |

Table 17: Des0129 vs. Des0080 principal data

More information regarding both models can be found in tables 15 and 16. The main differences between the two variants can be spotted in their $L_{BP}$ and beam values. In particular, Des0080 features a smaller $L_{BP}$, whereas its one extra row produces a wider hull, compared to Des0129. The result is a much lower lightship weight, as far as Des0080 is concerned. Moreover, the *Deadweight/Displacement* ratio is higher in Des0080 than in Des0129. In addition, the $c_B$ value of Des0080 is considerably lower than Des0129's one. These observations help us understand why Des0080 achieves both a lower freight rate and a lower total resistance (table 18).

| **Objective** | **Des0129** | **Des0080** |
|---|---|---|
| RFR ($/TEU) | 579.99 | 562.93 |
| Capacity ratio | 0.5179 | 0.5344 |
| EEDI | 8.58 | 8.98 |
| Stowage ratio | 1.3191 | 1.6250 |
| Total ship resistance (KN) | 1,688 | 1,582 |

Table 18: Des0129 vs. Des0080 objective values

In table 18, it is visible that Des0129's EEDI value is a bit lower than Des0080's one. It should be noted though that this is the only objective where Des0129 outmatches Des0080. As far as the stowage ratio is concerned, the one extra tier above the main deck in Des0080, results in a higher ratio. Finally, the capacity ratio in Des0080 is marginally higher than in Des0129's case.

The information provided above is sufficient for us to proceed to the decision making process. Since Des0080 outranks Des0129 in every objective but the EEDI, it is safe to declare Des0080 as the optimal design of the optimization process carried out in this thesis. The improvement is visible through the tables provided above, however, an overall comparison of both base models and their improved variants is presented below.

In figure 47, the attained EEDI value is compared to the number of bays. The lowest EEDI value is achieved by Des0129. Both improved models have a lower attained EEDI value than the baseline models.

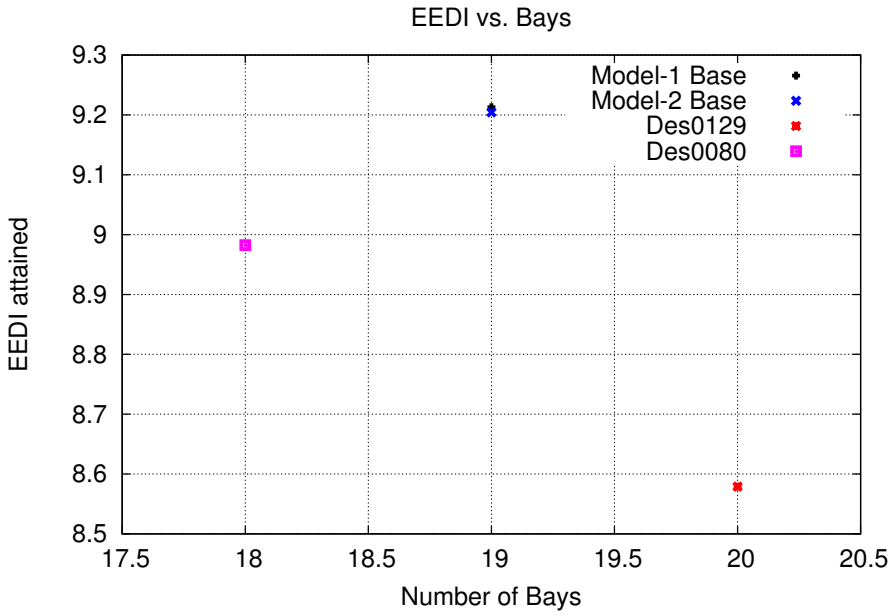


Figure 47: Overall comparison – EEDI vs. Bays

As far as figure 48 is concerned, it is clear that Des0080 achieves the best combination of stowage and capacity ratios. Des0129 is characterized by a higher stowage ratio than both baseline models, however, it scores the lowest capacity ratio.

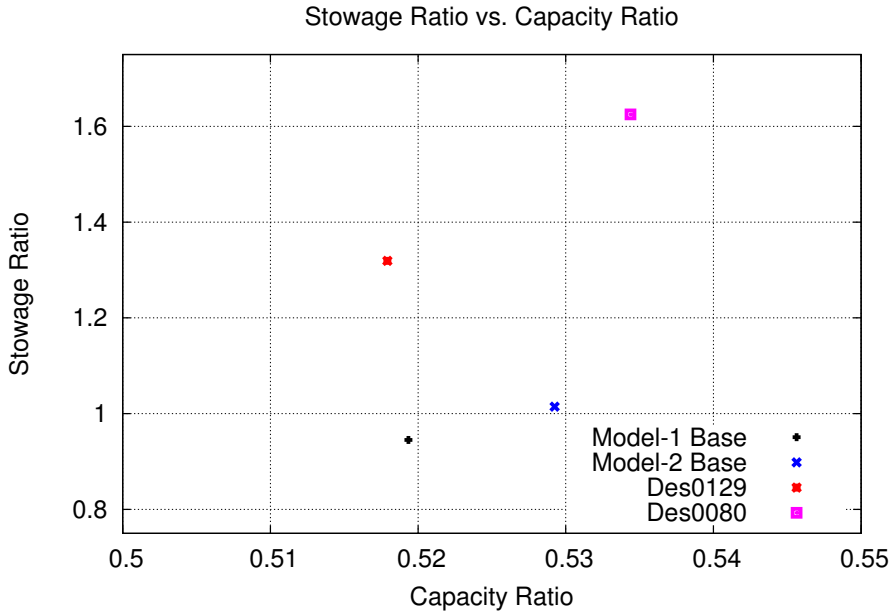


Figure 48: Overall comparison – Stowage ratio vs. Capacity ratio

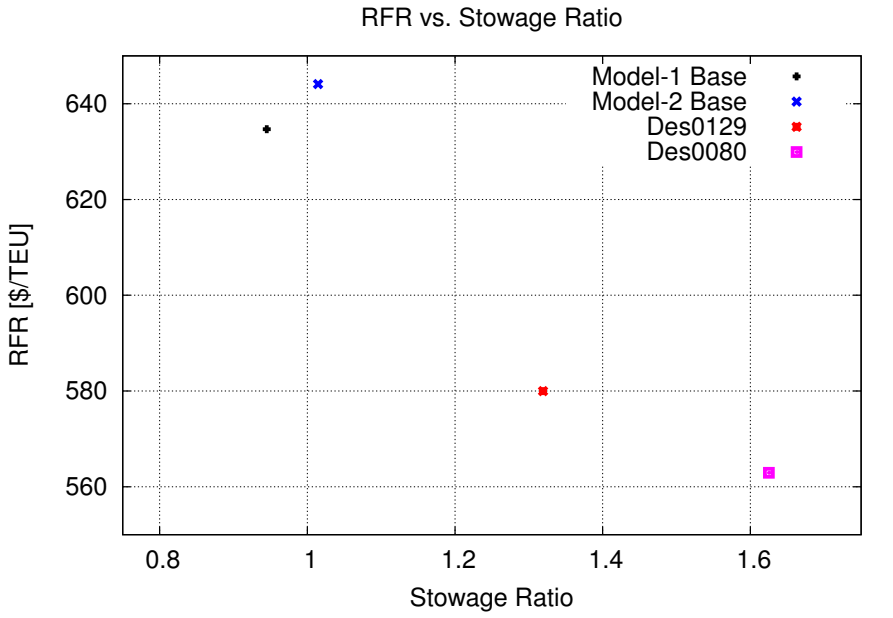


Figure 49: Overall comparison – RFR vs. Stowage ratio

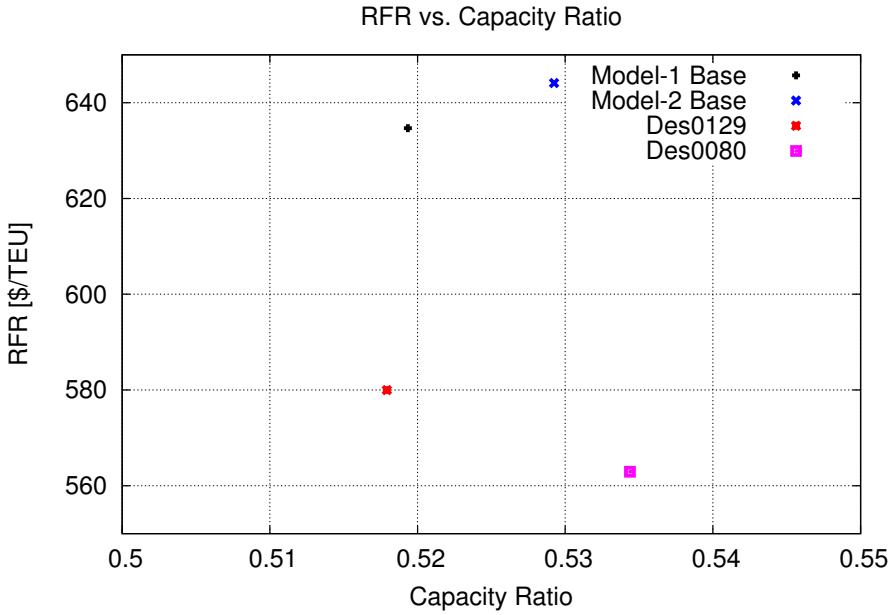


Figure 50: Overall comparison – RFR vs. Capacity ratio

In regard to the freight rate of the designs, we can observe a noticeable decrease in the RFR value of both improved designs, compared to the base models. However, the percentage difference between Model-2 and Des0080 is higher than the other pair of designs, as seen in figures 49 and 50. Des0080 manages to combine a low freight rate, as well as satisfactory stowage and capacity ratios.

## 5.6 Optimal Design Evaluation

In order to further elaborate on the selection of Des0080 as the optimal variant, a detailed comparison with some of the existing vessels that were used as input during the creation of the parametric model is made and can be seen in table 19.

Before commenting on the information found in table 19, it should be mentioned that the calculation of both the RFR and the EEDI of the existing container ships –Ship 1, 2 and 3– was performed using the same methods as in our model in Friendship-Framework, so as to be fair in this procedure. For this reason, the stowage and capacity ratios are not included in this process, as there were not sufficient data available to perform a candid comparison regarding these objectives. Moreover, every ship is supposed to operate at 20 Knots, in order for their required main engine power to be more or less the same and consequently, the comparison to be realistic.

| Data | Des0080 | Ship 1 | Ship 2 | Ship 3 |
|---|---|---|---|---|
| $L_{BP}$ (m) | 276.00 | 287.00 | 306.58 | 286.00 |
| Beam (m) | 41.45 | 40.00 | 40.06 | 42.84 |
| Depth (m) | 22.21 | 23.90 | 24.20 | 24.50 |
| Displacement (t) | 112,611 | 110,715 | 115,832 | 111,270 |
| Deadweight (t) | 88,683 | 82,275 | 87,534 | 88,700 |
| Lightship (t) | 23,928 | 28,440 | 28,298 | 22,570 |
| Max. TEU capacity | 6,980 | 6,208 | 6,478 | 6,802 |
| RFR ($/TEU) | 562.93 | 666.37 | 667.05 | 644.37 |
| EEDI | 8.98 | 10.06 | 9.57 | 9.36 |
| Total ship resistance (KN) | 1,582 | 1,603 | 1,620 | 1,588 |
| $P_{B_{ME}}$ (KW) | 26,829 | 27,882 | 28,242 | 27,987 |

Table 19: Overall comparison

All in all, the superiority of Des0080 is evident in table 19. At similar dimensions, Des0080 is able to carry the highest number of TEUs. Des0080's RFR value is considerably lower than the rest of the ships. The same stands for the attained EEDI value, where Des0080 achieves the lowest number. Furthermore, the overall resistance of Des0080 is lower than the one of the existing ships, but it is worth mentioning that Ship 3 achieves a low overall resistance as well.

As far as the rest of the data is concerned, the Displacement and the main engine's required power values seem to be nearly the same in every vessel, however, Ship 1 and 2 are described by higher lightship values, thus their deadweight is a bit lower than in Des0080's and Ship 3's case.

Apart from the freight rate and the EEDI, various differences can be spotted in the main dimensions of the ships. Des0080 features the lowest length and depth, while its beam is the second biggest. The twin-isle arrangement however, offers the advantage of an increased number of TEUs stored above the main deck, since the visibility line rule is practically not a restriction in this configuration, contrary to the rest of the ships, which feature a traditional arrangement.

Finally, a one-to-one comparison between the initial and the improved design is made, to show the percentage differences in several elements. The comparison is found in table 20. Overall, the improvement of the initial container ship design is obvious. Des0080 manages to perform much better, reducing the required freight rate by 12.6% and the attained EEDI by 2.39%. Moreover, the capacity ratio is increased, which means that the zero ballast TEU capacity is improved, while at the same time, more TEUs can be stored above the main deck, simplifying the cargo loading/unloading process.

As far as the weight per TEU in maximum and zero ballast capacity conditions is concerned (tables 17 and 20), it should be noted that in our model, we assume homogeneous loading. Of course, in reality, the weight of the TEUs stacked on board would vary, depending on the position of the heavier and lighter containers. Moreover, taking into account that the maximum weight per TEU cannot

exceed the twenty tons limit due to structural reasons, we should clarify that the numbers achieved in this project are theoretical and in real conditions may vary. The main point that should be noted is that the capacity ratio of the initial model was improved after the optimization runs.

| **Data** | **Model-2** | **Des0080** | **Difference** |
|---|---|---|---|
| Bays | 19 | 18 | -1 |
| Rows | 16 | 17 | +1 |
| Tiers in hold | 9 | 8 | -1 |
| Tiers on deck | 6 | 8 | +2 |
| Double bottom (m) | 2.00 | 2.52 | +0.52 m |
| Double side (m) | 2.10 | 2.69 | +0.59 m |
| Total ship resistance (KN) | 1,635 | 1,582 | -3.24% |
| Max. TEU capacity | 6,394 | 6,980 | +9.16% |
| Z.B. TEU capacity | 3,384 | 3,730 | +10.22% |
| Capacity ratio | 0.5292 | 0.5344 | +0.98% |
| Stowage ratio | 1.0145 | 1.6250 | +60.17% |
| Weight per TEU (Max. capacity) (t) | 8.17 | 7.69 | -5.87% |
| Weight per TEU (Z.B. capacity) (t) | 24.74 | 22.42 | -9.37% |
| RFR ($/TEU) | 644.10 | 562.93 | -12.60% |
| EEDI | 9.20 | 8.98 | -2.39% |

Table 20: Model-2 vs. Des0080

# 6 Conclusion

This diploma thesis dealt with the multi-disciplinary optimization of a mid-sized, 6,500 TEU container ship. The project covered every aspect of the process, beginning with the preliminary design of the model, utilizing the principles of parametric ship design. The optimization procedure was carried out afterwards, incorporating the inspection of the design space through the design of experiment phase. The NSGA-II algorithm was utilized during the formal optimization rounds, which proved to be a felicitous choice, as the results were satisfactory.

Through the work presented in this thesis, the advantages of the utilization of design optimization in the shipbuilding industry are demonstrated. By incorporating the optimization process in the early stages of ship design, a much improved design can be produced, providing numerous benefits to a potential buyer.

Furthermore, it is proved that using modern CAD/CAE systems, the optimization can effortlessly become part of the design process, yielding excellent results without causing any delays. The areas of optimization are of course not limited to the objectives examined in this project. Aspects such as structural strength or seakeeping, can become the main objectives of design optimization as well, allowing naval architects to achieve a greater degree of holism in the design process.

As far as the results of the current project are concerned, some general observations can be made. First of all, the consideration of twin-isle arrangements in such container ship sizes seems to be substantial, as the best variant proved to feature such a configuration. In addition, it is worth mentioning that shorter and wider designs appear to be more cost-efficient than longer and narrower ones. A decrease in the ship's length can lead to a much lower lightship value, thus increasing the deadweight of the ship and, consequently, its overall cost-efficiency.

Of course, the work performed in this thesis can be applied to different ship sizes and types in future research projects. More phases of the ship's life cycle can be integrated to future studies, resulting in a more detailed investigation.

# A Sobol Diagrams

## Model-1 Results

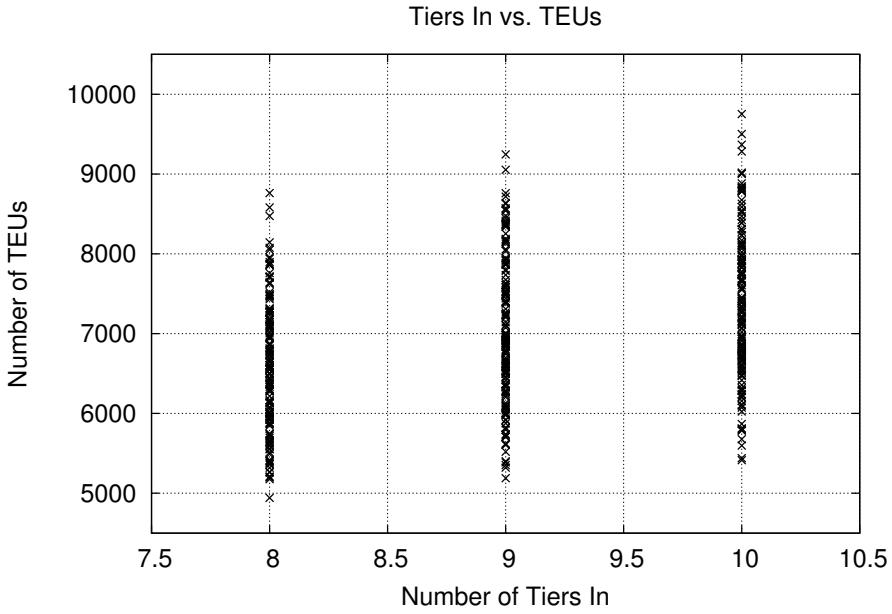


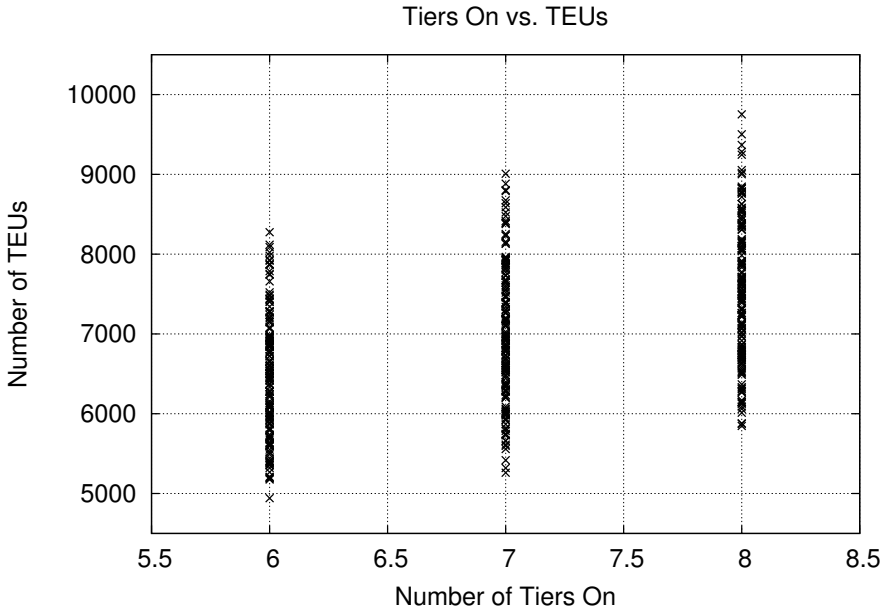

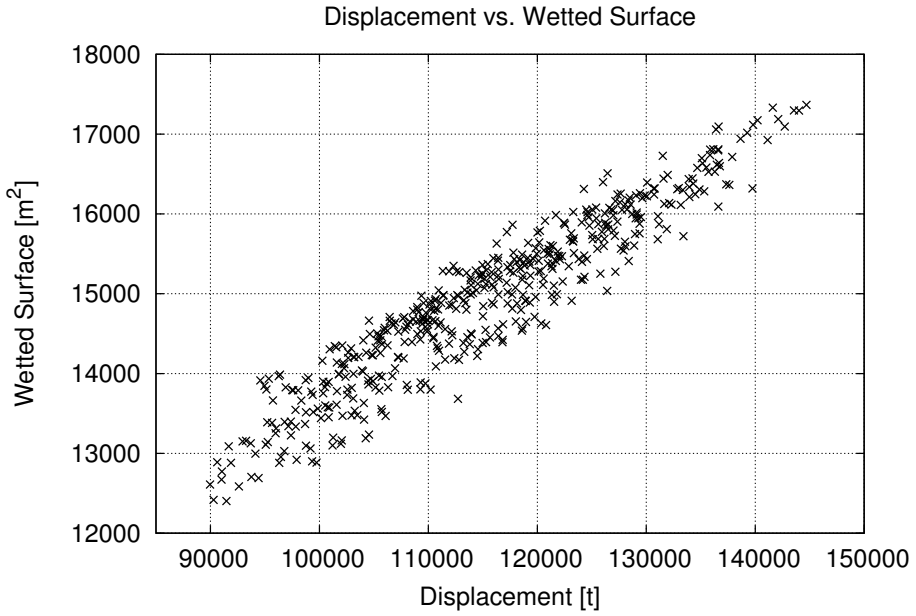
Displacement vs. Wetted Surface
Wetted Surface [m$^2$]
18000
17000
16000
15000
14000
13000
12000
90000
100000
110000
120000
130000
140000
150000
Displacement [t]

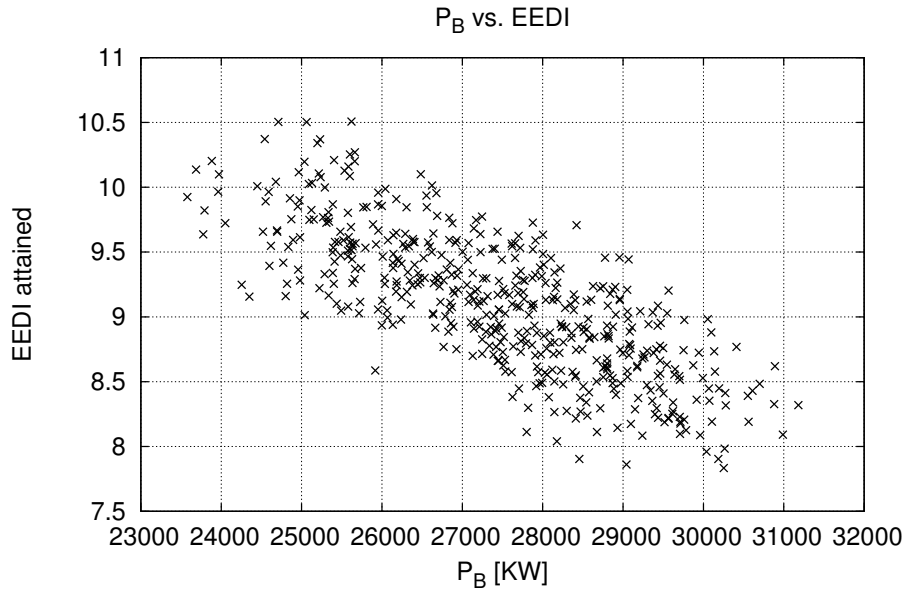
$P_B$ vs. EEDI
EEDI attained
11
10.5
10
9.5
9
8.5
8
7.5
23000
24000
25000
26000
27000
28000
29000
30000
31000
32000
$P_B$ [KW]

### Model-2 Results

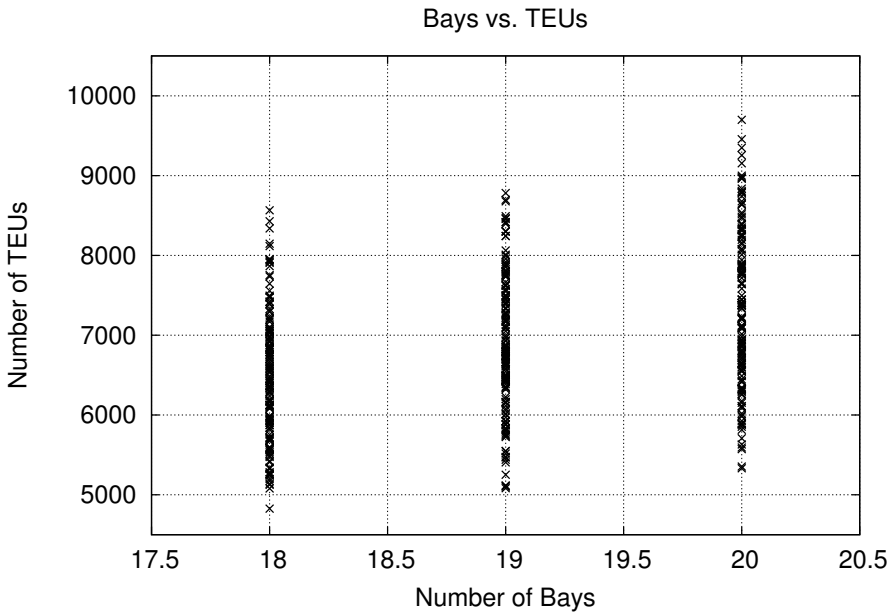


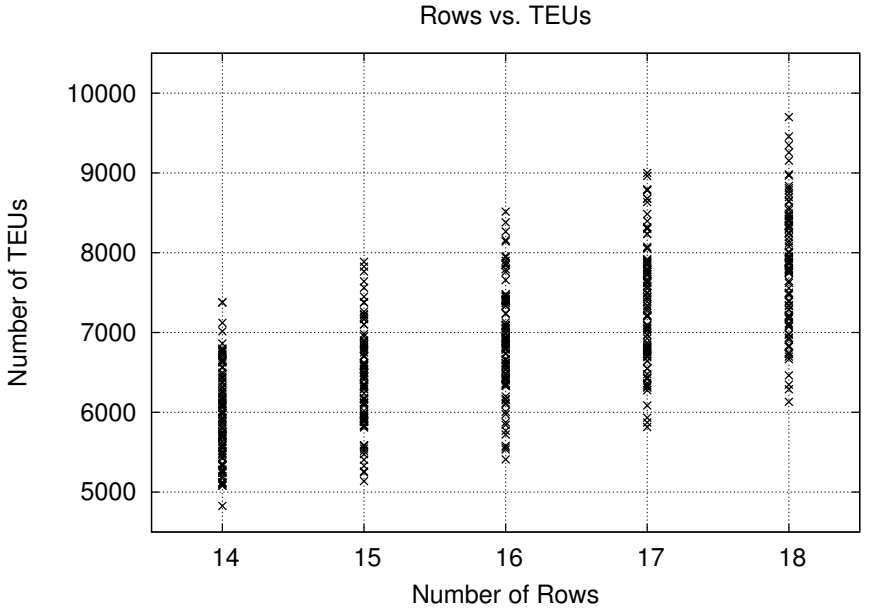

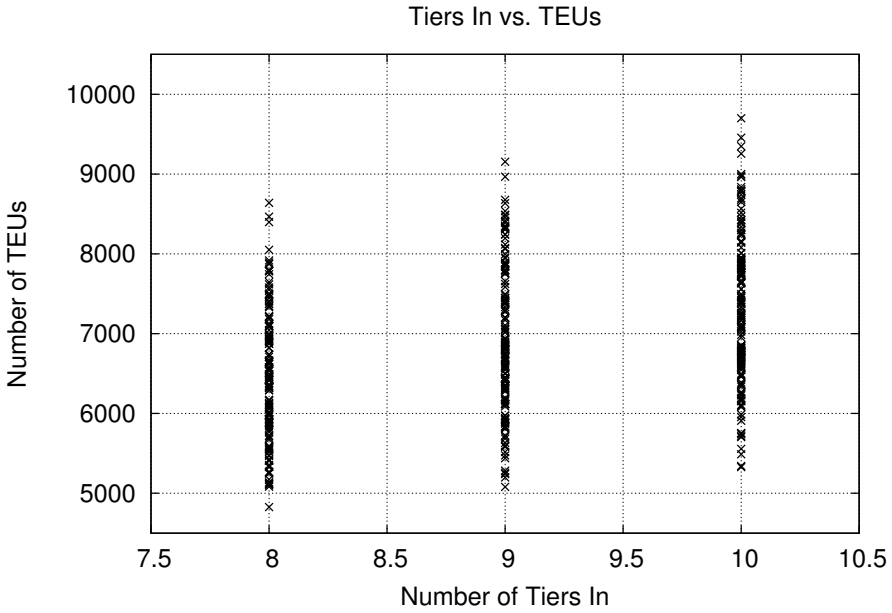
Tiers In vs. TEUs
Number of TEUs
10000
9000
8000
7000
6000
5000
7.5
8
8.5
9
9.5
10
10.5
Number of Tiers In

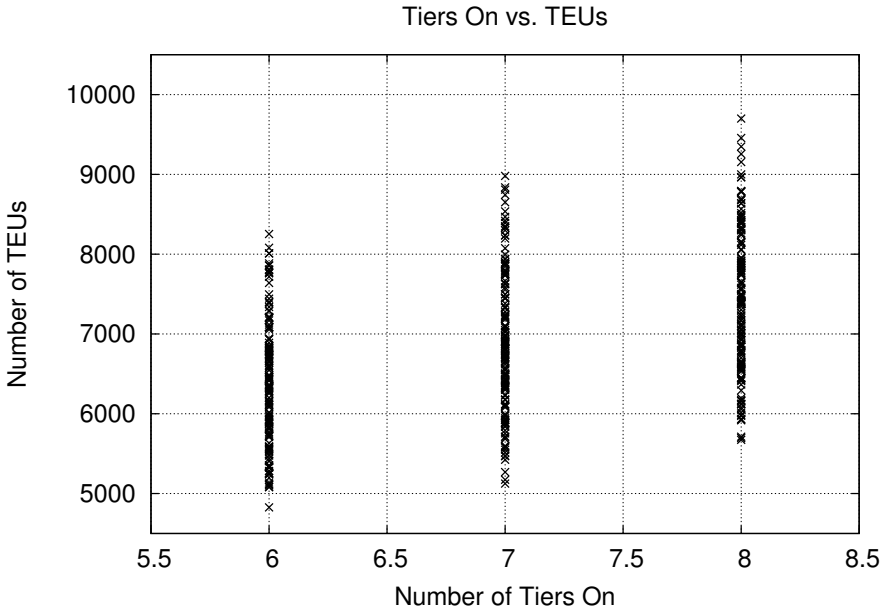
Tiers On vs. TEUs
Number of TEUs
10000
9000
8000
7000
6000
5000
5.5
6
6.5
7
7.5
8
8.5
Number of Tiers On

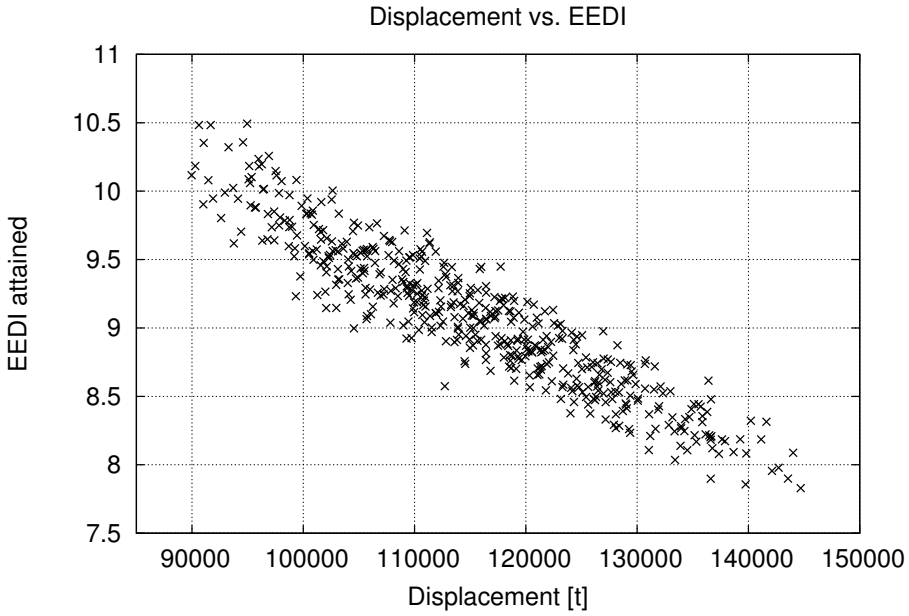
Displacement vs. EEDI
EEDI attained
Displacement [t]
11
10.5
10
9.5
9
8.5
8
7.5
90000
100000
110000
120000
130000
140000
150000

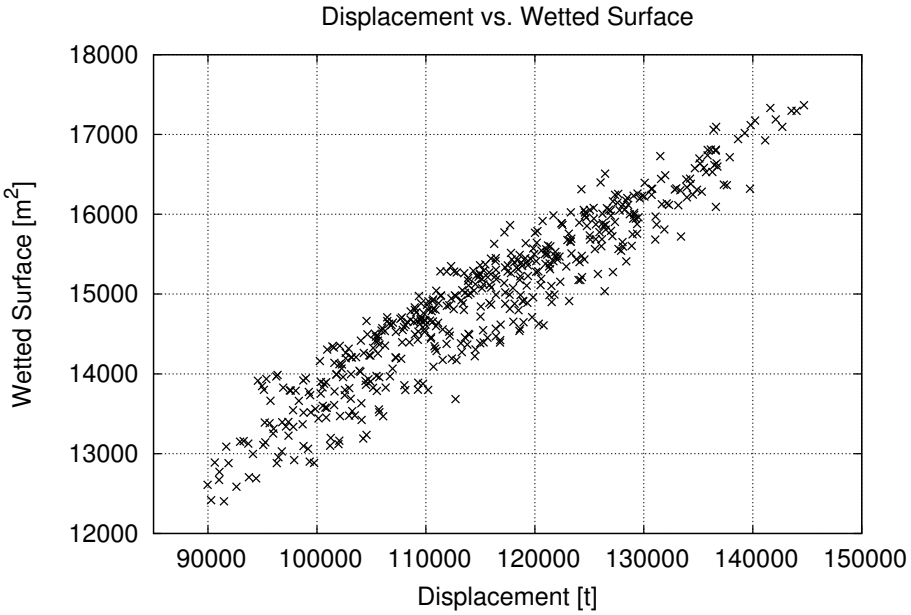
Displacement vs. Wetted Surface
Wetted Surface [m2]
Displacement [t]
18000
17000
16000
15000
14000
13000
12000
90000
100000
110000
120000
130000
140000
150000

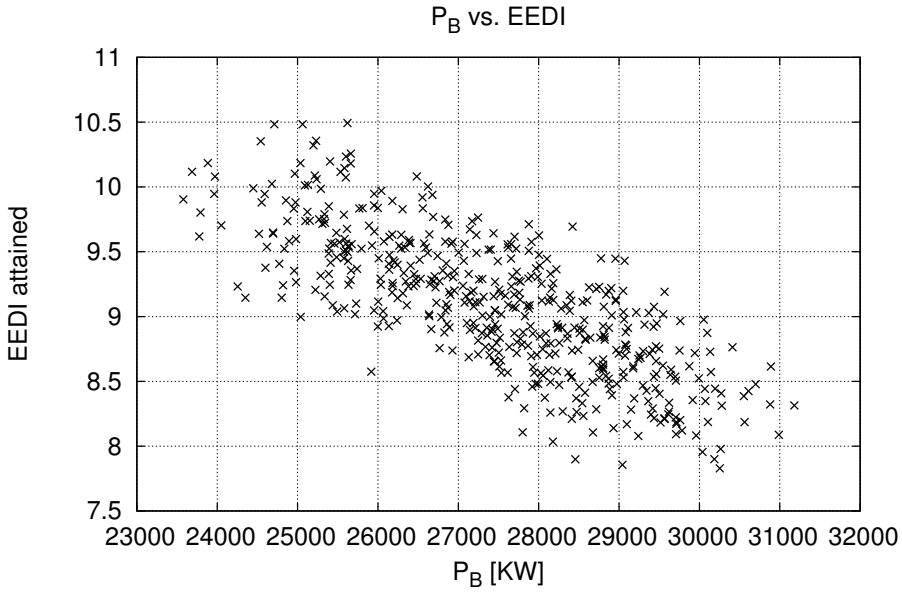
$P_B$ vs. EEDI
EEDI attained
11
10.5
10
9.5
9
8.5
8
7.5
23000 24000 25000 26000 27000 28000 29000 30000 31000 32000
$P_B$ [KW]

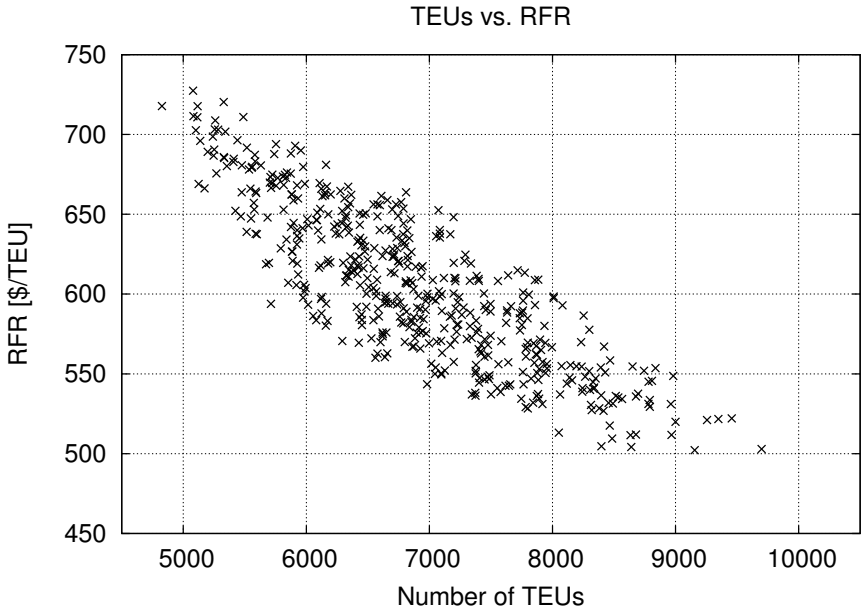
TEUs vs. RFR
RFR [$/TEU]
750
700
650
600
550
500
450
5000
6000
7000
8000
9000
10000
Number of TEUs

# B NSGA-II Results

## Model-1 Results

| Variant | $R_T$ (KN) | Capacity ratio | Stowage ratio | RFR ($/TEU) | EEDI |
|---|---|---|---|---|---|
| Nsga2_01_des0022 | 1,613 | 0.4963 | 1.1647 | 662.20 | 9.36 |
| Nsga2_01_des0027 | 1,631 | 0.5490 | 0.8224 | 627.89 | 9.39 |
| Nsga2_01_des0033 | 1,636 | 0.5050 | 1.0914 | 612.70 | 8.60 |
| Nsga2_01_des0039 | 1,648 | 0.5472 | 0.8285 | 628.73 | 9.24 |
| Nsga2_01_des0047 | 1,604 | 0.5293 | 0.9677 | 657.90 | 9.22 |
| Nsga2_01_des0058 | 1,688 | 0.5199 | 0.9247 | 611.68 | 8.82 |
| Nsga2_01_des0061 | 1,618 | 0.4609 | 1.1710 | 641.22 | 9.26 |
| Nsga2_01_des0066 | 1,579 | 0.4931 | 1.1141 | 641.76 | 9.15 |
| Nsga2_01_des0071 | 1,641 | 0.5481 | 0.8254 | 628.17 | 9.45 |
| Nsga2_01_des0086 | 1,672 | 0.4786 | 1.0908 | 619.37 | 8.77 |
| Nsga2_01_des0088 | 1,580 | 0.4953 | 1.1680 | 656.40 | 9.18 |
| Nsga2_01_des0089 | 1,545 | 0.5383 | 0.8952 | 665.73 | 9.93 |
| Nsga2_01_des0090 | 1,642 | 0.5306 | 0.9553 | 656.05 | 9.03 |
| Nsga2_01_des0107 | 1,624 | 0.5496 | 0.8204 | 626.24 | 9.37 |
| Nsga2_01_des0111 | 1,675 | 0.4789 | 1.0894 | 619.62 | 8.80 |
| Nsga2_01_des0114 | 1,594 | 0.5447 | 0.8369 | 646.29 | 9.67 |
| Nsga2_01_des0116 | 1,637 | 0.5308 | 0.9553 | 655.47 | 9.00 |
| Nsga2_01_des0121 | 1,715 | 0.5284 | 0.9495 | 621.53 | 8.60 |
| Nsga2_01_des0126 | 1,601 | 0.5008 | 1.1413 | 640.16 | 8.99 |
| Nsga2_01_des0129 | 1,688 | 0.5179 | 1.3191 | 579.99 | 8.58 |
| Nsga2_01_des0134 | 1,611 | 0.5486 | 0.8237 | 620.47 | 9.06 |
| Nsga2_01_des0143 | 1,580 | 0.5284 | 0.9703 | 652.57 | 9.08 |
| Nsga2_01_des0145 | 1,657 | 0.4784 | 1.0918 | 616.58 | 8.75 |
| Nsga2_01_des0153 | 1,613 | 0.5019 | 1.1558 | 650.67 | 9.08 |
| Nsga2_01_des0156 | 1,584 | 0.5304 | 0.9699 | 654.26 | 9.10 |
| Nsga2_01_des0159 | 1,637 | 0.4802 | 1.0841 | 644.00 | 8.87 |
| Nsga2_01_des0160 | 1,604 | 0.4575 | 1.1873 | 636.08 | 8.77 |
| Nsga2_01_des0161 | 1,565 | 0.5027 | 1.1692 | 631.31 | 8.97 |
| Nsga2_01_des0163 | 1,605 | 0.5132 | 1.3790 | 615.33 | 9.00 |
| Nsga2_01_des0164 | 1,632 | 0.4970 | 1.1157 | 650.21 | 9.11 |
| Nsga2_01_des0167 | 1,605 | 0.4984 | 1.1107 | 646.11 | 9.27 |
| Nsga2_01_des0168 | 1,573 | 0.5292 | 0.9686 | 652.46 | 9.09 |
| Nsga2_01_des0171 | 1,630 | 0.5482 | 0.8250 | 626.14 | 9.39 |
| Nsga2_01_des0173 | 1,566 | 0.4725 | 1.1177 | 624.08 | 8.77 |
| Nsga2_01_des0174 | 1,726 | 0.5147 | 0.9441 | 620.84 | 8.58 |
| Nsga2_01_des0176 | 1,545 | 0.5383 | 0.8952 | 665.74 | 9.93 |
| Nsga2_01_des0179 | 1,657 | 0.4688 | 1.1345 | 612.51 | 8.64 |
| Nsga2_01_des0181 | 1,786 | 0.4768 | 1.0985 | 626.59 | 8.29 |
| Nsga2_01_des0182 | 1,769 | 0.4775 | 1.0958 | 624.09 | 8.24 |
| Nsga2_01_des0186 | 1,567 | 0.4614 | 1.1686 | 632.37 | 8.96 |
| Nsga2_01_des0187 | 1,621 | 0.4959 | 1.1662 | 663.59 | 9.39 |
| Nsga2_01_des0189 | 1,654 | 0.5528 | 0.8098 | 626.50 | 9.52 |

| Variant | $R_T$ (KN) | Capacity ratio | Stowage ratio | RFR ($/TEU) | EEDI |
|---|---|---|---|---|---|
| Nsga2_01_des0191 | 1,740 | 0.5296 | 0.9479 | 637.41 | 8.62 |
| Nsga2_01_des0192 | 1,576 | 0.5256 | 0.9528 | 630.73 | 9.23 |
| Nsga2_01_des0195 | 1,601 | 0.4941 | 1.1315 | 629.23 | 9.07 |
| Nsga2_01_des0196 | 1,659 | 0.5506 | 0.8272 | 630.22 | 9.41 |
| Nsga2_01_des0198 | 1,664 | 0.4788 | 1.0897 | 617.10 | 8.73 |
| Nsga2_01_des0199 | 1,654 | 0.5302 | 0.9550 | 658.65 | 9.10 |
| Nsga2_01_des0203 | 1,636 | 0.5482 | 0.8250 | 627.09 | 9.42 |
| Nsga2_01_des0207 | 1,831 | 0.5103 | 0.9609 | 635.17 | 8.48 |
| Nsga2_01_des0208 | 1,648 | 0.5489 | 0.8229 | 651.81 | 9.44 |
| Nsga2_01_des0209 | 1,532 | 0.5095 | 1.3345 | 610.22 | 9.41 |
| Nsga2_01_des0212 | 1,538 | 0.5402 | 0.8523 | 643.19 | 9.34 |
| Nsga2_01_des0214 | 1,758 | 0.5110 | 1.1007 | 625.13 | 8.31 |
| Nsga2_01_des0218 | 1,564 | 0.5016 | 1.1701 | 630.27 | 8.72 |
| Nsga2_01_des0219 | 1,646 | 0.4278 | 1.3389 | 578.55 | 8.59 |
| Nsga2_01_des0220 | 1,587 | 0.5137 | 1.3958 | 601.23 | 9.29 |
| Nsga2_01_des0222 | 1,654 | 0.4736 | 1.1127 | 626.67 | 8.94 |
| Nsga2_01_des0225 | 1,791 | 0.5101 | 1.0937 | 627.21 | 8.34 |
| Nsga2_01_des0226 | 1,531 | 0.5209 | 0.9934 | 659.66 | 9.25 |
| Nsga2_01_des0230 | 1,642 | 0.5386 | 0.8578 | 643.81 | 9.51 |
| Nsga2_01_des0234 | 1,764 | 0.5261 | 0.9577 | 629.35 | 8.35 |
| Nsga2_01_des0235 | 1,690 | 0.5284 | 0.9620 | 642.59 | 8.95 |
| Nsga2_01_des0237 | 1,596 | 0.5045 | 1.1111 | 626.89 | 8.78 |
| Nsga2_01_des0243 | 1,658 | 0.5142 | 0.9460 | 632.61 | 9.28 |
| Nsga2_01_des0246 | 1,605 | 0.5399 | 0.8532 | 654.97 | 9.73 |
| Nsga2_01_des0248 | 1,564 | 0.4984 | 1.1145 | 639.35 | 9.08 |
| Nsga2_01_des0249 | 1,535 | 0.5386 | 0.8947 | 663.26 | 9.86 |
| Nsga2_01_des0252 | 1,577 | 0.5270 | 0.9392 | 621.65 | 9.10 |
| Nsga2_01_des0254 | 1,644 | 0.5429 | 0.8690 | 647.19 | 9.50 |
| Nsga2_01_des0255 | 1,686 | 0.5231 | 0.9129 | 622.52 | 8.87 |
| Nsga2_01_des0256 | 1,546 | 0.5383 | 0.8952 | 665.74 | 9.93 |
| Nsga2_01_des0257 | 1,660 | 0.5528 | 0.8098 | 627.45 | 9.56 |
| Nsga2_01_des0258 | 1,643 | 0.5476 | 0.8270 | 628.32 | 9.48 |

## Model-2 Results

| Variant | $R_T$ (KN) | Capacity ratio | Stowage ratio | RFR ($/TEU) | EEDI |
|---|---|---|---|---|---|
| Nsga2_02_des0031 | 1,671 | 0.5013 | 0.9960 | 618.92 | 8.73 |
| Nsga2_02_des0035 | 1,741 | 0.5506 | 0.8722 | 642.51 | 9.07 |
| Nsga2_02_des0039 | 1,648 | 0.5277 | 0.8960 | 641.17 | 9.23 |
| Nsga2_02_des0040 | 1,779 | 0.5265 | 1.3798 | 598.68 | 8.27 |
| Nsga2_02_des0055 | 1,597 | 0.5268 | 1.0153 | 664.33 | 9.40 |
| Nsga2_02_des0063 | 1,725 | 0.5338 | 0.8742 | 641.12 | 8.99 |
| Nsga2_02_des0064 | 1,735 | 0.5115 | 1.1926 | 631.47 | 8.37 |
| Nsga2_02_des0072 | 1,702 | 0.5091 | 1.1641 | 649.05 | 8.92 |
| Nsga2_02_des0080 | 1,582 | 0.5344 | 1.6250 | 562.93 | 8.98 |
| Nsga2_02_des0085 | 1,635 | 0.5344 | 0.9983 | 618.35 | 8.68 |
| Nsga2_02_des0086 | 1,664 | 0.5278 | 1.0059 | 633.49 | 8.94 |
| Nsga2_02_des0090 | 1,778 | 0.4208 | 1.3782 | 598.34 | 8.28 |
| Nsga2_02_des0091 | 1,644 | 0.4645 | 1.1543 | 632.34 | 8.63 |
| Nsga2_02_des0092 | 1,685 | 0.4541 | 1.2034 | 618.59 | 8.27 |
| Nsga2_02_des0097 | 1,691 | 0.5499 | 0.8793 | 639.07 | 9.03 |
| Nsga2_02_des0098 | 1,652 | 0.5277 | 0.8960 | 641.90 | 9.24 |
| Nsga2_02_des0100 | 1,687 | 0.5311 | 1.0629 | 639.27 | 8.75 |
| Nsga2_02_des0103 | 1,598 | 0.5065 | 1.2453 | 644.42 | 8.72 |
| Nsga2_02_des0105 | 1,621 | 0.5281 | 1.0142 | 646.47 | 9.05 |
| Nsga2_02_des0106 | 1,594 | 0.5102 | 1.2462 | 642.08 | 9.06 |
| Nsga2_02_des0110 | 1,676 | 0.5295 | 0.8897 | 640.76 | 9.38 |
| Nsga2_02_des0111 | 1,657 | 0.5330 | 0.9974 | 619.28 | 8.65 |
| Nsga2_02_des0113 | 1,711 | 0.5311 | 1.0597 | 643.15 | 8.83 |
| Nsga2_02_des0115 | 1,625 | 0.4455 | 1.2462 | 649.18 | 8.86 |
| Nsga2_02_des0116 | 1,642 | 0.5025 | 0.9913 | 615.07 | 8.51 |
| Nsga2_02_des0117 | 1,630 | 0.5263 | 1.0146 | 632.31 | 8.99 |
| Nsga2_02_des0120 | 1,686 | 0.5303 | 1.0118 | 628.69 | 8.79 |
| Nsga2_02_des0121 | 1,591 | 0.4446 | 1.2506 | 644.82 | 8.92 |
| Nsga2_02_des0122 | 1,660 | 0.5475 | 0.8965 | 643.66 | 9.32 |
| Nsga2_02_des0123 | 1,707 | 0.5090 | 1.1599 | 648.33 | 8.90 |
| Nsga2_02_des0130 | 1,611 | 0.5294 | 1.0104 | 641.57 | 9.16 |
| Nsga2_02_des0131 | 1,631 | 0.5106 | 1.1541 | 630.03 | 8.55 |
| Nsga2_02_des0133 | 1,701 | 0.5486 | 0.8776 | 635.02 | 8.86 |
| Nsga2_02_des0134 | 1,693 | 0.5077 | 1.1643 | 647.32 | 8.86 |
| Nsga2_02_des0135 | 1,749 | 0.5423 | 0.8748 | 644.51 | 9.11 |
| Nsga2_02_des0140 | 1,623 | 0.5281 | 1.0142 | 647.28 | 9.05 |
| Nsga2_02_des0144 | 1,660 | 0.5477 | 0.8818 | 655.00 | 9.29 |
| Nsga2_02_des0148 | 1,644 | 0.5477 | 0.8866 | 640.15 | 9.22 |
| Nsga2_02_des0149 | 1,743 | 0.5114 | 1.1434 | 647.13 | 8.67 |
| Nsga2_02_des0151 | 1,624 | 0.5234 | 1.0040 | 641.02 | 8.94 |
| Nsga2_02_des0152 | 1,645 | 0.4504 | 1.2219 | 640.98 | 8.66 |
| Nsga2_02_des0156 | 1,665 | 0.5292 | 0.8907 | 642.75 | 9.33 |
| Nsga2_02_des0160 | 1,751 | 0.5464 | 0.8852 | 649.51 | 9.35 |
| Nsga2_02_des0161 | 1,678 | 0.5094 | 1.1633 | 644.30 | 8.78 |

| Variant | $R_T$ (KN) | Capacity ratio | Stowage ratio | RFR ($/TEU) | EEDI |
|---|---|---|---|---|---|
| Nsga2_02_des0162 | 1,668 | 0.5279 | 0.8955 | 644.51 | 9.33 |
| Nsga2_02_des0163 | 1,627 | 0.5478 | 0.8886 | 637.93 | 9.13 |
| Nsga2_02_des0164 | 1,656 | 0.4973 | 1.0122 | 652.39 | 9.26 |
| Nsga2_02_des0165 | 1,698 | 0.5485 | 0.8849 | 643.21 | 9.37 |
| Nsga2_02_des0166 | 1,602 | 0.4462 | 1.2426 | 647.03 | 8.75 |
| Nsga2_02_des0167 | 1,772 | 0.4652 | 1.1512 | 650.45 | 8.84 |
| Nsga2_02_des0169 | 1,772 | 0.5307 | 1.0405 | 667.74 | 8.78 |
| Nsga2_02_des0170 | 1,659 | 0.5110 | 1.1569 | 635.14 | 8.70 |
| Nsga2_02_des0171 | 1,806 | 0.4207 | 1.3787 | 603.78 | 8.39 |
| Nsga2_02_des0172 | 1,747 | 0.5423 | 0.8748 | 644.02 | 9.09 |
| Nsga2_02_des0174 | 1,583 | 0.5441 | 0.9141 | 637.68 | 9.55 |
| Nsga2_02_des0175 | 1,774 | 0.5495 | 0.8643 | 639.58 | 8.92 |
| Nsga2_02_des0176 | 1,710 | 0.5101 | 1.1435 | 663.66 | 8.92 |
| Nsga2_02_des0178 | 1,689 | 0.5143 | 0.9454 | 659.31 | 9.25 |
| Nsga2_02_des0179 | 1,732 | 0.5168 | 1.1332 | 608.70 | 8.53 |
| Nsga2_02_des0181 | 1,597 | 0.5268 | 1.0153 | 664.33 | 9.40 |
| Nsga2_02_des0182 | 1,655 | 0.5463 | 0.8883 | 635.27 | 9.30 |
| Nsga2_02_des0183 | 1,656 | 0.5467 | 0.8842 | 659.40 | 9.23 |
| Nsga2_02_des0184 | 1,614 | 0.5066 | 1.2479 | 646.37 | 8.81 |
| Nsga2_02_des0186 | 1,638 | 0.4515 | 1.2166 | 639.85 | 8.43 |
| Nsga2_02_des0187 | 1,702 | 0.5512 | 0.8729 | 636.36 | 8.89 |
| Nsga2_02_des0188 | 1,710 | 0.5320 | 1.0579 | 640.64 | 8.81 |
| Nsga2_02_des0189 | 1,647 | 0.5456 | 0.8957 | 641.95 | 9.27 |
| Nsga2_02_des0190 | 1,615 | 0.5440 | 0.8989 | 660.58 | 9.53 |
| Nsga2_02_des0191 | 1,651 | 0.5280 | 1.0113 | 648.17 | 9.21 |
| Nsga2_02_des0196 | 1,682 | 0.5516 | 0.8795 | 633.83 | 8.85 |
| Nsga2_02_des0197 | 1,592 | 0.5072 | 1.2425 | 642.49 | 8.84 |
| Nsga2_02_des0198 | 1,623 | 0.5109 | 1.2296 | 620.17 | 8.45 |
| Nsga2_02_des0199 | 1,599 | 0.5069 | 1.2387 | 640.92 | 8.80 |
| Nsga2_02_des0202 | 1,623 | 0.5281 | 1.0142 | 647.28 | 9.05 |
| Nsga2_02_des0203 | 1,660 | 0.5475 | 0.8965 | 643.66 | 9.32 |
| Nsga2_02_des0205 | 1,597 | 0.5112 | 0.9574 | 678.98 | 9.67 |
| Nsga2_02_des0206 | 1,642 | 0.5328 | 0.9950 | 614.38 | 8.70 |
| Nsga2_02_des0208 | 1,714 | 0.5054 | 1.2227 | 668.29 | 8.98 |
| Nsga2_02_des0209 | 1,818 | 0.5149 | 1.1626 | 626.05 | 8.02 |
| Nsga2_02_des0211 | 1,780 | 0.4913 | 1.0368 | 666.42 | 8.83 |
| Nsga2_02_des0213 | 1,689 | 0.5299 | 1.0050 | 651.65 | 9.06 |
| Nsga2_02_des0214 | 1,776 | 0.5156 | 1.1078 | 602.84 | 8.01 |
| Nsga2_02_des0218 | 1,637 | 0.5293 | 1.0685 | 637.40 | 9.00 |
| Nsga2_02_des0219 | 1,694 | 0.5155 | 1.1476 | 635.77 | 8.76 |
| Nsga2_02_des0220 | 1,806 | 0.4586 | 1.1822 | 655.75 | 8.32 |
| Nsga2_02_des0221 | 1,677 | 0.5001 | 1.0006 | 628.37 | 8.86 |
| Nsga2_02_des0222 | 1,719 | 0.5110 | 1.1437 | 643.04 | 8.57 |
| Nsga2_02_des0223 | 1,680 | 0.5292 | 1.0564 | 642.31 | 8.90 |
| Nsga2_02_des0224 | 1,740 | 0.5495 | 0.8781 | 648.18 | 9.31 |
| Nsga2_02_des0225 | 1,649 | 0.5299 | 1.0717 | 639.18 | 8.93 |
| Nsga2_02_des0226 | 1,628 | 0.5394 | 0.8913 | 637.66 | 9.20 |

| Variant | $R_T$ (KN) | Capacity ratio | Stowage ratio | RFR ($/TEU) | EEDI |
|---|---|---|---|---|---|
| Nsga2_02_des0227 | 1,620 | 0.5237 | 1.3989 | 587.52 | 8.27 |
| Nsga2_02_des0228 | 1,742 | 0.5298 | 1.0074 | 643.35 | 8.89 |
| Nsga2_02_des0229 | 1,611 | 0.5305 | 1.0174 | 644.91 | 9.35 |
| Nsga2_02_des0230 | 1,771 | 0.5468 | 0.8749 | 650.22 | 9.23 |
| Nsga2_02_des0231 | 1,660 | 0.4485 | 1.2314 | 625.61 | 8.62 |
| Nsga2_02_des0232 | 1,568 | 0.5282 | 1.0212 | 663.91 | 9.23 |
| Nsga2_02_des0234 | 1,620 | 0.5452 | 0.8966 | 661.57 | 9.57 |
| Nsga2_02_des0236 | 1,607 | 0.4596 | 1.1771 | 632.78 | 8.79 |
| Nsga2_02_des0237 | 1,684 | 0.5159 | 0.9396 | 658.20 | 9.28 |
| Nsga2_02_des0238 | 1,671 | 0.5108 | 1.2160 | 645.43 | 8.60 |
| Nsga2_02_des0240 | 1,601 | 0.5444 | 0.9124 | 638.43 | 9.56 |
| Nsga2_02_des0241 | 1,695 | 0.5463 | 0.9245 | 655.71 | 8.92 |
| Nsga2_02_des0242 | 1,730 | 0.5111 | 1.1535 | 622.57 | 8.44 |
| Nsga2_02_des0243 | 1,762 | 0.5141 | 1.1776 | 647.58 | 8.31 |
| Nsga2_02_des0244 | 1,576 | 0.4479 | 1.2343 | 634.23 | 8.75 |
| Nsga2_02_des0245 | 1,637 | 0.5316 | 1.0100 | 622.50 | 8.65 |
| Nsga2_02_des0246 | 1,617 | 0.4959 | 1.0177 | 652.33 | 9.34 |
| Nsga2_02_des0247 | 1,741 | 0.5131 | 1.1844 | 618.43 | 8.08 |
| Nsga2_02_des0249 | 1,715 | 0.5467 | 0.8884 | 644.87 | 9.59 |
| Nsga2_02_des0250 | 1,705 | 0.5514 | 0.8640 | 650.66 | 9.10 |
| Nsga2_02_des0251 | 1,717 | 0.5166 | 1.1342 | 608.10 | 8.52 |
| Nsga2_02_des0252 | 1,774 | 0.5486 | 0.9094 | 657.31 | 8.91 |
| Nsga2_02_des0253 | 1,654 | 0.5099 | 1.1791 | 612.90 | 8.60 |
| Nsga2_02_des0254 | 1,628 | 0.5296 | 1.0081 | 643.04 | 9.11 |
| Nsga2_02_des0255 | 1,662 | 0.5315 | 1.0023 | 621.56 | 8.83 |
| Nsga2_02_des0256 | 1,710 | 0.4695 | 1.1311 | 605.83 | 8.43 |
| Nsga2_02_des0257 | 1,720 | 0.5080 | 1.1625 | 650.56 | 8.97 |
| Nsga2_02_des0259 | 1,620 | 0.5470 | 0.8957 | 640.44 | 9.23 |

# C NSGA-II Diagrams

## Model-1 Results

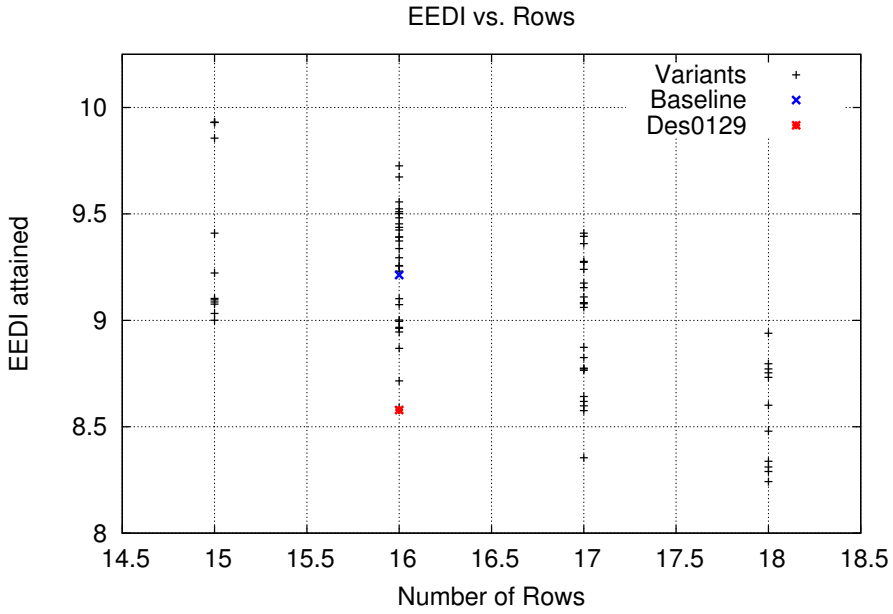


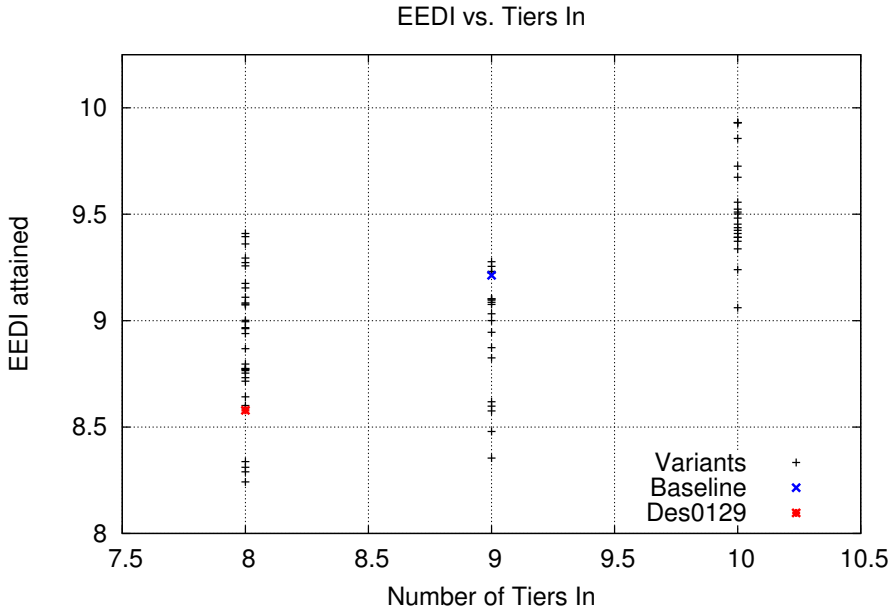

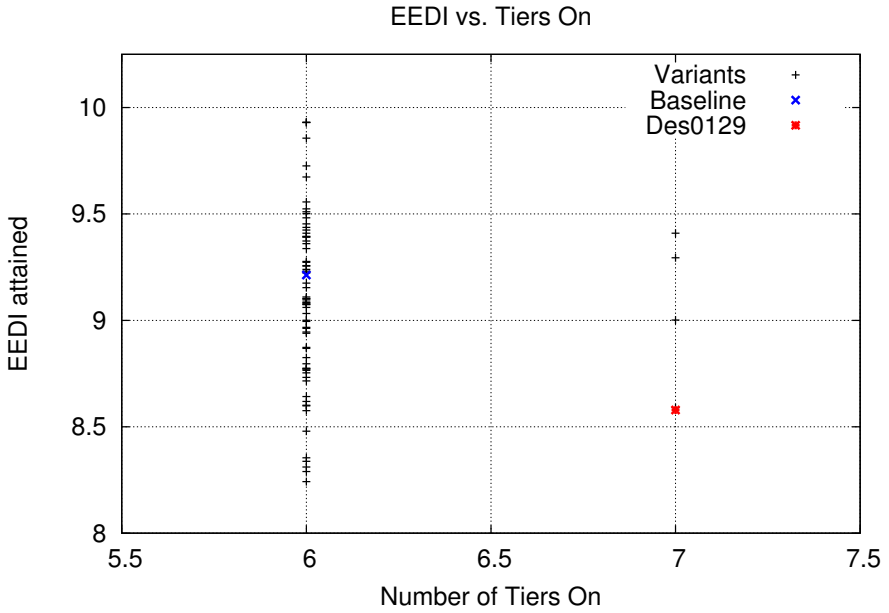
EEDI vs. Tiers On
Variants
Baseline
Des0129
EEDI attained
10
9.5
9
8.5
8
5.5
6
6.5
7
7.5
Number of Tiers On

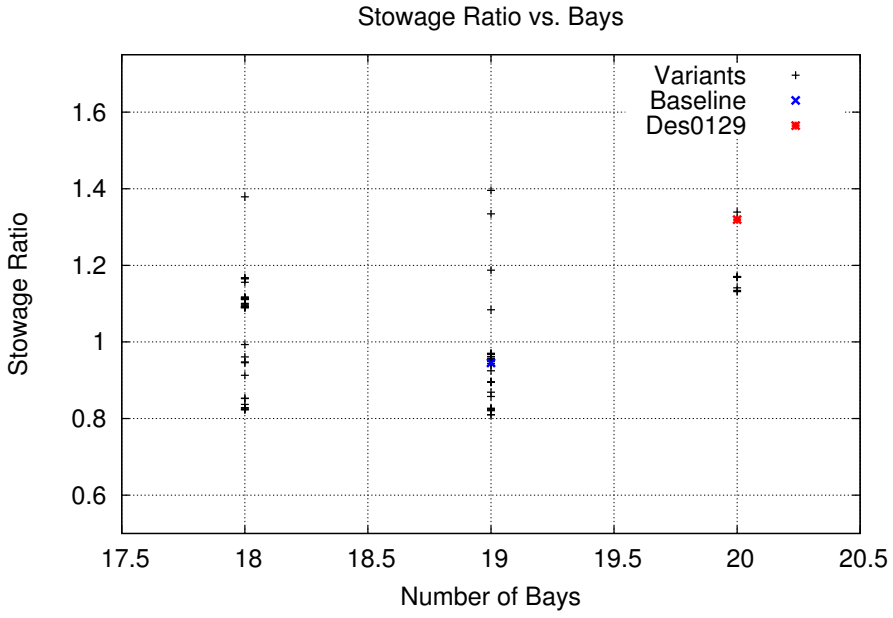
Stowage Ratio vs. Bays
Variants
Baseline
Des0129
Stowage Ratio
1.6
1.4
1.2
1
0.8
0.6
17.5
18
18.5
19
19.5
20
20.5
Number of Bays

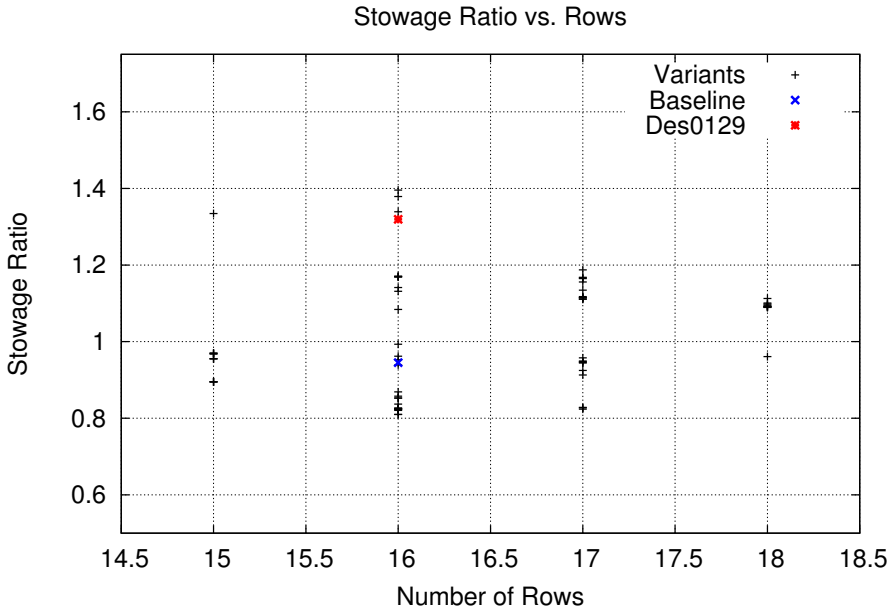
Stowage Ratio vs. Rows
Variants
Baseline
Des0129
Stowage Ratio
1.6
1.4
1.2
1
0.8
0.6
14.5
15
15.5
16
16.5
17
17.5
18
18.5
Number of Rows

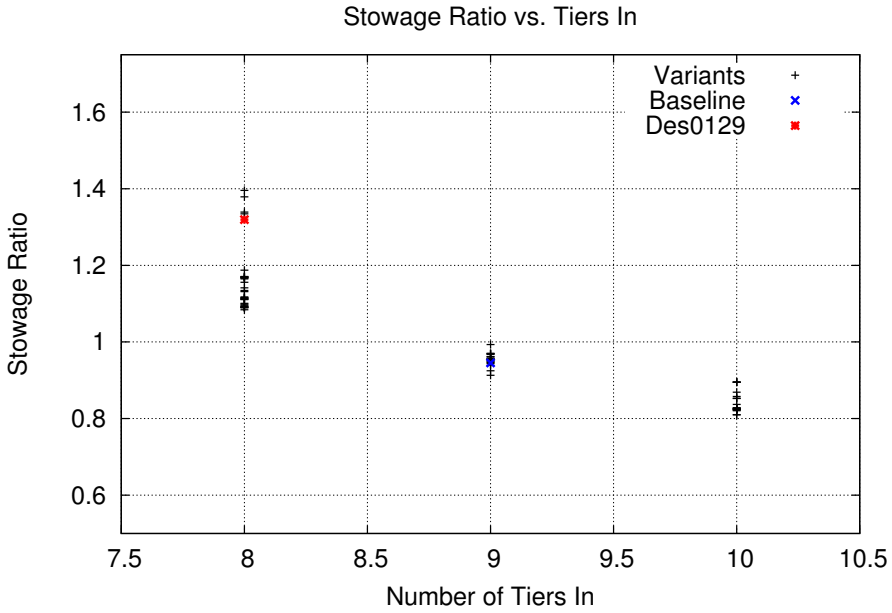
Stowage Ratio vs. Tiers In
Variants
Baseline
Des0129
Stowage Ratio
1.6
1.4
1.2
1
0.8
0.6
7.5
8
8.5
9
9.5
10
10.5
Number of Tiers In

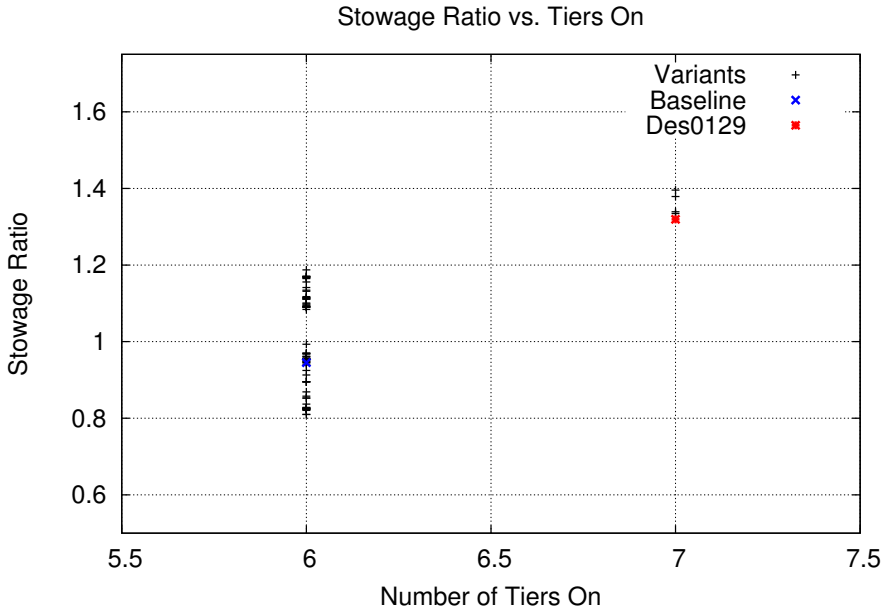
Stowage Ratio vs. Tiers On
Variants
Baseline
Des0129
Stowage Ratio
1.6
1.4
1.2
1
0.8
0.6
5.5
6
6.5
7
7.5
Number of Tiers On

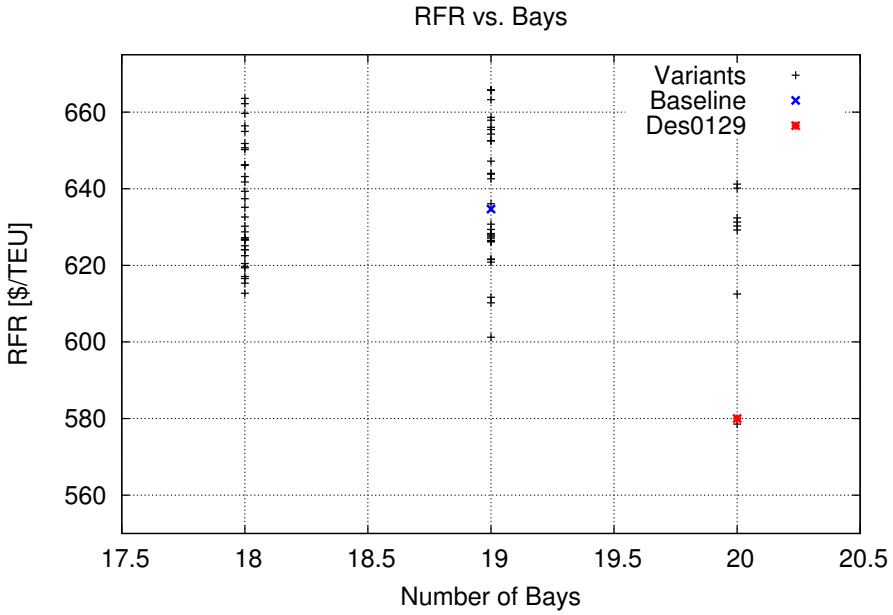
RFR vs. Bays
Variants
Baseline
Des0129
RFR [$/TEU]
660
640
620
600
580
560
17.5
18
18.5
19
19.5
20
20.5
Number of Bays

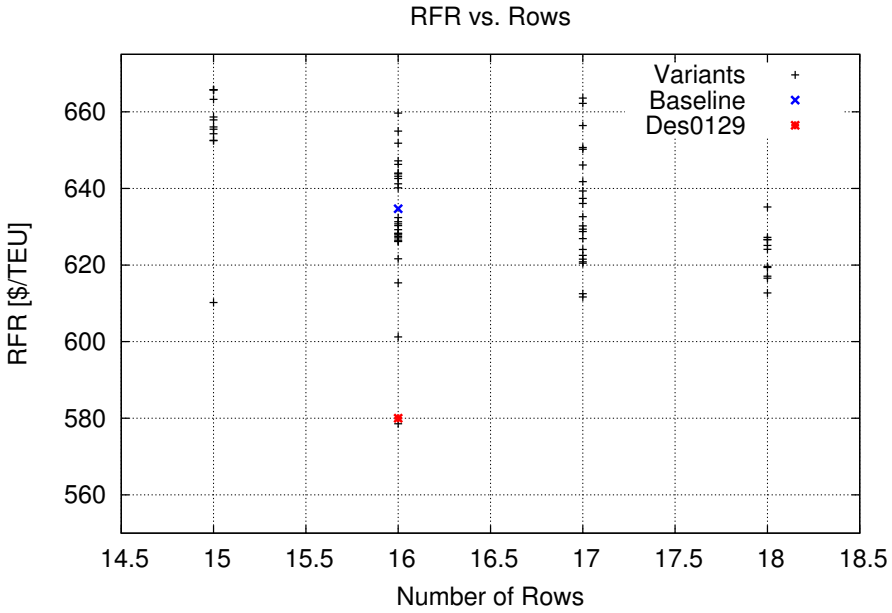
RFR vs. Rows
RFR [$/TEU]
Number of Rows
Variants
Baseline
Des0129
660
640
620
600
580
560
14.5
15
15.5
16
16.5
17
17.5
18
18.5

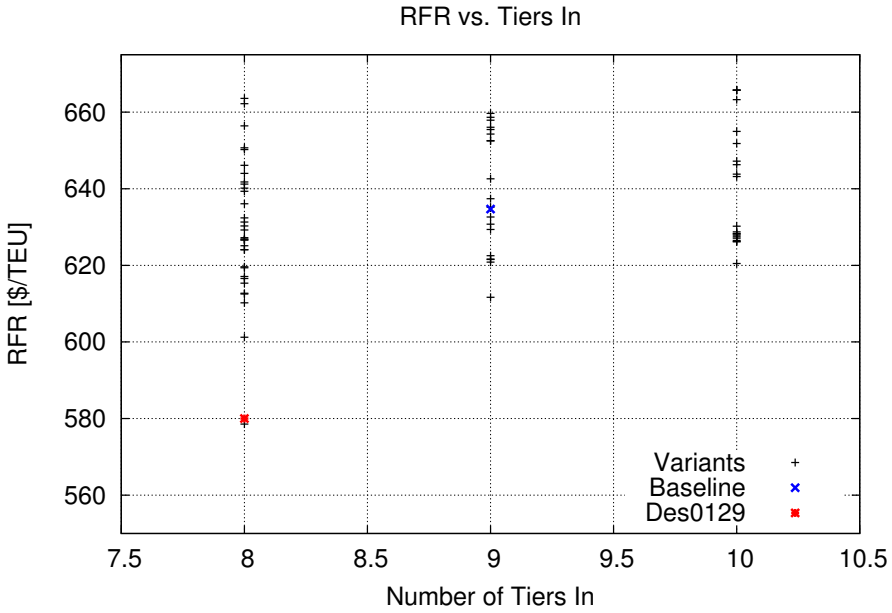
RFR vs. Tiers In
RFR [$/TEU]
Number of Tiers In
Variants
Baseline
Des0129
660
640
620
600
580
560
7.5
8
8.5
9
9.5
10
10.5

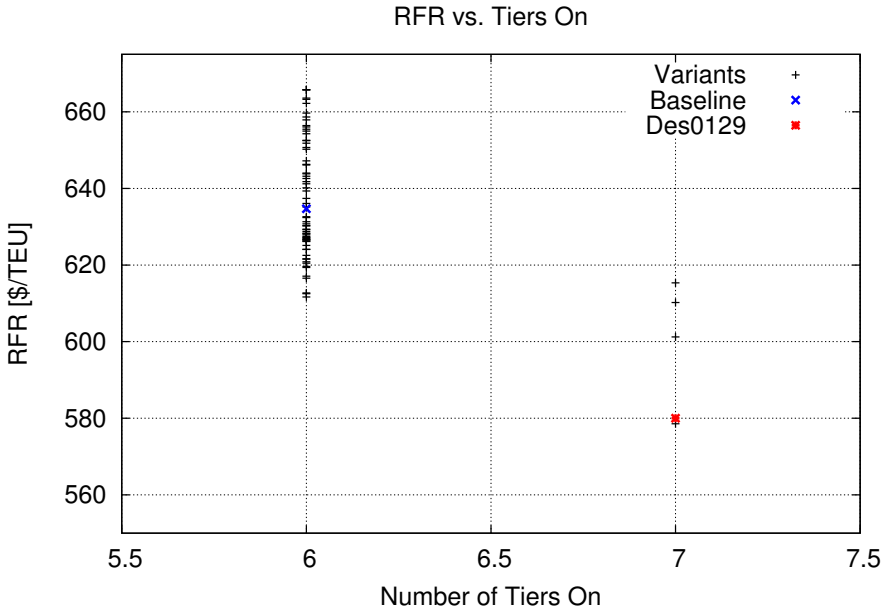
RFR vs. Tiers On
Variants
Baseline
Des0129
RFR [$/TEU]
660
640
620
600
580
560
5.5
6
6.5
7
7.5
Number of Tiers On

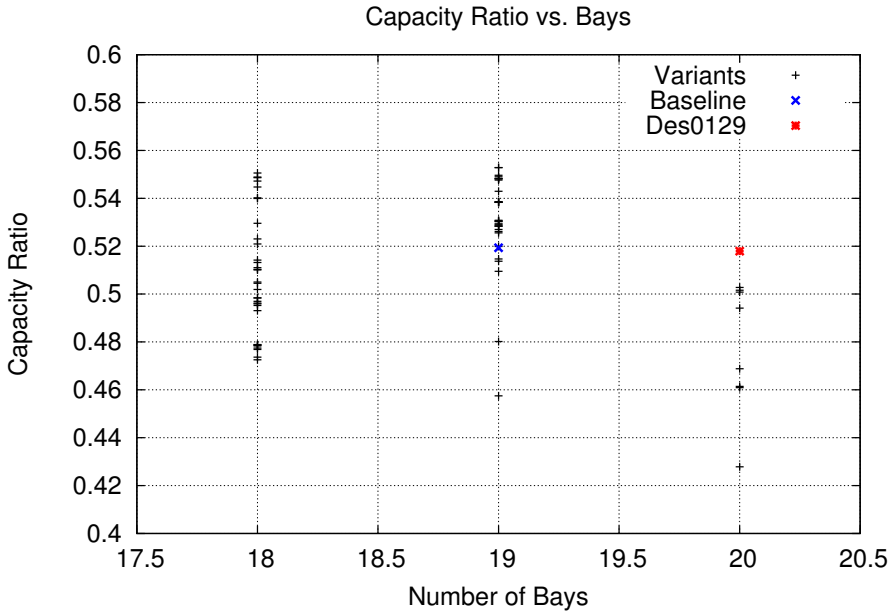
Capacity Ratio vs. Bays
Variants
Baseline
Des0129
Capacity Ratio
0.6
0.58
0.56
0.54
0.52
0.5
0.48
0.46
0.44
0.42
0.4
17.5
18
18.5
19
19.5
20
20.5
Number of Bays

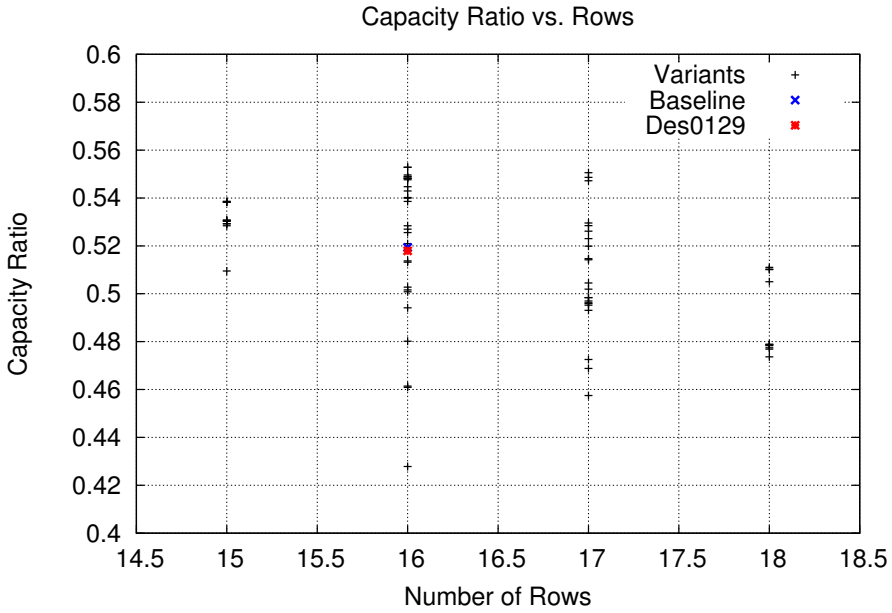
Capacity Ratio vs. Rows
Capacity Ratio
Number of Rows
Variants
Baseline
Des0129
0.6
0.58
0.56
0.54
0.52
0.5
0.48
0.46
0.44
0.42
0.4
14.5
15
15.5
16
16.5
17
17.5
18
18.5

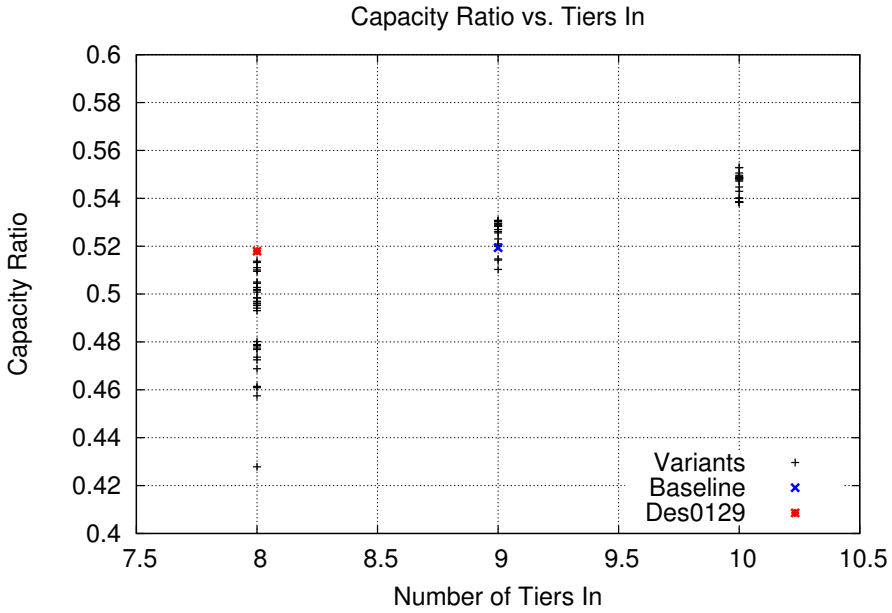
Capacity Ratio vs. Tiers In
Capacity Ratio
Number of Tiers In
Variants
Baseline
Des0129
0.6
0.58
0.56
0.54
0.52
0.5
0.48
0.46
0.44
0.42
0.4
7.5
8
8.5
9
9.5
10
10.5

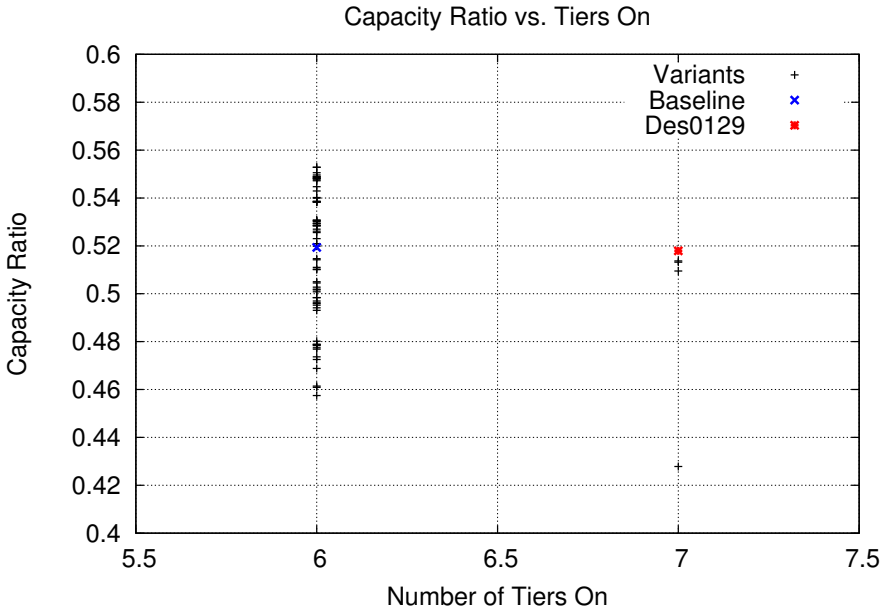
Capacity Ratio vs. Tiers On
Capacity Ratio
Number of Tiers On
Variants
Baseline
Des0129
0.6
0.58
0.56
0.54
0.52
0.5
0.48
0.46
0.44
0.42
0.4
5.5
6
6.5
7
7.5

## Model-2 Results

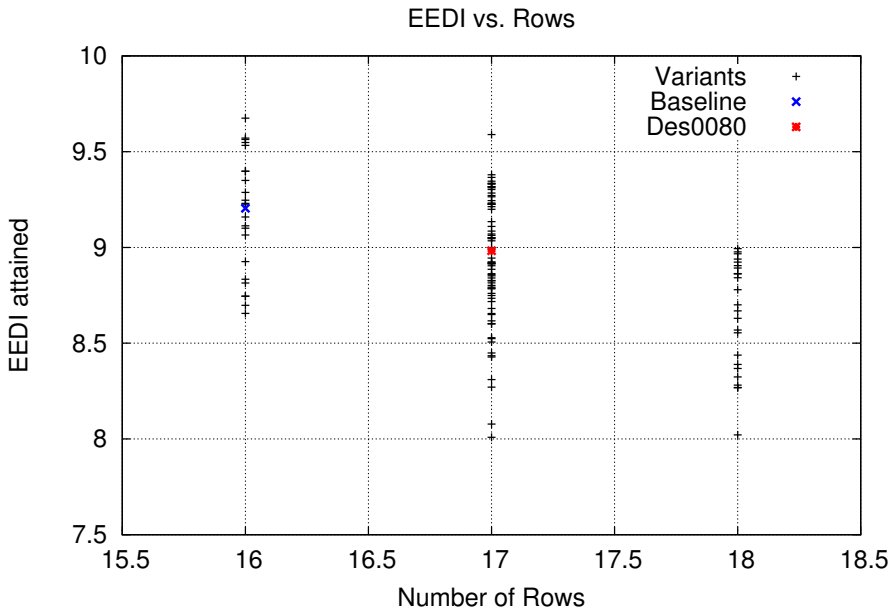


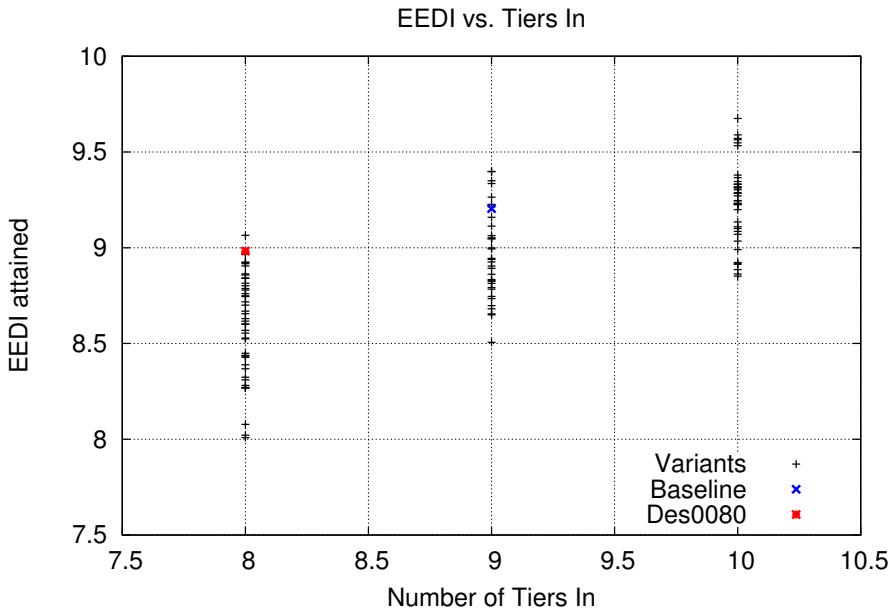

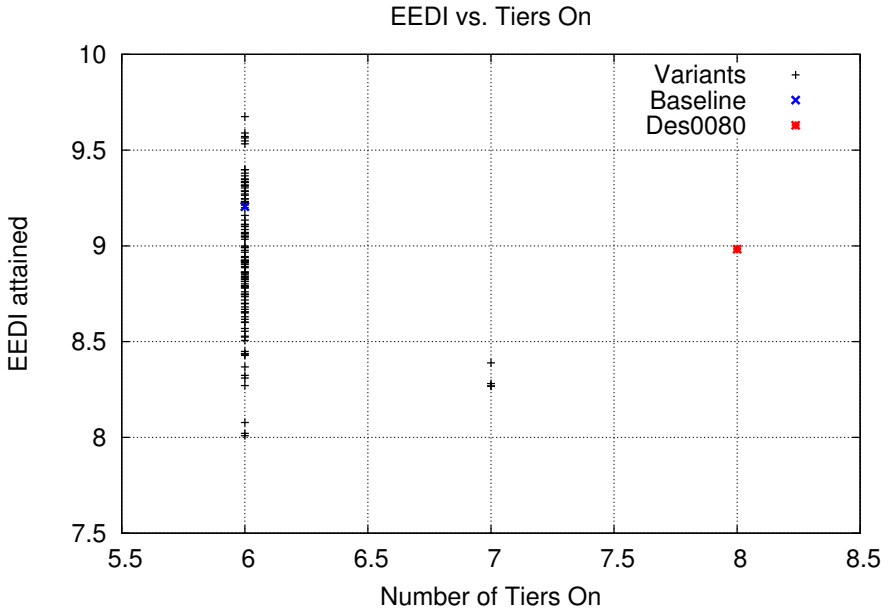
EEDI vs. Tiers On
EEDI attained
Number of Tiers On
Variants
Baseline
Des0080
10
9.5
9
8.5
8
7.5
5.5
6
6.5
7
7.5
8
8.5

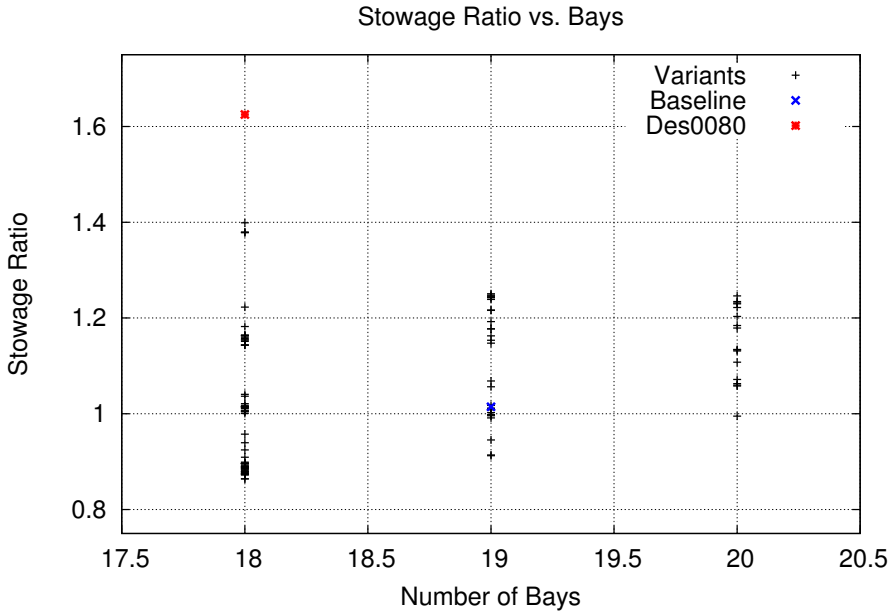
Stowage Ratio vs. Bays
Stowage Ratio
Number of Bays
Variants
Baseline
Des0080
1.6
1.4
1.2
1
0.8
17.5
18
18.5
19
19.5
20
20.5

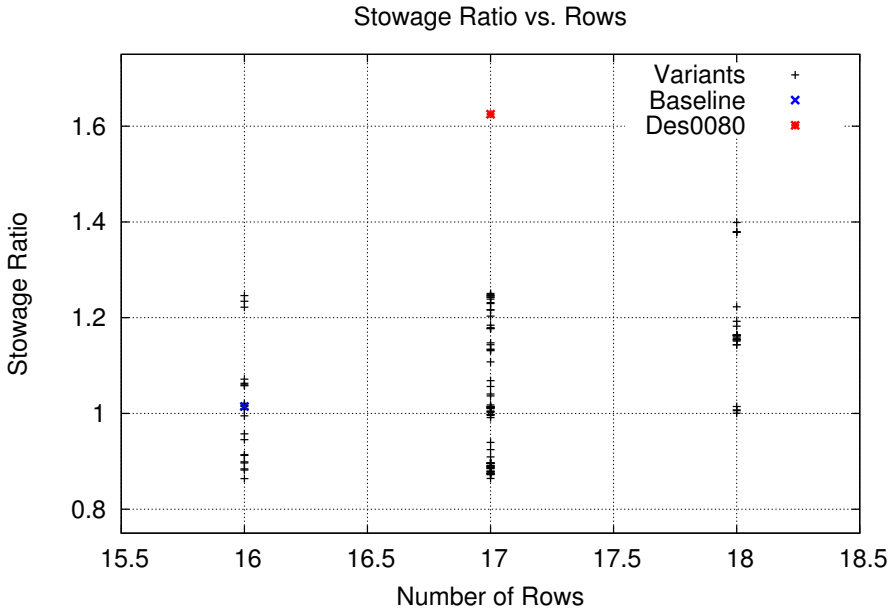
Stowage Ratio vs. Rows
Variants
Baseline
Des0080
Stowage Ratio
1.6
1.4
1.2
1
0.8
15.5
16
16.5
17
17.5
18
18.5
Number of Rows

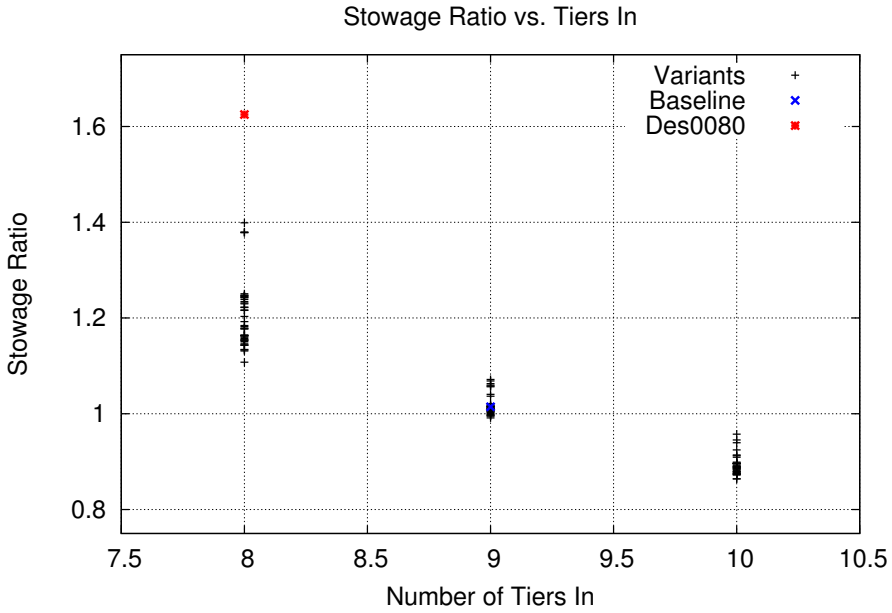
Stowage Ratio vs. Tiers In
Variants
Baseline
Des0080
Stowage Ratio
1.6
1.4
1.2
1
0.8
7.5
8
8.5
9
9.5
10
10.5
Number of Tiers In

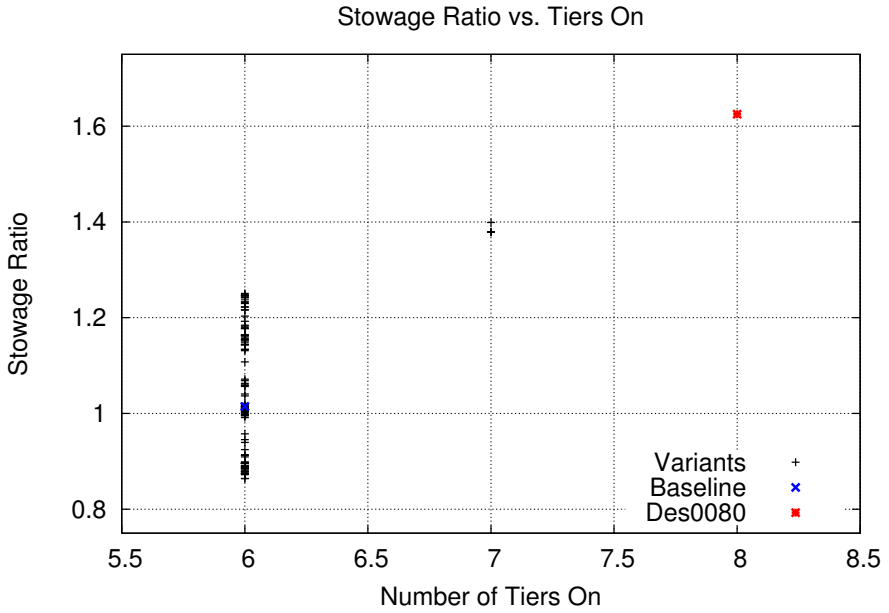
Stowage Ratio vs. Tiers On
Stowage Ratio
1.6
1.4
1.2
1
0.8
5.5
6
6.5
7
7.5
8
8.5
Number of Tiers On
Variants
Baseline
Des0080

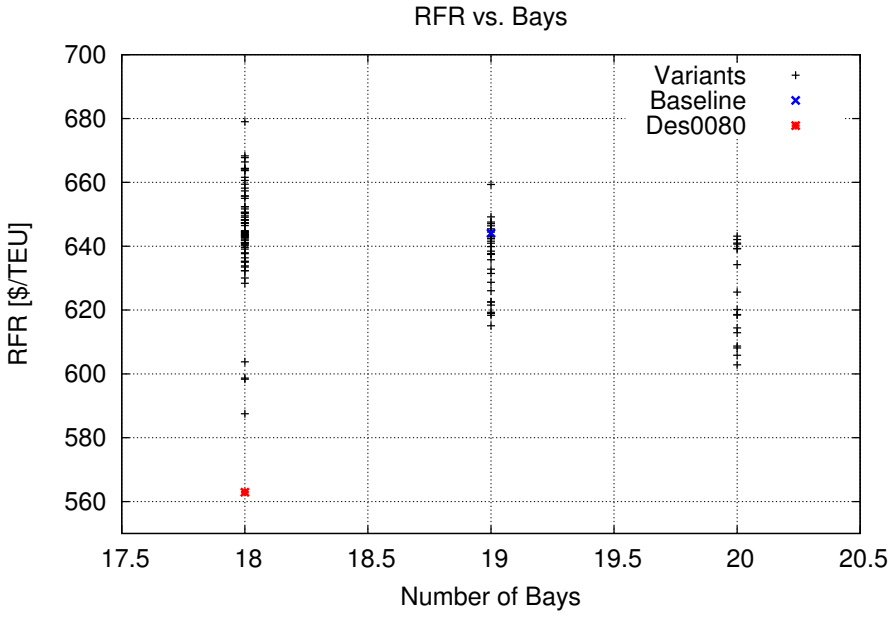
RFR vs. Bays
RFR [$/TEU]
700
680
660
640
620
600
580
560
17.5
18
18.5
19
19.5
20
20.5
Number of Bays
Variants
Baseline
Des0080

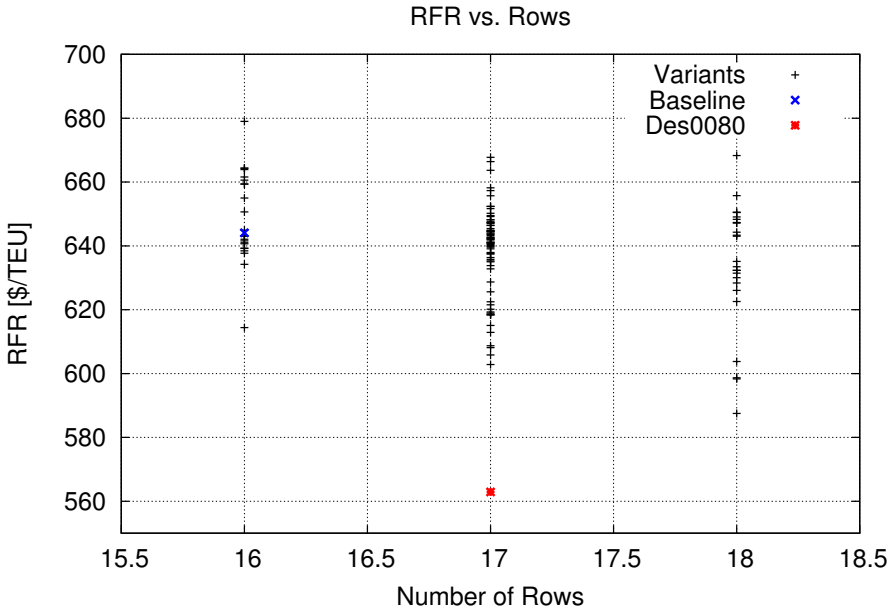
RFR vs. Rows
RFR [$/TEU]
Number of Rows
Variants
Baseline
Des0080
700
680
660
640
620
600
580
560
15.5
16
16.5
17
17.5
18
18.5

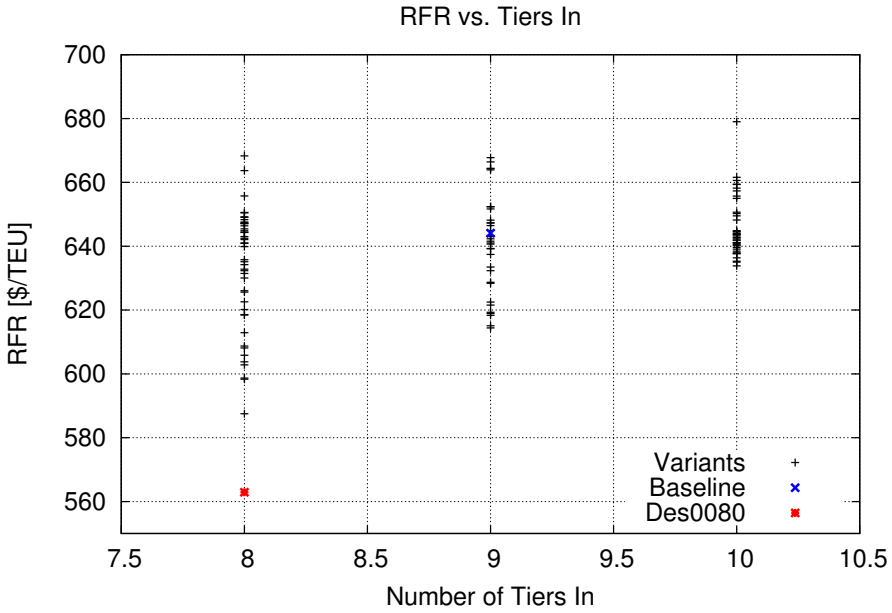
RFR vs. Tiers In
RFR [$/TEU]
Number of Tiers In
Variants
Baseline
Des0080
700
680
660
640
620
600
580
560
7.5
8
8.5
9
9.5
10
10.5

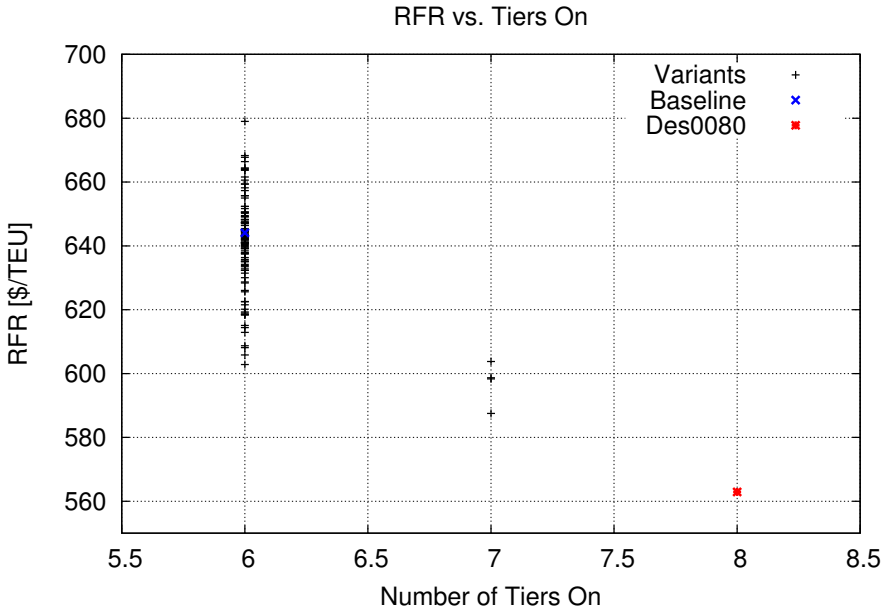
RFR vs. Tiers On
RFR [$/TEU]
Number of Tiers On
Variants
Baseline
Des0080
700
680
660
640
620
600
580
560
5.5
6
6.5
7
7.5
8
8.5

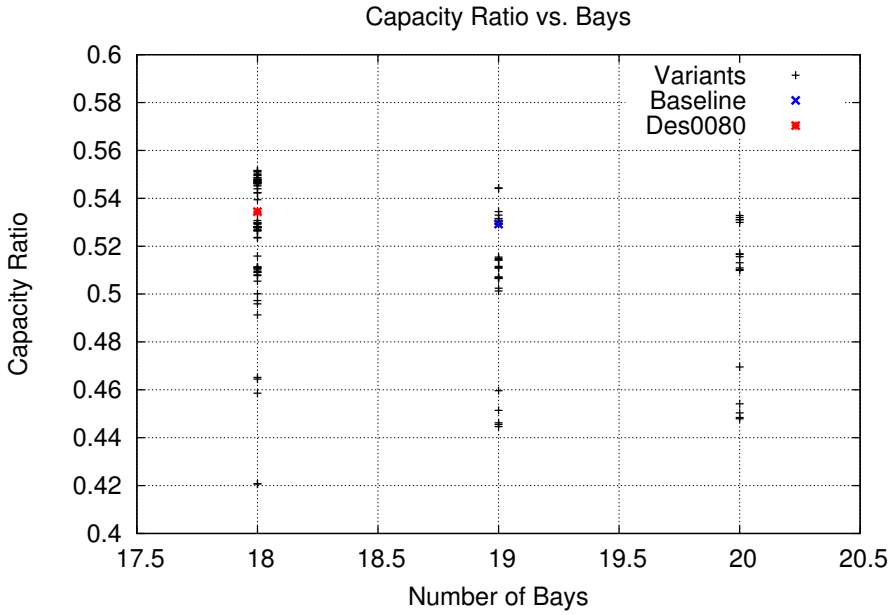
Capacity Ratio vs. Bays
Capacity Ratio
Number of Bays
Variants
Baseline
Des0080
0.6
0.58
0.56
0.54
0.52
0.5
0.48
0.46
0.44
0.42
0.4
17.5
18
18.5
19
19.5
20
20.5

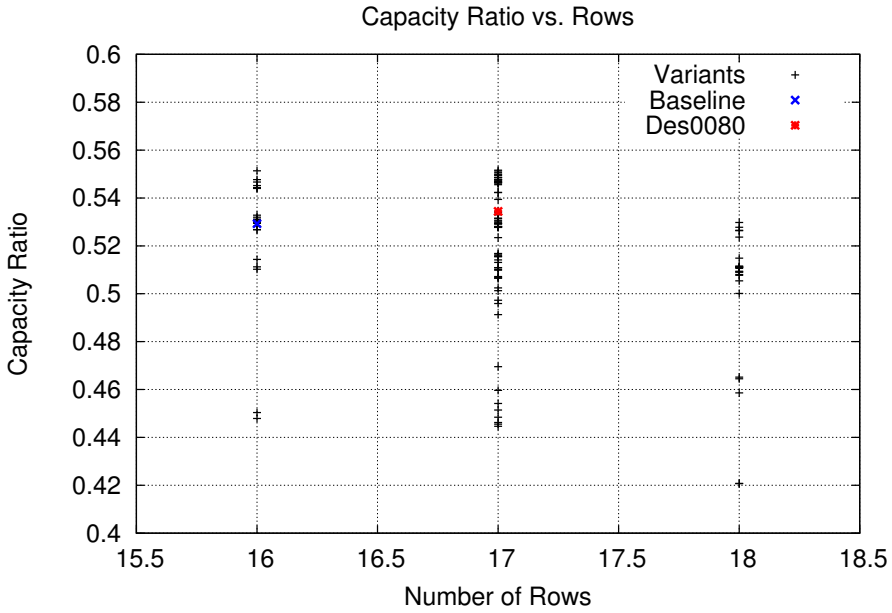
Capacity Ratio vs. Rows
Capacity Ratio
Number of Rows
Variants
Baseline
Des0080
0.6
0.58
0.56
0.54
0.52
0.5
0.48
0.46
0.44
0.42
0.4
15.5
16
16.5
17
17.5
18
18.5

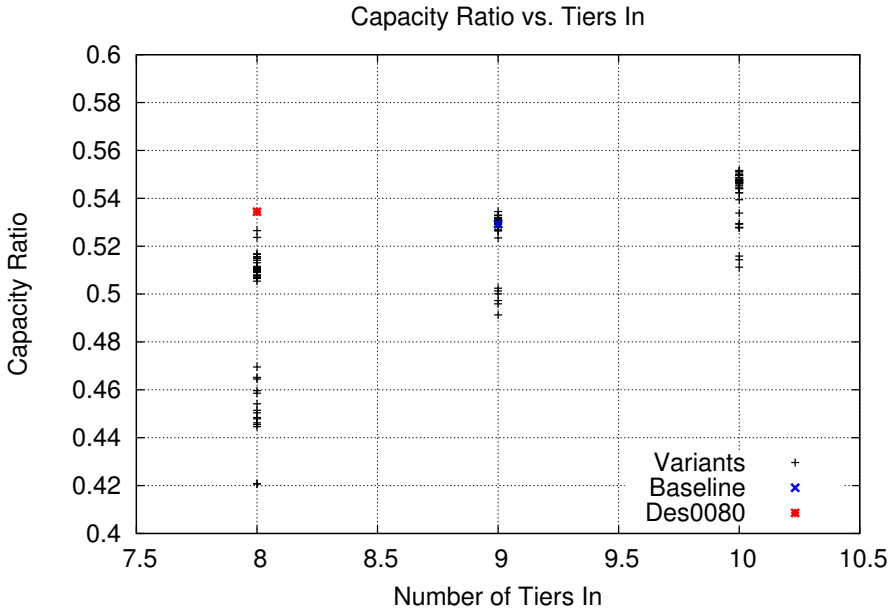
Capacity Ratio vs. Tiers In
Capacity Ratio
Number of Tiers In
Variants
Baseline
Des0080
0.6
0.58
0.56
0.54
0.52
0.5
0.48
0.46
0.44
0.42
0.4
7.5
8
8.5
9
9.5
10
10.5

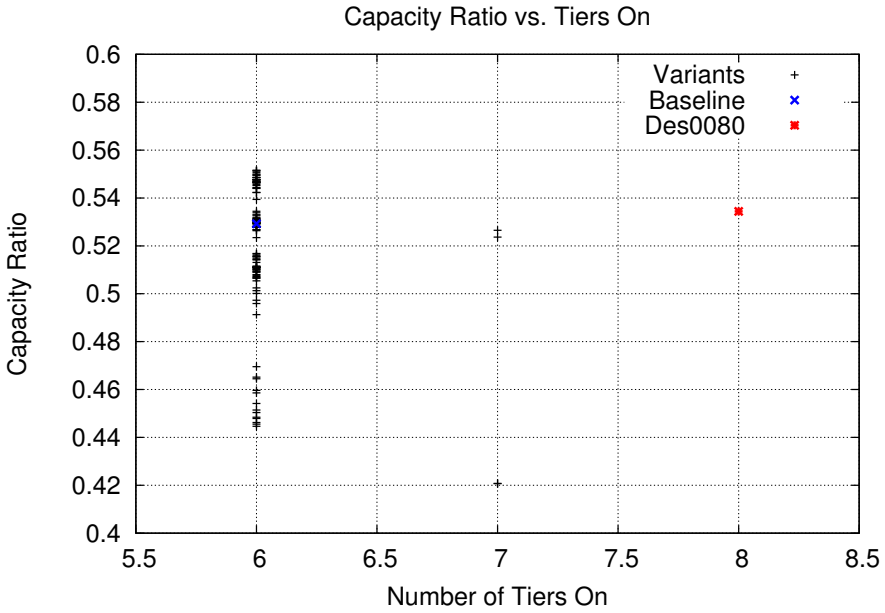
Capacity Ratio vs. Tiers On
Capacity Ratio
Number of Tiers On
Variants
Baseline
Des0080
0.6
0.58
0.56
0.54
0.52
0.5
0.48
0.46
0.44
0.42
0.4
5.5
6
6.5
7
7.5
8
8.5

# References


[1] http://en.wikipedia.org/wiki/Container_ship. March 2015.

[2] http://en.wikipedia.org/wiki/Pareto_efficiency. March 2015.

[3] http://www.bunkerworld.com/prices. March 2015.

[4] http://www.container-transportation.com/worlds-largest-container-ship.html. March 2015.

[5] http://www.worldshipping.org/about-the-industry/global-trade/trade-routes. March 2015.

[6] C. Abt and S. Harries. Hull Variation and Improvement Using the Generalised Lackenby Method of the Friendship-Framework. *The Naval Architect*, pages 166 – 167, September 2007.

[7] F.M. Azmin and R. Stobart. Benefiting from Sobol Sequences Experiment Design Type for Model-based Calibration. *SAE International*, 2015.

[8] J. Bergmann. Future Development of Ultra Large Container Ships. *DNV - GL*, April 2014.

[9] B.J. Cudahy. The Containership Revolution: Malcom McLean's 1956 Innovation Goes Global. *TR News*, (246):5 – 9, September - October 2006.

[10] K. Deb, A. Pratap, S. Agarwal, and T. Meyarivan. A Fast and Elitist Multi-objective Genetic Algorithm: NSGA-II. *IEEE Transactions on Evolutionary Computation*, 6(2), April 2002.

[11] MAN Diesel and Turbo. Energy Efficiency Design Index.

[12] DNV GL. Additional Rules and Guidelines - Energy Efficiency. *Rules for Classification and Construction*, 2013.

[13] J. Holtrop and G.G.J. Mennen. An Approximate Power Prediction Method. *International Shipbuilding Progress*, 25, October 1978.

[14] H.J. Koelman. *Computer Support for Design, Engineering and Prototyping of the Shape of Ship Hulls*. PhD thesis, SARC, 1999.

[15] M. Köpke, A. Papanikolaou, S. Harries, L. Nikolopoulos, and P. Sames. CONTiOPT - Holistic Optimisation of a High Efficiency and Low Emission Containership. *Transport Research Arena*, 2014.

[16] G.L. Koutroukis. Parametric Design and Multi-objective Optimization Study of an Ellipsoidal Containership. Master's thesis, National Technical University of Athens, January 2012.

[17] H. Nowacki. Five Decades of Computer-aided Ship Design. *Computer-Aided Design*, 42(11):956 – 969, November 2010.

[18] A. Papanikolaou. Holistic Ship Design Optimization. *Computer-Aided Design*, (42):1028 – 1044, 2010.

[19] A. Papanikolaou. *Ship Design: Methodologies of Preliminary Design*. Springer, 2014.

[20] A. Papanikolaou, S. Harries, M. Wilken, and G. Zaraphonitis. Integrated Design and Multi-objective Optimization Approach to Ship Design. *15th International Conference on Computer Applications in Shipbuilding*, 2011.

[21] T. Ray, R.P. Gokarn, and O.P. Sha. A Global Optimization Model for Ship Design. *Computers in Industry*, (26):175 – 192, 1995.

[22] I. Soultanias. Parametric Ship Design and Holistic Design Optimization of a 9K TEU Container Carrier. Master's thesis, National Technical University of Athens, November 2014.

[23] D. Tozer. Container Ship Speed Matters. *Lloyd's Register*, September 2008.

[24] UNCTAD. Review of Maritime Transport. pages 17 – 20, 2014.

[25] R.D. White. Ocean Shipping Lines Cut Speed to Save Fuel Costs. *Los Angeles Times*, July 2010.